UNIVERSITAT POLITÈCNICA DE VALÈNCIA

Wideband Electromagnetic Body Phantoms for the Evaluation of Wireless Communications in the Microwave Spectrum

Institute of Telecommunications and Multimedia Applications
Centre for Biomaterials and Tissue Engineering
Universitat Politècnica de València

A thesis for the degree of

PhD in Technologies for Health and Well-Being

Valencia, October 2019

Author:
Sergio Castelló Palacios

Supervisors:
Dr. Concepción García Pardo
Prof. Narcís Cardona Marcet
Prof. Ana Vallés Lluch

"No tingueu més conviccions que les decididament imprescindibles"
Joan Fuster

Abstract

The constant evolution of technology and the search for new applications that improve people's lives has led to the arrival of the incorporation of these technologies in the organism. Body area networks (BANs) are a good example of this, consisting of communications networks located in the body itself, both on the surface and implanted inside it through the use of wireless devices. The main application of this technology is the biosanitary one, which seeks to monitor the activity of the body with the analysis of different parameters, and thus send the information collected inside the body to an external device that records it.

But it is not only these networks that interact with the body itself, as the presence of conventional networks in all the environments is increasing everyday. New generations of mobile communications, such as 5G, are moving towards making use of ever-increasing frequencies, as is the case of millimetre waves. These frequencies have much higher losses due to their interaction with the medium where they propagate, including people themselves. Therefore, it is increasingly necessary to take into account the presence of the human body in the propagation of wireless signals.

The research and design of new antennas and devices that take into account the human body requires testing in the environment where they are going to be used. In order to avoid experimentation on humans, or on animals that might have similar characteristics, phantoms are to be obtained in order to carry out experiments in the transmission of electromagnetic signals and thus observe the losses that own. In addition, the influence of these electromagnetic waves on the tissues themselves could be studied with regard to the specific absorption rate (SAR) of power.

The final objective of this thesis is to obtain phantoms that can be both in liquid and gel form, so that the appropriate medium can be chosen according to the type of experiment. For the gel form it is intended to use polymeric materials capable of providing mechanical consistency and with the possibility of being synthesized with the desired shape, i.e., that of the tissue in question.

In the case of liquids, these could be confined in containers with the shape of the tissues in order to adapt them to the type of test.

The property of a medium or material that defines how an electromagnetic wave propagates through it is the relative permittivity. Therefore, that is the main parameter that is studied in this thesis. It is a complex value, consisting of a real part commonly called the dielectric constant, and an imaginary part called the loss factor. The intention is to imitate the values of relative permittivity of the tissues from the human body, since from the point of view of a wireless communications link, it is enough to imitate this feature to replace the body itself. To this end, databases have been used to obtain this information, which has been taken as a reference.

Before trying to imitate the dielectric properties of human tissues, it has previously been necessary to analyse how different chemical compounds influence them within the frequency band of interest. The selected bands have been the main ones for biomedical use, as well as the new millimetre wave frequencies that will be used in the new 5G generation. Once the ideal compounds have been chosen to adjust the values of relative permittivity, the maximum number of tissues from the body has been imitated, prioritising those of greatest relevance for the cases of use. First, liquid mixtures with these properties have been achieved, which have later been converted into gel through the use of polymeric gels that are capable of absorbing these compounds. In addition, the main 3D printing materials have been studied from the point of view of degradation in time with the presence of these liquid mixtures. The choice of the best material is key to be able to print a container with the shape of the human tissue to imitate, which can be filled with liquids that have their dielectric properties.

Finally, it has been possible to use phantoms in different real tests that have served to obtain useful information for the design of future wireless communication devices. These experiments include the SAR assessment, the characterization of the propagation channel, the study of the signal penetration for microwave imaging, the influence of the body on the matching of an antenna in a medical smartband, and the validation of an early detection system for colon cancer based on differences in dielectric properties.

Resumen

La constante evolución de la tecnología y la búsqueda de nuevas aplicaciones con las que mejorar la vida de las personas trae consigo la llegada de la incorporación de dichas tecnologías en el organismo. Las redes de área corporal son un buen ejemplo de ello, que consisten en redes de comunicaciones situadas en el propio cuerpo, tanto en la superficie como implantadas en el interior del mismo mediante el uso de dispositivos inalámbricos. La principal aplicación que se desprende de esta tecnología es la biosanitaria, que busca monitorizar la actividad del organismo con el análisis de diferentes parámetros, y así enviar la información registrada del interior del cuerpo hacia un dispositivo externo que la registre.

Pero no solo estas redes son las que interaccionan con el propio cuerpo, pues la presencia de las redes convencionales en todos los entornos es cada vez más cotidiana. Y es que las nuevas generaciones de comunicaciones móviles, como el 5G, van en la dirección de hacer uso de frecuencias cada vez mayores, como es el caso de las milimétricas. Estas frecuencias tienen pérdidas mucho mayores debido a su interacción con el medio por el que se propagan, incluyendo las propias personas. Por tanto, cada vez resulta más necesario tener en cuenta la presencia del cuerpo humano en la propagación de las señales inalámbricas.

La investigación y el diseño de nuevas antenas y dispositivos que tengan en cuenta el cuerpo humano requiere de pruebas de testeo en el propio medio donde van a ser usados. Con el fin de evitar la experimentación en humanos, o en animales que pudieran tener características similares, se pretenden obtener modelos sintéticos de los tejidos humanos con los que poder realizar los experimentos de transmisión de señales electromagnéticas y así observar las pérdidas que se producen. Además, se podría estudiar la influencia de dichas ondas electromagnéticas sobre los propios tejidos en lo que se refiere a la tasa de absorción específica de potencia.

El objetivo final de esta tesis es la obtención de materiales sintéticos que puedan estar tanto en forma líquida como en forma gel, de modo que se pueda escoger el medio adecuado según el tipo de experimento. Para la forma gel se

pretenden usar materiales poliméricos capaces de aportar consistencia mecánica y con la posibilidad de ser sintetizados con la forma deseada, es decir, con la del tejido en cuestión. En el caso de los líquidos, estos podrían ser confinados en recipientes con la forma de los tejidos para adecuarlos al tipo de prueba.

La propiedad de un medio o material que influye en cómo se propaga una onda electromagnética a través de él es la permitividad relativa. Por tanto, ese es el parámetro principal que se estudia en esta tesis. Es un valor complejo, que consta de una parte real denominada comúnmente constante dieléctrica, y una parte imaginaria llamada factor de pérdidas. Lo que se pretende es imitar los valores de permitividad relativa de los tejidos del cuerpo humano, ya que desde el punto de vista de un enlace de comunicaciones inalámbricas, basta con imitar esta característica para sustituir al propio cuerpo. Para ello, se ha recurrido a bases de datos que ofrecen esta información, que se ha tomado como referencia.

Para tratar de imitar las propiedades dieléctricas de los tejidos humanos, previamente se ha tenido que analizar cómo influyen distintos compuestos químicos en la banda de frecuencias de interés. Las bandas seleccionadas han sido las principales de uso biomédico, así como las nuevas frecuencias milimétricas de uso en la nueva generación 5G. Una vez escogidos los compuestos idóneos para ajustar los valores de la permitividad relativa, se ha pasado a imitar el máximo número de tejidos del cuerpo, priorizando aquellos de mayor relevancia para los casos de uso. Primero se han conseguido mezclas líquidas con dichas propiedades, que más adelante se han tratado de convertir en gel mediante el uso de geles poliméricos que son capaces de absorber dichos compuestos. Además, se han estudiado los principales materiales de impresión 3D desde el punto de vista de degradación en el tiempo con la presencia de estas mezclas líquidas. La elección del mejor material es crucial para poder imprimir un recipiente con la forma del tejido humano a imitar, que pueda ser rellenado con los líquidos que poseen sus propiedades dieléctricas.

Finalmente, se han podido usar los modelos sintéticos en diferentes pruebas reales que han servido para obtener información útil para el diseño de los futuros dispositivos de comunicaciones inalámbricas. Estos experimentos incluyen la tasa de absorción específica, la caracterización del canal de propagación, el estudio de la penetración de la señal para imágenes de microondas, la influencia del cuerpo sobre la adaptación de una antena en una pulsera médica, y la validación de un sistema de detección precoz de cáncer de colon basado en diferencias en las propiedades dieléctricas.

Resum

L'evolució constant de la tecnologia i la recerca de noves aplicacions amb les quals millorar la vida de les persones porta l'arribada de la incorporació d'aquestes tecnologies en l'organisme. Les xarxes d'àrea corporal són un bon exemple d'això, que consisteixen en xarxes de comunicacions situades en el propi cos, tant en la superfície com implantades a l'interior del mateix mitjançant l'ús de dispositius sense fil. La principal aplicació que es deriva d'aquesta tecnologia és la biosanitària, que busca monitoritzar l'activitat de l'organisme amb l'anàlisi de diferents paràmetres, i així enviar la informació registrada de l'interior del cos cap a un dispositiu extern que la registre.

Però no són només aquestes xarxes les que interaccionen amb el propi cos, ja que la presència de les xarxes convencionals en tots els entorns és cada vegada més quotidiana. I és que les noves generacions de comunicacions mòbils, com el 5G, van en la direcció de fer ús de freqüències cada vegada més grans, com és el cas de les mil·limètriques. Aquestes freqüències tenen pèrdues molt més grans a causa de la seua interacció amb el medi pel qual es propaguen, incloent les persones mateixes. Per tant, cada vegada resulta més necessari tenir en compte la presència del cos humà en la propagació dels senyals sense fils.

La investigació i el disseny d'antenes i dispositius nous que tinguen en compte el cos humà requereix de proves de testeig en el propi medi on van a ser usats. Per tal d'evitar l'experimentació en humans, o en animals que hi puguen tenir característiques similars, es pretenen obtenir models sintètics dels teixits humans amb els quals poder realitzar els experiments de transmissió de senyals electromagnètics i així observar les pèrdues que s'hi produeixen. A més, es podria estudiar la influència d'aquestes ones electromagnètiques sobre els propis teixits pel que fa a la taxa d'absorció específica de potència.

L'objectiu final d'aquesta tesi és l'obtenció de materials sintètics que puguen estar tant en forma líquida com en forma gel, de manera que es puga escollir el medi adequat segons el tipus d'experiment. Per a la forma gel es pretenen utilitzar materials polimèrics capaços d'aportar-hi consistència mecànica i amb la possibilitat de ser sintetitzats amb la forma desitjada, és a dir, amb la del teixit

en qüestió. En el cas dels líquids, aquests podrien ser confinats en recipients amb la forma dels teixits per a adequar-los al tipus de prova.

La propietat d'un medi o material que influeix en com es propaga una ona electromagnètica a través d'ell és la permitivitat relativa. Per tant, eixe és el paràmetre principal que s'estudia en aquesta tesi. És un valor complex, que consta d'una part real anomenada comunament constant dielèctrica, i una part imaginària anomenada factor de pèrdues. El que es pretén és imitar els valors de permitivitat relativa dels teixits del cos humà, ja que des del punt de vista d'un enllaç de comunicacions sense fil, només cal imitar-ne aquesta característica per a substituir al cos mateix. Per a això, s'ha recorregut a bases de dades que ofereixen aquesta informació, que s'ha pres com a referència.

Per a tractar d'imitar les propietats dielèctriques dels teixits humans, s'ha hagut d'analitzar prèviament com hi influeixen diferents compostos químics en la banda de freqüències d'interès. Les bandes seleccionades han sigut les principals d'ús biomèdic, així com les noves freqüències mil·limètriques d'ús en la nova generació 5G. Un cop escollits els compostos idonis per a ajustar els valors de la permitivitat relativa, s'ha passat a imitar el màxim nombre de teixits del cos, prioritzant-ne aquells de major rellevància per als casos d'ús. Primer s'han aconseguit mescles líquides amb aquestes propietats, que més endavant s'han tractat de convertir en gel mitjançant l'ús de gels polimèrics que són capaços d'absorbir aquests compostos. A més, s'han estudiat els principals materials d'impressió 3D des del punt de vista de degradació en el temps amb la presència d'aquestes barreges líquides. L'elecció del millor material és clau per a poder imprimir un recipient amb la forma del teixit humà que es vol imitar, que puga ser omplit amb els líquids que tenen les seues propietats dielèctriques.

Finalment, s'han pogut fer servir els models sintètics en diferents proves reals que han servit per obtenir informació útil per al disseny dels futurs dispositius de comunicacions sense fils. Aquests experiments inclouen la taxa d'absorció específica, la caracterització del canal de propagació, l'estudi de la penetració del senyal per a imatges de microones, la influència del cos sobre l'adaptació d'una antena en una polsera mèdica, i la validació d'un sistema de detecció precoç de càncer de còlon basat en diferències en les propietats dielèctriques.

Acknowledgements

This thesis is the result of the effort, influence, affection, advice and help of many people. Some of these people are still in my life, while others have gone their own way. In any case, they have all made their contribution to get here.

The first person I want to mention is Ana, one of my supervisors. This whole thing started with her. She has become one of the people who has changed the course of my life. She trusted me from the very first moment and it was she who convinced me to take this opportunity. She always has a smile in her mouth and a motivational phrase to offer. Thank you so much for making me live this experience. My second supervisor is no less important, because she has always been there when it has been necessary, with her advice and her proverbs. Thanks, Conchi, for everything you have taught me and contributed as a person, I think I am a little wiser because of you. You have been a great support on which to lean in the face of any problem. Last but not least, I would like to thank Narcís for giving me the opportunity to join this fantastic team in which I have felt like one more from the beginning. Thank you for trusting me and doing the impossible to grow and compete in this world of research. Without your support, I would not be here right now.

On the side of the Centre for Biomaterials and Tissue Engineering, I'm very happy with the people that have surrounded me over the years. I am especially grateful to Guille for helping me with everything I have asked him and for making me think about a great deal of things. Of course, Laura, whom I can never thank for everything that has helped me over the years. This centre would not work at all without her. This centre is full of people with a lot of vocation, who enjoy the time they spend there, and you can feel that in the great environment you experience. I had a great time there, especially my first year of doctorate, when we made a great group of students of all modalities. I would like to thank Fran, Marina, Adri, Álvaro, Belén, Arnau, Yess, Ana, Leydi, María and others that I know for sure I forget. You made all the hours in the hideout more bearable. Thanks also to María, my passing trainee, for all your help in the lab. In the end I think I learned more from you than the other

way around. The teachers who inhabit the place are of the most endearing, always with a reflection or a different point of view. I want to give special thanks to Gloria, David and Isabel for sharing their life experience and lessons. Finally, thanks also to the rest of my colleagues, who facilitate your work as much as possible and make it more enjoyable, such as María, Rubén, Silvia, Sandra, Laura, Hayk, Sergiy, Cristina, etc.

My stay in Ghent was an amazing experience that I will never forget. I want to thank Wout for welcoming me for three months in his group and for helping me with everything I need. I especially want to thank Reza and Gemma for all they did for me those months. They made me feel at home. We made a great group of friends with whom we had a great time. Thanks to Rodney, Sunil, Sarah, Greta and the rest of the group for such wonderful moments. Thanks also to Günter, Margot, Arno and the other members for the lunchtime talks. I do not want to forget the people of the residence, with whom I also lived many experiences and spent memorable moments. Thanks to Carlos, Lolo, Javi, Carlotta, Clara, Caroline, Víctor and many others. The stay was made much easier thanks to your company.

The Mobile Communications Group (MCG) has become my new home. There are a lot of people here who have become my new friends. Edu, thank you for your nonsense and for taking care of your friends so much. Gerardo, thanks for your constant interest in people problems and your thoughts about life. Manuel, thank you for your straightforward way of looking at life and for your sincere honesty. José Luis, thank you for the moments of laughs, for your kindness and for your maturity that serves as an example. Barjau, thanks for your madness and for making the world an unexpected place. Although the craziest person of all is Alicia, who always has a feeling to confess. Thank you for your ray of light and your positive energy. Of course, thanks to my groupmates, Sofía and Martina, for breaking schemes and contributing so much to the wheels of this research. They are unique and irreplaceable, with their special oddities. Thanks to Tere for all her infinite warmth and patience. Irene, for taking care of everyone. Thanks also to Carlos Herranz, David García, Barquero and Martín-Sacristán, Sandra, Josetxo and Dani. Thank you all for making me feel one more of you.

From the rest of the colleagues from the iTEAM I also have to mention some people. Thanks to J.J. for introducing me to the world of 3D printing and for letting me use the printer to mess around. Thanks to the Electromagnetic Radiation Group (GRE) for helping us with all the antennas we needed and for the collaborations we have carried out. Without them, much of our group research would not have been possible. Thanks to Marta, Eva, Hamza and Marc for being so friendly and willing to do things together. I want to highlight Toni,

a wonderful person with infinite solidarity who has helped us in everything that has been within his reach.

The people who have supported me the most in this adventure have been Álex and Carlos. Their help has been invaluable in all aspects. We have had good times and bad times, but they have all made me grow as a person. Without them this would not have been the same, not by a long shot. They have made me enjoy and work in a way that did not cost any effort. Both have always put friendship ahead of work. They have become two great friends, and we have lived many experiences together that I will always carry with me. I love them so much for everything they mean to me. Álex, you are the other person it all started with. You have always been like my extra supervisor. I admire you very much as a person and as a professional. I never stop learning from you. You have helped me whenever it was needed and practically all I have achieved is thanks to you. You have dared with chemistry and with everything that has been put in front of you. Thank you for your advice and wisdom. I will never be able to reach your level. Carlos, you came into my life unexpectedly and you have become indispensable. I started helping you and you ended up getting involved in everything I did, as an inseparable team. You are like an unstoppable engine because of the passion you put into what you do. Your motivation made us progress a lot and work intensely when it was necessary without becoming hard. Thank you for all you have endured for me, for all you have taught me, and for your special way of being.

Thanks to all the friends who have given me their support and motivated to continue until the end. Those who are always present and who have a gap of time to make me enjoy life.

I would finally like to thank my family. My brother, Jordi, who has helped me in every way he has been able to, with ideas and gadgets, always with a great predisposition and enthusiasm. My father, Toni, who has always supported me to get where I wanted to go. And my mother, Isabel, who has always given everything for me.

Financial Support

This thesis has been possible thanks to the funding contribution of the Universitat Politècnica de València through the PAID-01-16 programme. This work was also supported by the UPV-IIS La Fe programme (STUDER, 2016 and EMOTE, 2017). The research stay was supported by the European Union's Erasmus+ funding programme under a traineeship grant.

Table of contents

Abstract **v**

Acknowledgements **xi**

List of Figures **xvii**

List of Tables **xxiii**

1 Introduction **1**
1.1 The Human Body in the Propagation Medium 1
1.2 The Permittivity of the Medium 7
1.2.1 Polarisation Mechanisms 7
1.2.2 Nature of Dielectric Materials 11
1.3 Objectives and Scope 12
1.4 State-of-the-Art 14
1.5 Thesis Outline 19

2 Materials & Methods **23**
2.1 Semisolid Gels 24
2.1.1 Types of Gels 24
2.1.2 Hydrogels in Biomedical Applications 28
2.2 Gel Synthesis 29
2.3 Experimental Design 36
2.3.1 Characterisation of the Relative Permittivity 36
2.3.2 Degradation Analysis 41

3 Phantom Engineering **45**
3.1 Basic Common Compounds 45
3.2 Materials Selection for Liquid Phantoms 52
3.3 Liquid Phantoms Tailoring 58

3.4 Material Selection for Gel Phantoms 63
3.5 Gel Phantoms Design 67
3.6 Printing Materials 69

4 Tissue Phantoms **73**
4.1 Narrowband Models 73
4.1.1 Industrial, Scientific and Medical Band 73
4.2 Ultrawideband Liquid Phantoms 76
4.3 Ultrawideband Synthetic Gels 87
4.4 5G New Radio Frequency Range 2 95
4.4.1 Data Modelling with Mixing Rules 98
4.4.2 Cole-Cole Fitting 101
4.4.3 Gelling of the Mixtures 102

5 Applications in Biomedical Engineering **105**
5.1 Effect of the Arm on the Antenna Matching of a Wearable . . . 105
5.2 Assessment of Specific Absorption Rate 107
5.3 Channel Characterisation at Ultrawideband Frequencies 110
5.4 Validation of a Colon Tumour Diagnosis System 114
5.5 Study of the Penetration Ratio for Microwave Imaging 116

6 Conclusions & Perspective **121**
6.1 Concluding Remarks 122
6.2 Future Work 127

A Dielectric Properties of the Human Body **129**
A.1 Dispersion Regions 129
A.2 Variability Factors 130
A.3 Cole-Cole Parametric Fitting 131

Thesis Contributions **133**

Acronyms **139**

References **141**

List of Figures

1.1 Endoscopic capsule for recording the gastrointestinal tract. . . 3
1.2 Reflected and transmitted signal when changing propagation medium. 4
1.3 Simulation environments. 6
1.4 Movement of the electrical charges of a medium when applying an external field. 8
1.5 Diagram of the polarisation by electronic distortion. 9
1.6 Diagram of the distribution of charges in a polar molecule. . . . 10
1.7 Relationship between polarisation mechanisms and frequency. . 11
1.8 Relative permittivity of water compared to muscle and fat. . . 15
1.9 Relative permittivity of the phantoms for the muscle and liver included in Table 1.1, compared to their corresponding reference values according to Gabriel. 18

2.1 Examples of different physical and chemical gelification mechanisms. 25
2.2 Gelification of κ-carrageenan by means of cooling a hot solution in presence of a salt. 27
2.3 Diagram of gel formation, from polymerisation reaction through the swelling of the cross-linked structure to its final state. . . . 29
2.4 Mechanism of initiation and propagation of the polymerisation reaction for the cross-linked PHEA. 30
2.5 Mechanism of initiation and propagation of the polymerisation reaction for the cross-linked PAM. 31
2.6 Glass moulds that allowed the passage of UV light to induce the polymerisation of the reacting mixture. 32
2.7 Glass flask containing the polymers immersed in a mixture of water and ethanol. 33

2.8 Glass flask with the coil vapour condenser connected to a refrigerant recirculation system. 34
2.9 Desiccator with a glass cover and thermal plate with adjustable temperature. 35
2.10 Hammer and die cutter with a diameter of 7 mm and the die-cut samples before swelling. 36
2.11 Setup of the characterisation system of the relative permittivity through the open-ended coaxial method. 37
2.12 Immersion of the coaxial probe within the MUT. 39
2.13 Measurement of a semisolid material with the open-ended coaxial probe. 40
2.14 Single point load cell connected to the strain meter, which shows the strength applied to the red surface in newton. 41
2.15 Pelletiser machine. 42
2.16 Hydraulic press with heating plates where the polymer specimens were shaped. 43
2.17 PLA specimens of a 4×1 cm^2 area and 200-300 μm of thickness. 44
2.18 Tensile testing setup with serrated grips for subjecting the specimens. 44

3.1 Relative permittivity of water with 0% sucrose with different concentrations of NaCl. 46
3.2 Relative permittivity of water with 17% sucrose with different concentrations of NaCl. 47
3.3 Relative permittivity of water with 34% sucrose with different concentrations of NaCl. 47
3.4 Relative permittivity of water with 51% sucrose with different concentrations of NaCl. 48
3.5 Evolution of the dielectric constant at 2.4 GHz according to the concentration of salt and sucrose in aqueous solutions. 50
3.6 Evolution of the loss factor at 2.4 GHz according to the concentration of salt and sucrose in aqueous solutions. 51
3.7 Relative permittivity of water, 50% aqueous mixtures of different polar liquids, and that of the muscle tissue according to Gabriel. 53
3.8 Hydrogen bonds of a single water molecule with four other water molecules. 54
3.9 Loss factor of aqueous solutions with a 2.5% of NaCl, KCl and NaBr compared with deionised water. 55
3.10 Relative permittivity of 30% acetonitrile mixtures with different concentrations of NaCl. 56

3.11 Relative permittivity of 40% acetonitrile mixtures with different concentrations of NaCl. 57
3.12 Relative permittivity of 50% acetonitrile mixtures with different concentrations of NaCl. 57
3.13 Relative permittivity of 60% acetonitrile mixtures with different concentrations of NaCl. 58
3.14 Evolution of the dielectric constant at 2.4 GHz according to the concentration of acetonitrile and salt in aqueous solutions. . . . 59
3.15 Evolution of the loss factor at 2.4 GHz according to the concentration of acetonitrile and salt in aqueous solutions. 60
3.16 Average swelling index and standard deviation of the PHEA and PAM gels, swollen in water and in a 50% acetonitrile aqueous mixture. 64
3.17 Average swelling index and standard deviation of PHEA gels, with different cross-linking degrees, when swollen in water and in a 50% acetonitrile aqueous mixture. 65
3.18 Box-and-whisker diagram of the ultimate strength for gels made of agar, κ-carrageenan and PHEA in water. 66
3.19 Box-and-whisker diagram of the ultimate strength for PHEA gels, swollen in water and in a 50% acetonitrile aqueous mixture, with different cross-linking degrees. 67
3.20 Relative permittivity of the PHEA gel, swollen in water, with different percentages of cross-linker. 68
3.21 Relative permittivity of the PHEA gel, with a fixed cross-linking degree of 0.05%, swollen in different acetonitrile aqueous mixtures. 69
3.22 Stress-strain curve of a PP specimen after being immersed in the degradation mixture for 9 months. 70
3.23 Box-and-whisker diagram of the ultimate strength for ABS, PLA and PP. 70
3.24 Box-and-whisker diagram of the ultimate strength for PP specimens, after being immersed in the degradation mixture for the indicated time. 71
3.25 Box-and-whisker diagram of the ultimate strength for PLA specimens, after being immersed in the degradation mixture for the indicated time. 72

4.1 Relative permittivity of the wideband liquid phantom for the muscle. 76
4.2 Relative permittivity of the wideband liquid phantom for the heart. 77

4.3 Relative permittivity of the wideband liquid phantom for the pancreas. . . . 78
4.4 Relative permittivity of the wideband liquid phantom for the colon. . . . 79
4.5 Relative permittivity of the wideband liquid phantom for the liver. 80
4.6 Relative permittivity of the wideband liquid phantom for the cartilage. . . . 80
4.7 Relative permittivity of the wideband liquid phantom for the wet skin. . . . 81
4.8 Relative permittivity of the wideband liquid phantom for the grey matter. . . . 82
4.9 Relative permittivity of the wideband liquid phantom for the kidney. . . . 83
4.10 Relative permittivity of the wideband liquid phantom for the cornea. . . . 83
4.11 Relative permittivity of the wideband liquid phantom for the blood. . . . 84
4.12 Relative permittivity of the wideband liquid phantoms for the infiltrated and non-infiltrated fat. . . . 86
4.13 Relative permittivity of the wideband gel phantom for the cerebellum. . . . 88
4.14 Relative permittivity of the wideband gel phantom for the wet skin. . . . 89
4.15 Relative permittivity of the wideband gel phantom for the liver. 90
4.16 Relative permittivity of the wideband gel phantom for the tendon. 90
4.17 Relative permittivity of the wideband gel phantom for the colon. 91
4.18 Relative permittivity of the wideband gel phantom for the muscle. 91
4.19 Relative permittivity of the wideband gel phantom for the cartilage. . . . 92
4.20 Relative permittivity of the wideband gel phantom for the nerve. 93
4.21 Relative permittivity of methanol aqueous mixtures together with the average values of the dry and wet skin. . . . 97
4.22 Relative permittivity of 1-propanol aqueous mixtures together with the average values of the dry and wet skin. . . . 97
4.23 Comparison between the measured relative permittivity of 5% methanol aqueous mixtures and the predicted one by using the equations from the mixing rules. . . . 100
4.24 Relative permittivity of the κ-carrageenan gels. . . . 103

5.1 Study of the influence of the arm over the performance of a wearable in an anechoic chamber. . . . 106

5.2 Comparison between the simulated and measured reflection parameter (S_{11}) of the wearable antenna in contact with an arm phantom. 107
5.3 Setup for the SAR measurements, where the phantom container is fixed with the dipole under it, and the probe is moved by a 3D positioner system. 108
5.4 Specific Absorption Rate over the bottom of a 10 gram cube of muscle tissue by using the muscle phantom. 109
5.5 Specific Absorption Rate over the top of a 10 gram cube of muscle tissue by using the muscle phantom. 110
5.6 UWB antennas used in the studied scenarios. Large antenna, for the on-body location, and miniaturised antenna, for the in-body location. 111
5.7 Experimental measurement setup particularised for the in-body to on-body scenario. 112
5.8 Path loss as a function of the distance between the antenna centres in different layout scenarios. 113
5.9 Correlation coefficients at a z distance from the plane $z = 0$ in the experimental in-body to on-body scenario. 113
5.10 Endoscope from different perspectives and the probe that is inserted into the available cavity. 115
5.11 Relative permittivity of the healthy and malignant colon tissues according to Fornes-Leal *et al.* and that of their suggested phantoms. 116
5.12 Antenna designed for microwave imaging in the breast region. . 117
5.13 Representation of the setup for the penetration measuring system. 118
5.14 Scattering parameters of the transmitting and receiving antennas on fat phantom, when the transmitting one is placed 2 cm away from the surface of the container and the receiving one changes its distance from the same surface in reverse. 119
5.15 Scattering parameters of the transmitting and receiving antennas on muscle phantom, when the transmitting one is placed 2 cm away from the surface of the container and the receiving one changes its distance from the same surface in reverse. . . . 120

A.1 Dielectric properties of the muscle tissue and its dispersion regions, according to Gabriel. 130

List of Tables

1.1 Wideband phantoms of different body tissues reported for the UWB band. 15

2.1 Physical cross-linking methods. 26
2.2 Chemical cross-linking methods. 27

4.1 Phantoms made of aqueous solutions of sucrose and salt for the 2.4 GHz ISM band compared to tissues values from Gabriel. . . 74
4.2 Phantoms made of acetonitrile mixtures for the 2.4 GHz ISM band compared to tissues values from Gabriel. 75
4.3 Phantoms composition along with their corresponding RMSE values for real and imaginary part, compared with the reference values from Gabriel's report. 85
4.4 Composition of the synthetic gel phantoms along with their corresponding RMSE values for real and imaginary part, compared with the reference values from Gabriel. 94
4.5 RMSE values of the deviation of the values achieved by the different equations of the mixing rules from the real measured values. 101
4.6 RMSE values of the deviation produced with the Cole-Cole experimental models. 102

5.1 Phantom composition to fit the values of the healthy and malignant colon according to Fornes-Leal *et al.* 115

6.1 Comparison between the accuracy of some of the phantoms obtained in this thesis and those previously presented in the literature. 126

Chapter 1

Introduction

1.1 The Human Body in the Propagation Medium

Most of the modern telecommunication systems are based on wireless transmission due to its ease of adaptation to any environment as well as elimination of cables. This medium is usually the air, where the electromagnetic waves travel in a similar way to vacuum. The range of these waves depends on the path loss they suffer through the medium, which are very low in the air. However, there are always obstacles in the path on a real scenario, like buildings, mountains, trees, water or people. Changes of medium cause refraction, diffraction, reflection and absorption, different mechanisms that increase the losses of the signal, usually measured in decibels (dB). Thus, one needs to take into account the scenario in which the devices are going to work in and then design the antennas accordingly. There are models for specific scenarios that consider an average of buildings or different elements in order to estimate the required distribution of access points, distances or transmitting power. These models are obtained from the statistical results in field trials, where the losses are measured for different distances and conformations. Urban environments are characterised pretty well, since most signals travel in this area. Nevertheless, performing field trials is not always possible due to physical or legal limitations, or even because they involve a lot of time. It is also possible to estimate theoretically the propagation of signals in a particular region by solving the Maxwell's equations with the materials and layers involved, each one with its specific resistance to the passage of the signal. Results are not equally realistic, though.

Frequency is the key parameter for propagation issues because it determines how the waves interact with the matter of the surroundings and, therefore, the losses they suffer. In general, the higher the frequency, the higher the losses. Nowadays, the bands used in telecommunications are moving towards higher frequencies with the purpose of increasing the channel capacity. This fact leads to the increase of base stations, which will be closer to users. In addition to that, the Internet of Things brings an avalanche of connected devices, many of them in the vicinity of the body, i.e., the Wireless Personal Area Network (WPAN). All these factors have repercussions on the human influence over the telecommunications systems, so that body must be considered in the current propagation models. WPANs are the most critical case, because the body influences not only the losses, but also the radiation pattern and matching of the antennas. There is also the concern about the health effect of this nearby radiation. Communication devices must meet a number of requirements such as the maximum transmitting power or the Specific Absorption Rate (SAR) regulations.

Wireless Body Area Networks

A particular case of the WPANs are the Wireless Body Area Networks (WBANs), which are thought to transmit directly over the human body by using sensors or nodes that can be implanted, swallowed or on the skin, e.g., wearables. Certainly, WBANs are mostly used for medical purposes such as vital signs monitoring or endoscope imaging, even though there is a user niche for sports performance analysis. Normally, the information collected by a sensor that is placed in the body is transmitted to an external device and processed there. There are basically three positions for the nodes:

- In-Body. Sensor is placed inside the body.
- On-Body. Sensor is placed on the surface of the body.
- Off-Body. Sensor is placed away but near of the body.

These locations can be combined to create different scenarios, depending on the application. A typical in-body to on-body transmission case is an endoscopic capsule that records images from the intestinal tract and sends them to an external belt. It is not still common but the wireless pacemakers will clearly be a reality in the coming years. There are currently devices that send information through the human body, but their performance is far away from other communication systems that work in the air. These type of devices prioritize the low energy consumption due to the difficulty of changing the batteries, specially in the implanted sensors. Besides, regulations force these devices to

use really low powers because of the possible health effects. These two facts, coupled with the poor efficiency of the signal propagation, lead to insufficient data rates for modern applications. The scenario where the data rate is most important is probably the video transmission from the gastrointestinal capsules (Fig. 1.1).

(a) Endoscopic capsule

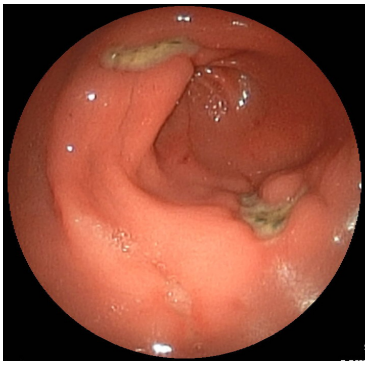

(b) Images from the gastrointestinal tract

Figure 1.1: Endoscopic capsule for recording the gastrointestinal tract. (a) Image by TMKO, licensed under CC BY 3.0.

Resolution and video quality are directly proportional to the bandwidth, and this is a vital aspect that should be improved in WBANs. Researchers try to improve this by looking for new bands of the spectrum that have better performance in the field of body communications. These communications normally take place at low frequencies due to the lower propagation losses, but the need of increasing the bandwidth is leading researchers to explore alternatives at higher frequencies.

Transmission Frequency Bands

The propagation medium for the waves depends on the configuration of the aforementioned nodes, i.e., the transmitting scenario. In the case that an implanted sensor sends a signal to another implanted sensor, waves travel exclusively through the body tissues. When, on the other hand, signal is sent outside the body, its path includes the free space. Apart from the inherent losses of the medium, which change depending on the material or tissue, there is the effect of the change of medium (Fig. 1.2). When a wave changes of medium, there is a part of the signal that is reflected to the original medium and a part that is transmitted into the new one.

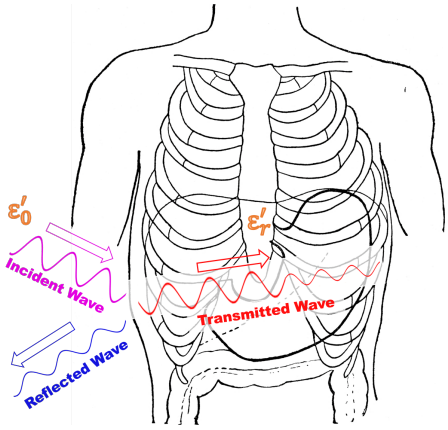

Figure 1.2: Reflected and transmitted signal when changing propagation medium.

The property of the matter that defines how an electromagnetic wave passes through a medium is the permittivity (ε). It determines the speed, wavelength and amplitude of the transmitted signal. The free space owns the lowest permittivity, $\varepsilon_0 = \frac{1}{36\pi} \times 10^{-9} F/m = 8.854 \times 10^{-12} F/m$, which means that this is the most suitable one for propagation in terms of resistance. Any other medium will have a higher permittivity and therefore will attenuate the signal more than the air itself.

Regarding the WBANs, tissues are part of the medium, and their composition makes them materials of high permittivity (see Appendix A). The medium is far from the usual for communications, so the propagation models are totally different in this case. The losses in this medium are much higher, that is why commercial solutions make use of low frequencies, where the penetration is high. The frequency bands that can be used in WBANs are defined in the standard IEEE 802.15.6-2012-Part 15.6. These include the Medical Implant Communication Service (MICS) bands, around 400 MHz, the Industrial, Scientific and Medical (ISM) bands, around 900 MHz and 2.4 GHz, and Ultrawideband (UWB), from 3.1 to 10.6 GHz. From those bands, the MICS one is chosen for intracorporal communications, but its bandwidth is not enough for the aforementioned requirements. The ISM bands have been suggested to solve this lack of bandwidth, but they own another drawback, which is their widespread use in all types of applications, including Bluetooth and WiFi networks. Sharing the spectrum with such a congested band could lead to interferences or inefficiency of the connections. UWB is a suggested band for WBANs, but only outside the body. It uses bandwidths from at least

500 MHz up to several gigahertz, which allows high data rates, miniaturisation capabilities and low consumptions. Some researchers are studying to use UWB for intracorporal communications as well, to solve the previous problems, but since interactions of the waves with the body are crucial, it must be further analysed.

WBANs are the most affected ones by the presence of the human body, but these are not the only ones. Tissues can reflect the signal when they are present in the conventional propagation medium, depending on the frequency of transmission. The higher the frequencies, the greater the propagation losses and the body influence on the signal. The upcoming 5G mobile technology is moving towards the use of frequencies above 24 GHz, which are higher than what is currently used in mobile networks. Precisely, the 5G radio access technology, known as New Radio, has been divided into two frequency ranges, the low and high [1]. The frequency range 2 includes the following bands: 26.5-29.5 GHz, 24.25-27.5 GHz, 37-40 GHz and 27.5-28.35 GHz. As stated before, these frequencies have a worse propagation, so it becomes necessary to place more base stations, which are closer to the users. The high frequency, together with the proximity of access points, make it indispensable to study the influence of the human body on the radiocommunications links.

Human Body Phantoms

This interaction with the human body is studied from different perspectives. From the one hand, the health concern, by means of the SAR, to ensure that the absorbed power is not harmful for the tissues. On the other hand, the devices performance, in order to ensure a suitable communication link and minimise the energy consumption. In any case, the actual human body cannot be used for testing because of ethical reasons. The choices that designers and manufacturers must do are between these ones:

- *In vivo* measurements on animals.
- Computer simulations.
- Artificial human phantoms.

Each methodology has its advantages and disadvantages, but all of them can be combined. For instance, the *in vivo* measurements are the most realistic environment (Fig. 1.3a). These are normally carried out in pigs, due to its the similarity with the human tissues. However, there are ethical reasons and the cost (in time and money) of the experiments is really high. They require specialised personal and a lot of legal permissions for using a surgery room. Furthermore, the real scenario of a WBAN can be simulated, either by

computer software or by experimental phantoms. The computer simulations involve commercial software in which one can create a virtual model (Fig. 1.3b) with the dielectric characteristics of the tissues that take part in the devices communication. The drawbacks of this method are the high cost of the licenses that must be renewed each year, the long times that take the computer to calculate the required equations, and the need of costly computer systems able to carry out these simulations. Finally, the artificial phantoms are models made of materials that own the dielectric properties of the body tissues (Fig. 1.3c). Their advantages are the approximation to a real scenario, cost-effective solution and quickness of the tests. Nevertheless, reproducing a tissue is not always a trivial task, so the number of available phantoms is limited to a few ones. Besides, phantoms are designed for a particular frequency band, not for the full spectrum, since this is not possible. Hence, researchers have to settle for the reported phantoms or try to create a particularised one.

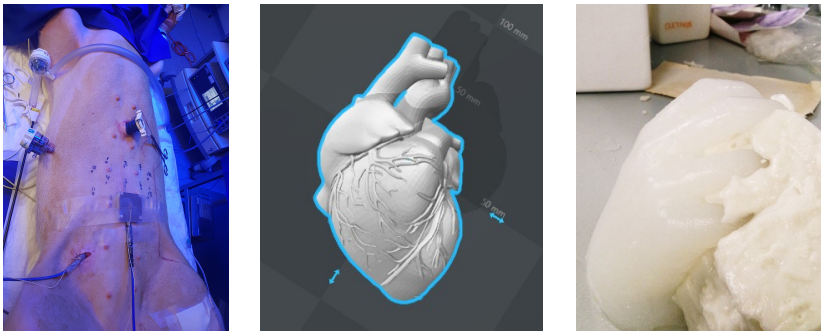

(a) (b) (c)

Figure 1.3: Simulation environments. (a) *In vivo* experiment with a pig subject (b) Virtual heart phantom (c) Artificial hand phantom.

The latter are the most reproduced experiments when it is possible. They are the easiest and cheapest way to perform experimental, instead of theoretical analyses, and are within the reach of nearly anyone. In addition to that, they are the only chance for certification issues. In fact, literature works usually prefer to show results of antennas working in a single tissue phantom, rather than in a heterogeneous complex modelled virtual chest. Current research on the topic is focused on the development of wideband phantoms that are able to cover as many frequencies as possible. This would allow the test of several different technologies at the same time and future bands which make use of wider bandwidths, e.g., UWB. Here, the trend of the dielectric properties of the tissues gains more importance than the values themselves. The number

of tissues is also a target to increase for getting more complex models like the virtual ones. As mentioned above, the change of medium has a significant effect on the waves (Fig. 1.2), so multilayer phantoms are preferable to the homogeneous ones.

1.2 The Permittivity of the Medium

Permittivity (ε) is the name of the property of a material or medium that defines its interaction with the electric fields. Permeability (μ) is the analogue property for the magnetic fields. Wireless communications are overwhelmingly based on electromagnetic waves, which actually are electric and magnetic fields perpendicular to each other that are propagated through a medium or the free space. These magnitudes are normally given in relative terms, compared to the free space, where $\varepsilon_\mathrm{r} = \frac{\varepsilon}{\varepsilon_0}$ and $\mu_\mathrm{r} = \frac{\mu}{\mu_0}$ are the relative permittivity and permeability. Under conventional conditions, $\mu_\mathrm{r} = 1$, i.e., permeability of most materials and media is the same as in the free space, given that they are not magnetic. Bearing this in mind, permittivity is the property that characterises the scenarios of wireless communications. This relation between the behaviour of the waves in the free space and in a material can be decomposed in two parts, the attenuation of the magnitude and its phase difference. Accordingly, the relative permittivity is a complex magnitude that can be separated in two parts, $\varepsilon_\mathrm{r} = \varepsilon'_\mathrm{r} - j\varepsilon''_\mathrm{r}$. The real part, ε'_r, is called dielectric constant, and it is related with the amount of energy that the material is able to storage. The second part, ε''_r, is called loss factor, and it is related with the phase deviation and other losses. This part is often expressed in absolute terms, by means of the dielectric conductivity, $\sigma(S/m) = \omega \cdot \varepsilon''_\mathrm{r} = 2\pi \cdot f \cdot \varepsilon_0 \cdot \varepsilon''_\mathrm{r}$. Relation between both parts of the relative permittivity is given by the loss tangent, $\tan\delta = \frac{\varepsilon''_\mathrm{r}}{\varepsilon'_\mathrm{r}}$. These parameters are totally defined by different mechanisms that take place in the matter.

1.2.1 Polarisation Mechanisms

When an electrical wave travels through a medium, it causes a polarisation of its charges. Then, there is a part of the energy that is absorbed and another part that is reflected or transmitted. Polarisation is the movement of the charges trying to follow the external electric field (Fig. 1.4). This rearrangement of the charges generates an opposite electric field that counteracts the external one, reducing its intensity.

Polarisation is not homogeneous for all kinds of charges. It consists in the movement of the medium charges to follow the applied electrical field,

whose changes depend on its frequency. Some charges take more time than others to follow the external field, usually the greatest ones. For instance, electrons are faster than atoms to move due to its smallest mass. Because of this, when the frequency is too high, the greatest charges are not able to reach the movements of the field. When this happens, a polarisation mechanism disappears, remaining the other ones.

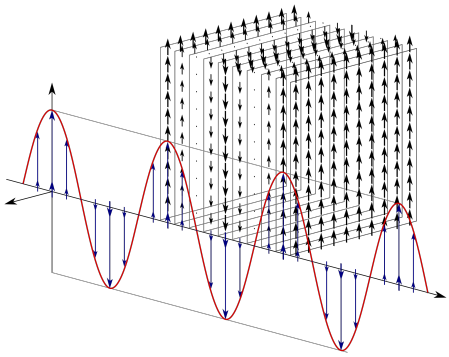

Figure 1.4: Movement of the electrical charges of a medium when applying an external field.

There are basically four polarisation mechanisms:

- Electronic distortion. One of the three types of particle that make up the atoms, the electrons, are relatively more free to move. The electron cloud is in the most external part of the atom, in the so-called orbitals, in which the negative charge is gathered. In the nucleus there are the positive charges, the protons, and the neutral particles, neutrons, so the overall charge is positive. When an external electric field is applied, the nucleus tends to move towards the negative part of the field and the electron cloud to the positive one (Fig. 1.5).

- Ionic or atomic distortion. Molecules are formed from atoms, which are bonded by electron sharing. Depending on how electronegative are the atoms that share the electrons, they have a greater or lesser tendency to attract the electron cloud to themselves. This fact causes a different distribution of charges over the molecule, creating areas with more negative or positive density. When applying an external field, bonds of the atoms are stretched out, since the regions or atoms with more negative charge move towards the positive part of the field and vice versa.

- Orientation. The aforementioned distribution of charges creates what are known as dipole moments inside the molecules. These moments have

magnitude and direction, which can be nullified between them if they are opposite and equal or they can form a polar molecule. Then, the geometry of the molecule is crucial for determining if a molecule is polar or not. This is mostly related with the bonding angles (see Fig. 1.6), according to the valence shell electron pair repulsion theory.

Within a material, polar molecules are randomly oriented in a way that the charges cancel each other out. Once an external electrical field is applied to the medium, a torque force whose effect is to spin the polar molecules appears. Then, the dipoles remain aligned to the field and the charges are no longer cancelled. In this way is how an internal electrical field is created in the material, which affects the external one.

- Interfacial polarisation. Media or materials can hold free charges like ions that are free to move in a certain way. The presence of an external electric field causes the charges to concentrate in the surfaces of the material. This accumulation of charges in some regions, opposite to the external ones, works against the applied field.

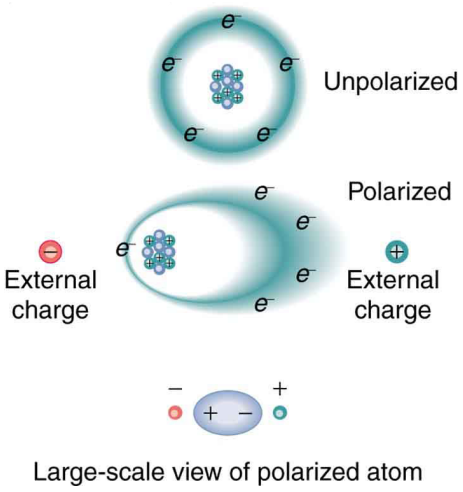

Figure 1.5: Diagram of the polarisation by electronic distortion. Reprinted from [2], licensed under CC BY 4.0.

The kind of mechanism that will dominate the polarisation on a material will depend on its charge distribution. Orientation takes place just in polar molecules, ionic distortion in molecules with ionic bonds (electronegatively different atoms), and interfacial polarisation only in materials with free charges.

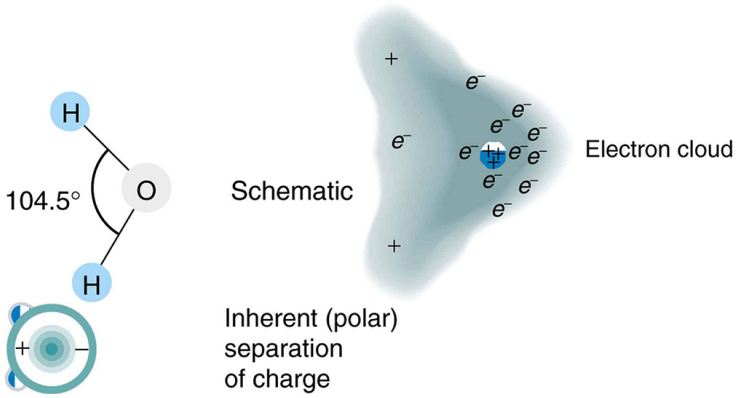

Figure 1.6: Diagram of the distribution of charges in a polar molecule. Reprinted from [2], licensed under CC BY 4.0.

Electronic distortion occurs in every material when an external field is present. The permittivity of the material is the sum of the four polarisation mechanisms. As mentioned before, not all mechanisms are equally fast, but they have a response time. The higher the involved mass is, the longer the mechanism. The particularity here lies in the fact that when the frequency is too high, certain mechanisms are not able to follow the changes of the field and those polarisations disappear. This relationship between these mechanisms and the frequency can be observed in Fig. 1.7.

In the figure, one can see different behaviours of the permittivity with the frequency. There are basically two ways in the mechanism disappearance: relaxation, in which the contribution of the mechanism falls gradually from a relaxation frequency. This is what happens with the orientation for the dielectric constant (red line), and the ionic polarisation for the loss factor (blue line); the other way to disappear for a mechanism is the resonance, where the influence of the mechanism is very small for most of the spectrum except for a resonance frequency, when there is a maximum in its influence. This effect can be appreciated in the dielectric constant (red line) for the atomic and electronic distortions. From this point, the mechanism disappears and the dielectric constant is no more influenced by its effect.

Both parts of the relative permittivity are not independent, they are related by the polarisation mechanisms. One can see in Fig. 1.7 that the relaxation and resonance of the dielectric constant (red line) have an effect on the loss factor (blue line). Every time a polarisation mechanism disappears, there is a rise in the loss factor, which is translated to thermal losses due to the resistance

of the medium to the dipole movement. The other main contribution to the loss factor are the free charges by means of ionic conductivity, but only up to a few gigahertz as can be seen in the same figure. In view of the above, the frequency will absolutely determine which mechanism is key in the permittivity of the medium. As mentioned in 1.1, the bands currently used in wireless communications are within the radiofrequency and microwave bands, which fall around the orientation relaxation. This means that this will be the crucial polarisation mechanism to take into account for most of the communication bands.

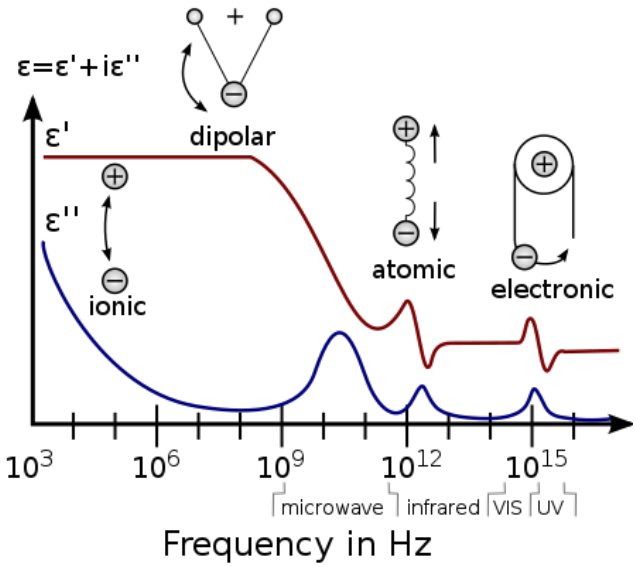

Figure 1.7: Relationship between polarisation mechanisms and frequency. Image by Prof. Kenneth A. Mauritz, with permitted use.

1.2.2 Nature of Dielectric Materials

The mechanisms explained above are related with dielectrics, which are materials capable of storing energy from the electromagnetic waves by means of polarisation. The permittivity depends on the quantity of polarised particles per unit volume. Then, the density of the material determines, in some way, its dielectric properties. Considering this, one can deduce that the physical phase of matter is key. Solids and liquids usually have higher dielectric properties than gases due to their higher density, since gases own few molecules

to polarise. Bigger molecules also have a poor level of compaction, so these normally have low permittivities. This is the case with polymers, which are formed by very long chains of atoms that have difficulty moving around. Ease of movement is another factor to consider in dielectric materials. In general, molecules of solids have more difficult to move than those of liquids. Orientation mechanism is the most affected by this restriction, precisely the most important one within the bands of interest in wireless communications. For those reasons, polymers are good electrical isolators in general.

Temperature is also a factor that defines the permittivity of a material. It is related to the kinetic energy of the molecules so, in a way, with their movement. The dipoles of the molecules are always in movement, even if they are aligned to a static field they are vibrating within a few margins. When temperature rises, this vibration becomes stronger, and alignment is not so clear and perfect. This worse alignment produces a reduction in the permittivity of the material. On the other side, in materials that are near the fusion point, an increase of the temperature produces precisely the contrary effect. In a solid, the crystal structure can move just in some directions, and molecules need a potential energy to change their direction. Temperature helps to reduce this required energy so that the energy provided by the external field is enough to polarise the molecules.

In the case of the body tissues, most of these are like semisolid materials with a large amount of water, especially the soft ones. Water owns a large polarisation ability in the microwave region, which means that tissues typically have high values of the relative permittivity. Tissues are complex structures with a multitude of constituents that change from one subject to another depending on parameters such as gender, age, etc. (see Appendix A). Additionally, different persons will have different tissue distribution or thickness, so there is a margin of heterogeneity in the dielectric properties. Researchers measure many samples from different specimens in order to average the data. The most referenced work in this aspect is that of Gabriel [3], which in addition to providing new measurements, makes an extensive compilation of what was previously published in the literature.

1.3 Objectives and Scope

The **main objective** of this dissertation is developing materials that own the dielectric properties of the main human body tissues. For that purpose, a thorough study of chemicals needs to be carried out in order to find out which ones are suitable to achieve those properties. Results will be compared with the highly referenced Gabriel's database [3]. This involves the characterisation of

the materials, which will be performed by means of a Vector Network Analyser (VNA) and a open-ended coaxial probe.

There are many recipes in the literature for preparing phantoms, which have been obtained from studying the influence of different additives over the relative permittivity. Most of these only cover a single frequency or small bands, since their dielectric properties change faster than those of the tissues. Then, it becomes necessary to find out other compounds that keep that stability with frequency in the values of permittivity. The candidates would be suitable within a wide frequency bandwidth, including the main WBAN bands. The phantom formulation has to take into account the final application in which it will be used, mainly its physical condition, i.e., solid, semisolid or liquid. References provide recipes for preparing phantoms in a single state, without being able to adapt it to another one. For instance, solids normally imitate tissues with low water content, regardless of the required application. One of the challenges of this thesis is the achievement of phantoms that imitate all kinds of tissues in different formats. Thus, the hydrogels will be studied with the aim of embedding liquids and therefore get a semisolid material. Regarding the solid phantoms, 3D printing arises as the best alternative to consider, since they could take the shape of the tissues while hosting the liquids inside. This solution can be positive to get solid phantoms with the dielectric properties of soft tissues. Print templates may be obtained from Magnetic Resonance Imaging (MRI) images. Before that, a suitable printing polymer must be chosen, which can be in constant contact with the phantom. A study of degradation for the most widespread printable polymers is desirable to ensure a long durability of these models. Considering all of the above, the main goals to be attached in this thesis can be summarised as follows:

- Study of the chemicals that have the required electromagnetic properties for using them in liquid mixtures that imitate different human tissues. This includes analysing the influence of these compounds when they are combined in order to predict the final properties for imitating the target tissues.

- Synthesising cross-linked polymers that are able to absorb the developed liquids and so form semisolid gels with the electromagnetic properties of the human tissues.

- Evaluate the electromagnetic response of the synthesised models by means of a VNA with the open-ended coaxial method. Choose those compounds with the greatest interest and review the level of approximation to the target tissues.

- Assess the chemical-physical interaction between the phantoms and the main 3D printing materials with the aim of selecting the most appropriate one.

1.4 State-of-the-Art

In Section 1.1, the need of synthetic environments that emulate the propagation medium in WBANs, i.e., the human body, has been explained. These are created by using materials with the same dielectric properties as those of human tissues called phantoms. They are commonly used in laboratory measurements, trying to imitate a realistic usage case scenario, for many types of studies such as SAR [4], microwave imaging [5], radiation dosimetry [6] or propagation through the human body [7]. The nature of these materials is defined by the handling requirements, either solid [8], semisolid [9] or liquid [10]. For instance, in-body communications are more suitable to be tested with liquids, where the antennas can be freely moved and placed. This nature defines the kind of materials that make up the phantom itself, and then restricts the attainable dielectric properties. Liquid phantoms are normally made by a great composition of water, similarly to soft tissues, so they are good candidates to mimic their high values. In contrast, polymers own low permittivities like bonds or other low water-content tissues. Fig. 1.8 shows a comparison between the high and close values of water and muscle values, and the radically different low values of fat. In general, the pursued properties for phantoms, apart from the permittivity, are the safety, low cost, ease of preparation and durability. Regarding the dielectric properties, there are three possibilities for obtaining the target values of the body tissues to imitate:

- Literature data. This is the most widespread choice for authors. There are values of real measurements for a lot of tissues in several bands that are reported in works. The most cited one is the Gabriel's reference [3], whose data have been parametrised and published online for ease of reference [11]. It contains a database of 55 tissues within a bandwidth from 10 Hz up to 100 GHz.

- Own measurements. Some authors perform their own measurements for the tissue of interest according to their requirements [12]. The advantage here lies in the use of the same measurement methodology for tissue and phantom, so that the error and uncertainty is maintained.

- Theoretical approach. There are mathematical models to estimate the relative permittivity of the tissues or any other material, taking into

account their constituents as a function of their shape, size and orientation [13].

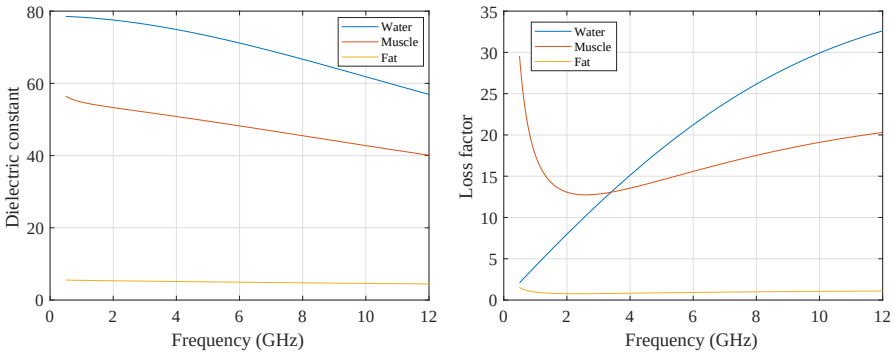

(a) Dielectric constant

(b) Loss factor

Figure 1.8: Relative permittivity of water compared to muscle and fat [3].

The phantoms of the literature are given for a concrete frequency band, along with the methodology to prepare them. Concerning the scope of this thesis, there are several reported phantoms that include the WBAN bands within the frequencies they imitate (see Section 1.1). For instance, in [14], the muscle phantom is given for some ISM and MICS bands, just in narrow band. The current trials are focused on modelling as much bandwidth as possible [9, 12, 15], but this is challenging. As mentioned above, the most promising band for wide bandwidth transmission in WBANs is UWB. Table 1.1 includes the phantoms found in literature that imitate tissues within the UWB band.

Table 1.1: Wideband phantoms of different body tissues reported for the UWB band.

Tissue phantom with accuracy (Real part/Imaginary part)	**Freq. (GHz)**	**T[1]**	**Components**	**Ref.**
Muscle (5.61/7.06) (accuracy in RMSE[2])	3.1-10.6	L	Water, sucrose	[10]
Breast (normal, three types, 0.5-6 GHz: [1.59, 1.90, 0.54]/[0.45, 0.83, 0.14]; 6-12 GHz: [0.53, 3.79, 0.31]/[1.12, 1.60, 0.16]); (malignant, 0.5-6 GHz: 0.99/0.11; 6-12 GHz: 1.39/0.65) (accuracy in RMSE)	0.5-12	L	Water, TX-100	[16]

Continued on next page

Table 1.1 – *Continued from previous page*

Tissue phantom with accuracy (Real part/Imaginary part)	**Freq. (GHz)**	**T[1]**	**Components**	**Ref.**
Breast (fat, malignant tissue, skin) (not imitating the actual values of the tissues but their contrast)	1-11	L	Water, oil, diacetin, FR4 glass epoxy printed circuit board	[17]
Infiltrated fat, non-infiltrated fat, muscle, wet skin, dry skin (accuracy not provided)	0.5-20	SS	Water, gelatin, oil, formaldehyde, surfactant, n-propanol, p-toluic acid	[18]
Two-thirds muscle (accuracy not provided)	2-10	SS	Water, agar, polyethylene powder, sodium chloride, TX-151, dehydroacetic acid (sodium salt)	[19]
Breast (fat, 9%; gland, 14%; tumour, 9%) (accuracy in deviation for real part)	3.1-10.6	SS	Water, gelatin, oil, propylene glycol, surfactant, formaldehyde, agar, p-toluic acid, 1-propanol, alizarin	[15]
Breast (low density, two types, [1.22, 2.59]/[2.39, 3.19]); (high density 2.89/2.17) (accuracy in RMSE at 7.5 GHz)	3-11	SS	Water, propylene glycol, gelatin, oil, surfactant, glyoxal, glutaraldehyde, agar, corn flour	[20]
Wet skin (6.87/5.97 S^2/m^2), fat (0.21/0.29 S^2/m^2), blood (25.38/1.12 S^2/m^2), muscle (21.14/6.21 S^2/m^2) (accuracy in MSE)	0.3-20	SS	Water, oil, gelatin, sodium chloride, detergent	[21]
Breast (muscle, fibrograndular tissue, skin, transitional tissue, fat, malignant tissue) (accuracy not provided)	3-10	SS	Water, glycerin, polyethylene powder, agar	[22]
Breast (fat, tumour, skin) (not imitating the actual values of the tissues but their contrast)	2-12	SS	Water, wheat flour, petroleum jelly (vaseline), oil, glass	[23]

Continued on next page

Table 1.1 – *Continued from previous page*

Tissue phantom with accuracy (Real part/Imaginary part)	Freq. (GHz)	T[1]	Components	Ref.
Fat, muscle, grey matter (first-order match)	0.001-10	S	Carbon black powder, polytetrafluoroethylene powder	[24]
Breast (normal, tumour) (accuracy not provided)	2-10	S	Polycarbonate, oil, epoxy	[25]
Skin (two types, [28, 10]/[21, 31]), bone (7/47), fat (2.46/0.15 S/m) (accuracy in relative error in 2-10 GHz, except absolute error for fat)	1-10	S	Carbon black powder, graphite powder, silicone rubber, urethane rubber	[26]
Liver (three models, [8.58, 8.55, 7.77]/[5.49, 5.77, 6.47]) (accuracy in RMSE[3])	0.7-20	S	Water, sucrose, sodium chloride, HEC 4400, Dowicil 75	[27]
Breast (muscle, fat, dry and wet skin, malignant tissue) (accuracy not provided)	2-15	V	Water, slime, egg white, egg yolk, butter, glycerol, moisturising lotion, corn starch	[28]

[1]Type. L: liquid, SS: semisolid, S: solid, V: various

[2]Own measurements after preparing and measuring the phantom within 3.1-10.6 GHz

[3]Calculation using the parametric models provided in the study within 3.1-10.6 GHz

The table includes the compounds that have been used in each work for mimicking the tissues. There is everything, from daily compounds [10, 28] to laboratory chemicals [15, 18]. The most recurrent ingredients are water, sodium chloride and oil. These have been proven to be suitable to define the dielectric properties of the phantoms. Water has a high dielectric constant whereas oil is just the opposite, with values more similar to those of the fat (see Fig. 1.8). Then, they are combined in different proportions by means of making an emulsion to fit the target tissue properties. This method has the disadvantage that droplets settle with time due to the lack of miscibility between oil and water. Sodium chloride, as an electrolyte, provides the mixture with ions, i.e., conductivity, which is related to the loss factor. Thus, adding this salt is the usual way to increase this value, but only up to several gigahertz (see ionic polarisation, Fig. 1.7). Other widely used substances are the polymer powder and different polar liquids. The first one has a similar effect to that of oil, i.e., decreasing the dielectric constant, and the polar liquids increase it, due to the orientation polarisation. Some additives are also often inserted into the

mixture, like gelatin or agar for obtaining a semisolid phantom, surfactants to allow mixtures with insoluble compounds, and alizarin as dye. These hardly affect the permittivity but contribute to achieve particular physical properties.

Authors typically show the dielectric properties of their proposed phantoms in a graph, comparing the values with those of the tissue reference. Fig. 1.9 shows and example of this kind of comparison, in which the order of magnitude is similar between phantom and tissue values, but not their trend. The visual comparison can be a suitable method to check the validity of phantoms, but sometimes this can be supplemented with numerical data. The most common parameters used by authors in this sense are the Root Mean Square Error (RMSE) (or Mean Square Error (MSE)) and the relative error. Table 1.1 includes this information when it is provided in the reference. One can notice the value disparity in terms of accuracy. Whereas the deviation of many phantoms is significant [10, 15, 21, 24, 26, 27], others do not even imitate the values of the tissue itself, but they recreate the values gap between different tissues [17, 23].

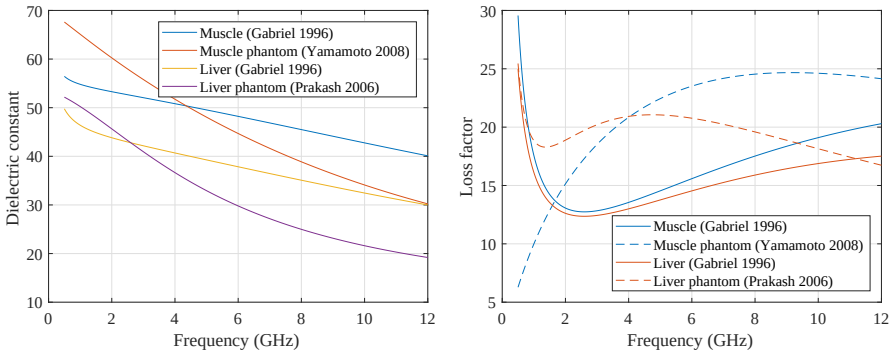

(a) Dielectric constant

(b) Loss factor

Figure 1.9: Relative permittivity of the phantoms for the muscle [10] and liver [27] included in Table 1.1, compared to their corresponding reference values according to Gabriel [3].

Target tissues are chosen depending on the application to test. One of the most pursued ones are the breasts for cancer detection issues, and they certainly achieve good results in some works [16, 20]. Muscle is another of the most sought-after tissues. It appears several times in Table 1.1, always with a remarkable deviation [10, 21] or even with just a first-order match [24]. Regarding the skin phantom, the works that report their accuracy give a 21% of deviation in [26], and a 6.87 MSE in [21], both in the dielectric constant, which are quite large deviations.

Replicating the values of the tissues in such wide bandwidths is challenging, particularly those with a high water content, since these normally change more with frequency. This can be seen in Fig. 1.8, where the slope of the fat in the dielectric constant is practically negligible, but not that of the muscle. This happens because of the relaxation frequency of the orientation polarisation (see Fig. 1.7), which makes this mechanism disappear, so that the values fall. Because of that, tissues with low content of water are usually obtained with more accuracy, e.g., the case of fat [18, 21, 26]. The desirable target is the possibility to assemble a heterogeneous model made up of several layers, representing the different body tissues. For that reason, the list of available phantoms needs to be enlarged. Some usage cases are more developed, like the breast cancer detection through microwave imaging, with phantoms of several layers [15–17, 20, 22, 23, 25, 28]. On the other side, parts like the gastrointestinal region are not so complete [10, 18, 27], which is key for the usage case of the capsule endoscopy. It is precisely in this scenario where devices could make use of the UWB benefits to improve the data transmission performance. Researchers usually simplify the region by using a single muscle phantom made of sugar [10], which can be easily reproduced and it is cheap. Others suggest a phantom with a relative permittivity of two thirds of the muscle values [19] in order to average the torso equivalent medium. The problem of using homogeneous phantoms is that reflections due to change of medium are not produced. Then, enlarging the number of mimicked tissues of this region is highly recommended. This would lead to the creation of realistic models by means of multilayer phantoms.

1.5 Thesis Outline

This thesis is divided in six chapters and one appendix. Each chapter covers a particular part of the research progress, from the problem definition to the discussion of the results. Chapter 2 describes the synthesis of the materials that have been studied and the methodology followed with the characterisation tests. Chapter 3 explains the effect of different factors over the final results and provides guidelines to adjust the materials to meet the target. Chapter 4 presents the main results of the thesis, which are the tissue-equivalent materials. Chapter 5 shows different use cases of the phantoms and the obtained results for these experiments. Chapter 6 depicts the conclusions of the dissertation and introduce the following steps that may be taken.

Appendix A describes the main features of the dielectric properties of the body tissues, including the polarisation mechanisms and their relationship with the frequency. It also explains the reasons for the variability of measurements

between specimens and the conditions that should be met to be a suitable reference. Moreover, the way in which researchers gather and provide the data is outlined.

The content of each chapter from this thesis is summarised hereinafter:

Chapter 2 introduces the polymeric materials that have been used for preparing the gel phantoms. First, a brief discussion about the most used materials in the literature for semisolid and solid phantoms is given. Then, the candidate materials for the new gel phantoms are described, which are based on hydrogels. These materials have been widely used as biomaterials due to their tailoring synthesis and controlled physical properties. A summary of the most used polymers in biomedical engineering is presented, together with their main advantages. Two polymers are selected because of their high swelling properties, which can be controlled from the synthesis. Thus, this synthesis procedure is detailed, along with the variations that can suffer for the final physical properties. The dielectric properties were analysed by means of the open-ended coaxial method, which is described in this section. The specific methodology for measuring gels is detailed here as well. This thesis also includes the study of the most common 3D printing materials with the aim of choosing the most suitable one to manufacture a container for the liquid phantoms. In this chapter, the degradation analysis and the characterisation tests are explained.

In **Chapter 3**, the selection of the compounds that will be included in the phantoms is carried out. The first step is to verify the usability in terms of frequency bandwidth of the basic compounds that are currently used in the literature. Then, the study is focused on the polar compounds, taking into account that are those with better orientation abilities, the most important one in this frequency range. The measurement of several compositions of both, polar and basic compounds, leads to the obtaining of a mathematical model in order to predict the relative permittivity of a mixture according to its concentration. Finally, the materials for the gel preparation are chosen based on different physical properties, which are also analysed. These semisolid materials are characterised by means of the open-ended coaxial technique, and some inference about the relation between the manufacturing procedure and the final dielectric properties is detailed. Finally, the 3D printing polymers are studied with the aim of choosing the most suitable one for manufacturing the solid models of tissues.

Chapter 4 is the main body of the results from this thesis. The mathematical models and the guidelines acquired in the previous chapter are used here to produce tissue-equivalent phantoms. The liquid models have been divided in three frequency bands. From the side of the narrowband models, there is the 2.4 GHz ISM band, which is covered by two kinds of phantom, those made

with basic compounds and those with the polar molecules. Regarding the wideband phantoms, these are first presented for UWB, reaching a considerable number of mimicked tissues in a large bandwidth. The accuracy achieved here is compared to phantoms previously reported in the literature within the same frequency band. Afterwards, the mixtures have been combined with the synthetic gels examined in the previous chapter in order to obtain semisolid models. The other wideband phantoms are those suggested for the millimetre waves, which are being considered for new communications. In this case, the target is just the skin tissue due to the low penetration rate at frequencies. Results have been adjusted to a theoretical and an experimental model to validate which fits best. Moreover, these latter have been gelled with a natural polymer without altering their dielectric properties.

In **Chapter 5**, several biomedical applications are put to the test through the use of the phantoms obtained here. The tests include both the study of the effect of the body tissues over the transmission of microwave signals, and the effect of those electromagnetic waves over the tissues by means of the SAR. Besides, two different tumour diagnosis methods have been tested thanks to the reproduction of malignant tissue.

This thesis concludes with **Chapter 6**, where the general conclusions are summarised and outlines the next steps that should be followed.

Chapter 2

Materials & Methods

A brief summary of the most used materials for preparing phantoms of different body parts and formats has already been discussed in Section 1.4, specially in Table 1.1. In a nutshell, there are many contributions in the literature that suggest phantom recipes for creating phantoms. Regarding the liquid format, sucrose is the most widespread ingredient for its easy, availability and quickness of preparation. Other works also suggest to add different compounds like vegetable oil and flour [29], polyethylene powder [30], or diethylene glycol monobutyl ether [31] to tune the phantoms. Taking into account that phantoms are usually intended to test biomedical applications, these are designed for authorised medical bands, mostly narrow [14]. In one of the frequently cited works [18], oil and water are combined in different ratios to match the dielectric trends of human tissues over a wide frequency range (0.5-20 GHz). Nonetheless, this work is limited to a few tissues with slight options to precise adjustment. Other attempts have been pursued taking the same formulation as reference [21]. This thesis addresses this problem on the basis of polar liquids, which are the key for the polarisation mechanisms in the frequency bands of interest (see Fig. 1.7). All percentages appearing in the thesis are weight by default.

Concerning the gels, these are normally created by adding around a 0.5-5% of a natural polymer [32], such as gelatin, within the liquid mixture, so that gels are mostly water in their composition. However, they have several drawbacks such as a poor durability ant the inability to coagulate the mixtures in the presence of solvents other than water. One of the greatly used materials for creating gels is the agar. Some attempts that include it achieve good approximations in different bands, like in [33], above 50 GHz, [12], within 55-65 GHz, and [34], within 15-40 GHz. Nevertheless, the number of tissues is still short

or focused in some parts of the body like breats [22, 23] or hands [9]. Besides, the accuracy of these phantoms is fairly low [15, 19, 20]. This thesis takes a different approach for making gels, which consists in synthetic polymers that can form three-dimensional structures capable of holding liquids.

2.1 Semisolid Gels

One of the goals of this thesis is the possibility of creating phantoms in different physical forms. This means that the initial liquid phantoms should be compatible with the semisolid or solid states. The suggested solution here for the semisolid materials is the gel formation with cross-linked polymers because of the multiple advantages they present such as high durability and tailoring capabilities. These features have been widely used for creating biomaterials in many different applications, such as regeneration of soft tissues, drug delivery, etc.

2.1.1 Types of Gels

Gels are made by polymer chains that are entangled or cross-linked by physical or chemical interactions, able to hold huge quantities of liquid (normally water), without being dissolved. They are basically liquids, due to the proportion of liquid in the composition, but they behave like a solid or semisolid. This is possible because the polymer chains have hydrophilic side groups (OH, COOH, $CONH_2$, CONH, SO_3H, electrolytes, etc.) that have affinity for water, which do not dissolve them because of the cross-linking. When these polymer networks are dried or without liquid inside their reticles they are called xerogels, and own physical characteristics completely different from those of their swollen state. There are two kinds of cross-linking according to its nature [35]:

- **Physical**: The joints of the polymer chains are made of physical interactions and not chemical covalent bonds. The network is actually composed of entangled chains that have electrostatic associative forces, hydrogen bonds and hydrophobic interactions. This is a weaker and reversible interaction, which depends on physical changes of the environment such as temperature, pH and ionic forces.

- **Chemical**: Polymer chains are cross-linked in a chemical reaction by substitution with a cross-linking agent, which is a molecule that creates a covalent bond (junction point) between two different chains. It is a strong and irreversible union that confers high stability against harsh environments such as high temperatures, acid or basic mixtures, or stress.

This type of hydrogels absorb great amounts of liquid until reaching a swelling point, which depends on the cross-linking degree and the affinity of the polymer to the solvent, which is estimated by the Flory-Huggins parameter (χ) [36].

Gels are also classified as a function of their natural or synthetic nature. In nature there are natural polymers such as proteins, which can form hydrogels, e.g., alginate and agarose [37]. Moreover, there are a great deal of publications that report several cross-linking methods for creating synthetic gels with customised physical properties according to their composition [35]. A general classification of the different gelification mechanisms for gels is depicted in Fig. 2.1.

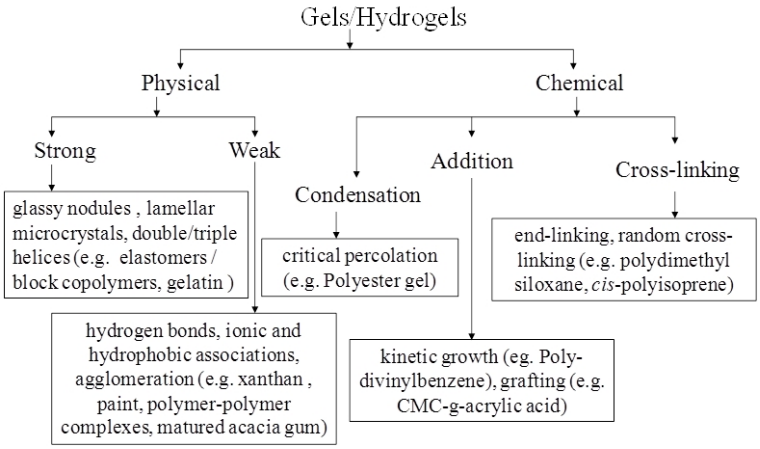

Figure 2.1: Examples of different physical and chemical gelification mechanisms. Reprinted from [35], licensed under CC BY-NC-SA 3.0.

These gelification mechanisms can be achieved by several cross-linking methods, either physical or chemical. The different ways to get cross-linked chains have been summarised in Tables 2.1 and 2.2. An example of a physical cross-linking method by means of heating and cooling a κ-carrageenan solution is shown in Fig. 2.2.

Gels are normally characterised by the swelling index, which represents the mass ratio between the liquid embedded within the gel and the polymer itself, i.e., the three-dimensional structure, when the gel reaches the swelling equilibrium. This relationship is obtained according to Eq. 2.1.

$$\text{Swelling Index } (\%) = \frac{m_{\text{liquid}}}{m_{\text{liquid}} + m_{\text{xerogel}}} \tag{2.1}$$

Table 2.1: Physical cross-linking methods. Adapted from [35], licensed under CC BY-NC-SA 3.0.

Method	Description
Heating/cooling a polymer solution	Some polymers such as gelatin or carrageenan get their chains in a random coil conformation in hot solution. Then, when cooled, they form rigid helixes with joint points between the chains (Fig. 2.2).
Ionic interaction	Ionic polymers can be cross-linked with the addition of counterions, which produce repulsions. The combination between this repulsion and the attraction of multivalent ions with their opposite charge generate chain reticles that are able to hold liquids.
Complex coacervation	An entangled complex is formed when a polycation and polyanion are mixed, which create repulsions between similar chains and attractions in different chains. This complex is soluble depending on the solution pH or insoluble instead.
H-bonding	Some hydrogels can be obtained through lowering the pH of a solution containing the polymer, which promote hydrogen bonding.
Maturation (heat induced aggregation)	Gums usually contain a low percentage of several proteins. Aggregation of proteins occurs by increasing their molecular weight when heat is applied, creating a hydrogel.
Freeze-thawing	This mechanism is based on the formation of microcrystals within the structure due to repeated freeze-thaw cycles.

Swelling index essentially depends on four factors:

1. Cross-linking degree: This parameter is related to the amount of connected nodes between polymer chains. A large amount of nodes and reticles leads to low possibilities of expansion for the network, so the swelling index will decrease.

2. Flory-Huggins parameter (χ): It indicates the affinity of the polymer with the solvent, and depends on the chemical nature of the polymer. The lower the value, the better the interaction of the polymer with the solvent.

3. Temperature: It affects the mobility of the chains as well as the χ parameter. Besides, the glass transition temperature fully determines its physical properties, so it is critical to know if the polymer is below (it behaves as a glass) or above (it behaves as a rubber) this point.

4. Water activity (a_w): This is the relationship between partial vapour pressure of water in a particular medium and that of pure water at the same temperature. The higher the water activity, the more the gel will swell. This parameter usually decreases with the solute concentration.

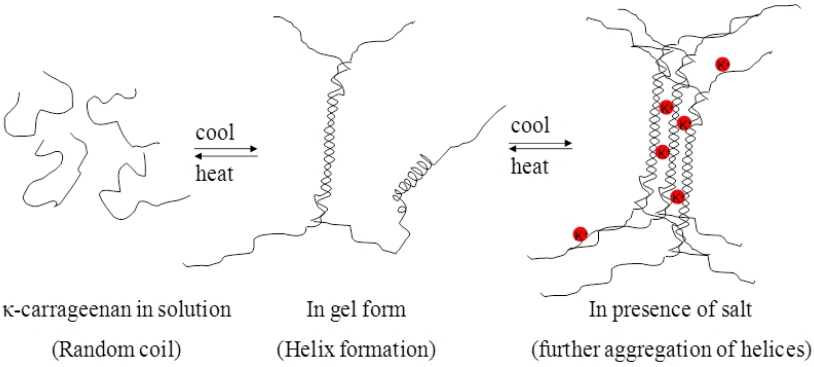

Figure 2.2: Gelification of κ-carrageenan by means of cooling a hot solution in presence of a salt. Reprinted from [35], licensed under CC BY-NC-SA 3.0.

Table 2.2: Chemical cross-linking methods. Adapted from [35], licensed under CC BY-NC-SA 3.0.

Method	**Description**
Copolimerisation of monomer with cross-linking agent	Starting from a monomer, a chain reaction begins due to radiation or by chemical reagents, in presence of a cross-linker. Free radicals react with both monomer and cross-linking molecules, forming long chains of polymers joined at particular points.
Aqueous state radiation	Irradiation of polymer aqueous solutions induces the generation of free radicals in the water molecules, which are the ones that mostly absorb the energy. These radicals react with the polymer and join the chains, creating a network that can absorb water.
Conversion of hydrophobic polymers into hydrophiles and cross-linking	A hydrophobic polymer is dissolved in water by changing the pH o grafting hydrophilic groups in its backbone. Then, it is cross-linked through a chemical reaction with a cross-linking agent.

2.1.2 Hydrogels in Biomedical Applications

Hydrogels are polymeric materials that are able to swell in water and hold a significant fraction of this water within its structure without being dissolved [38]. Because of their physical properties, these resemble human soft tissues more than any other material. The soft and rubbery consistency that these present minimize the irritation to surrounding cells and tissue, that is why these have a great potential to be used as biomaterials. The number of biomedical applications in which these have been used include sutures, vascular grafts, soft tissue substitute or drug delivery systems, among others.

The other important advantage from these materials is their tailoring ability, which allows to control physical parameters such as the pore size and permeation. These features determine the absorption and diffusion of solutes [39], key for tissue engineering. Hydrogels can be used as scaffolds, providing a bulk and mechanical construction where the damaged tissue can regenerate [40]. The structure can include peptides or other biological factors that induce cell adhesion and proliferation. Scaffolds are biodegradable, with a degradation time that can also be tailored according to the application. This is a critical factor, since that time should meet the regeneration and healing process of the tissue. After that, the hydrogel is reabsorbed and replaced by new healthy tissue.

As explained above, the behaviour of gels depend on many external factors, depending on their structure. This structure can be designed or modified to make it sensitive to changes in the medium. Some of the external factors that can affect the behaviour of hydrogels are temperature, pH, glucose concentration, electric signals, light, pressure, and specific ion or protein presence [41]. Hydrogels are designed to be responsive to these stimuli as required. The main application resulting from these possibilities is the drug delivery, which is based on the release of the hydrogel content in the particular region where it is needed. The polymer would increase the pore size when the environment conditions match those of the target, leading to the release of the contained particles.

The most used hydrogels in biomedical engineering are: Poly(2-Hydroxethyl Methacrylate) (PHEMA), which has been widely used for implant materials, mainly cornea [42]; Polyvinyl Alcohol (PVA) is a good replacement for avascular tissues like cartilage because it is stronger than other hydrogels and has a low coefficient of friction [43]; Polyethylene Glycol (PEG) has been one of the most used polymers for scaffolds due to its immunogenicity, antigenicity, protein binding and cell adhesion [44]; Hyaluronic Acid (HA), which has a high viscoelasticity, space filling properties and high biocompatibility, has been used in all kinds of applications [45]; alginate and fibrin [46, 47] have been used

for scaffolds, delivery vehicle for drugs and as model extracellular matrices; and collagen [48], which has been mainly used for drug delivery systems in ophthalmology.

2.2 Gel Synthesis

The synthetic polymers chosen for preparing the gel phantoms were the Poly(2-Hydroxyethyl Acrylate) (PHEA) and the Polyacrilamide (PAM), which were swollen in different aqueous mixtures. These can hold their shape, as a solid, but they can hold large quantities of liquid inside, like most of the tissues of interest. The main reason for choosing synthetic polymers is their high stability in time, in terms of degradation, and their ability to be chemically tailored to adjust the swelling properties. Another advantage is the fact that they can be swollen and dried reversibly with different mixtures. Both polymers are created from their corresponding monomers through a radical polymerisation. These chain reactions do not start spontaneously, but they require an initiator molecule and energy, which are defined further below. The scheme of this reaction is shown in Fig. 2.3. The two aforementioned polymers have a similar polymerisation reaction, but with their particular reagents, which are described below.

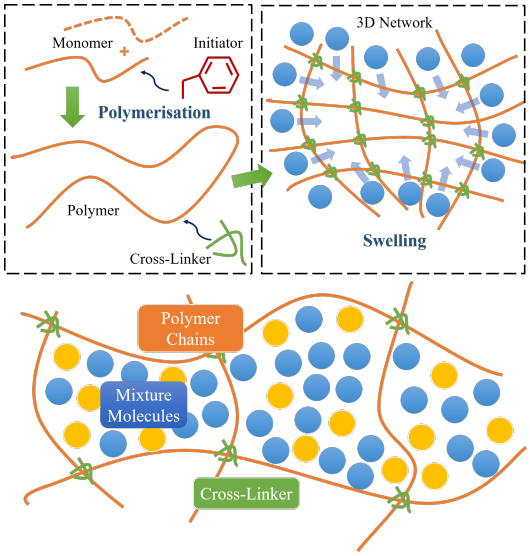

Figure 2.3: Diagram of gel formation, from polymerisation reaction (above) through the swelling of the cross-linked structure to its final state (below).

Poly(2-hydroxyethyl acrylate)

One of the suggested polymers for achieving the semisolid phantoms was the PHEA, which has a high mechanical resistance, great capacity of swelling water and high durability compared to natural polymers. These features allow the chance to carry out many tests with the same samples, taking away the need of preparing new ones. The ideal case is that the polymer absorbs the liquid and the resulting gel owns the same relative permittivity as the liquid. In this way it would be easier to control the dielectric properties to match them with those of the tissues. Then, the ratio between polymer and mixture should be decanted towards the latter, since the effective permittivity is related to the volume percentages (see Section 1.2). The polymer would act as a mere container of the liquid mixture and also provides mechanical resistance.

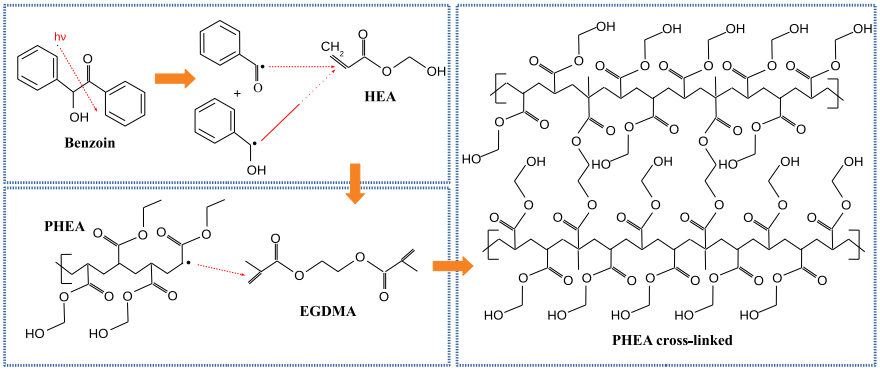

Figure 2.4: Mechanism of initiation and propagation of the polymerisation reaction for the cross-linked PHEA.

As mentioned above, these gels are made by polymerising the monomer in presence of a cross-linking agent, and then they are immersed in the liquid mixture in order to absorb it. The PHEA gels were synthesised from 2-Hydroxyethyl Acrylate (HEA) (Sigma-Aldrich), the monomer, Ethylene Glycol Dimethylacrylate (EGDMA) (Sigma-Aldrich), the cross-linking agent, and benzoin (Scharlab), the reaction initiator. Polymerisation takes place in a mixture with all the compounds present around. Benzoin suffers a homolytic fission with the energy of Ultraviolet (UV) light that generates free radicals, extremely unstable, capable of reacting with the surrounding molecules. These radicals react with the monomer molecules, mainly with the double bonds between carbons, because it leads to the most stable reaction intermediate. After breaking the bonds of the monomer, it also generates free radicals that interact with other HEA, and also EGDMA molecules. Thus, a long chain with hydrophilic side

groups is formed, joined at certain points as shown in Fig. 2.4. This reaction continues until there are no remaining monomer or cross-linker molecules. The more amount of cross-linker there is, the more connection points there will be, and so the reticles will be smaller.

Polyacrilamide

The other polymer considered is the PAM, which can also be cross-linked. It is one of the most superabsorbent hydrogels [49], with a strong stability in a wide range pH ans temperature, transparent and chemically inert. Its glass transition temperature is 165 °C, so it behaves like a glass at room temperature when it is not swollen. In the gel state, the polymer chains gain mobility and the temperature at which it behaves like a glass drops below that of the room. This gel is frequently used in protein eletrophoresis [50–52], which consists in a self-polymerisation of PAM in presence of water, creating a viscous liquid that desnaturalise proteins in a way they are classified by difference in weight, chain length and shape. Other uses include enzyme immobilisation, controlled drug delivery, regeneration of damaged tissues, or as a smart material that changes depending on the medium [53]. These features joint with its biocompatibility and biodegradability are make it a suitable biomaterial.

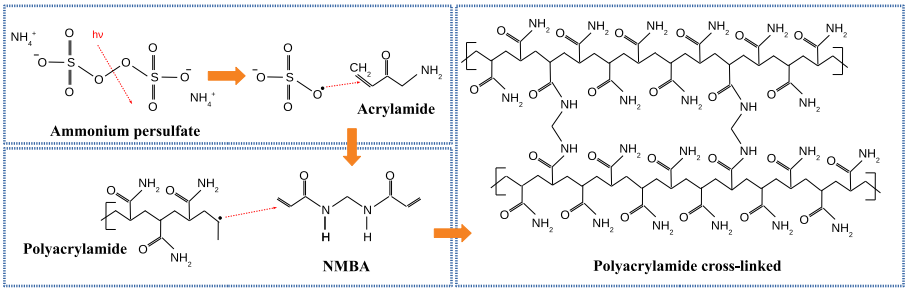

Figure 2.5: Mechanism of initiation and propagation of the polymerisation reaction for the cross-linked PAM.

The chemical compounds that were used here for creating the 3D structure with this polymer were acrylamide (Scharlau), which is the monomer, N,N'-Methylenebis(Acrylamide) (NMBA) (Sigma-Aldrich), as cross-linking agent, and Ammonium Persulfate (APS) (Avocado) as the reaction initiator. APS is broken homolitically in presence of UV light and generates the free radicals that interact with the monomer molecules. These molecules react progressively with all the remaining ones, forming the long main chain of PAM. Simultaneously,

these radicals react with the NMBA molecules, joining the chain at different points. This reaction mechanism is depicted in Fig. 2.5.

Acrylamide is supplied in powder form, so it needs to be dissolved in water to allow the reaction with the other polymerisation compounds. The methodology was the following: in a 20 mL ISO flask, there were introduced 8 grams of acrylamide, 0.1 grams of APS, the desired amount of NMBA, depending on the required cross-linking degree, and water to complete 20 grams. The resulting mixture was poured into the glass moulds shown in Fig. 2.6.

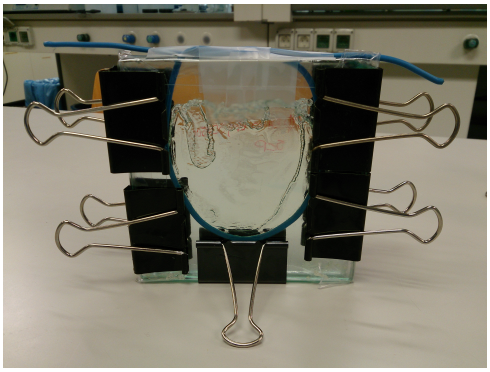

Figure 2.6: Glass moulds that allowed the passage of UV light to induce the polymerisation of the reacting mixture.

Preparation of the Mixtures

The mixtures mentioned above were prepared taking into account some safety measures in order to minimise the inherent risks associated with monomers. The reagents were all handled inside a gas extraction cabinet provided with an ozone injection system. Gas masks and security glasses were also needed. The gloves used were made of butyl and covered the entire forearm. Once the reactants were mixed in the flask with a magnetic stirrer, they were poured in a transparent mould made of two parallel glass plates. The plates were joint with several metal tongs with a cable in between, so that a gap of 3 mm was created between them. The cable surrounded all sides except one, forming an orifice through which the reagents can be introduced by means of a pasteur pipette. The plates were lined with transparent adhesive film as well, in order to avoid the glass contamination and to better remove the polymer afterwards. This procedure allows a better cleaning of the glass for further reuses without undesirable chemical reactions. The film must be transparent with the aim of allowing the passage of the UV light. In the same way, the metal tongs

have to avoid plugging the area where the liquid solution will be. In Fig. 2.6, the prepared mould is shown before introducing the liquid mixture with the reagents inside.

Polymerisation

After the moulds were prepared and filled with the reagents mixture, they were sealed with adhesive tape by the opening through which the pasteur pipette was introduced. Then, these were introduced in a UV oven, in vertical position to avoid monomer leaks. The plates were oriented in a way that they receive UV light on the whole surface on both sides and they do not cover each other. The moulds remained inside the oven for 24 hours. It is supposed that there are no longer monomer molecules after complete reaction, but to ensure that, a post-polymerisation procedure was pursued. Monomer molecules are harmful, so it is better to remove any remaining trace for health issues. Thus, the post-polymerisation consisted in 24 extra hours in a heat oven. After that there should not be any remaining monomer molecules, but there is the possibility of some non reacting free radicals. The gels were washed later with the aim of avoiding unnecessary risks. This was performed in a glass flask containing a mixture of water and ethanol (Fig. 2.7). There was a heating blanket under the flask and a coil vapour condenser connected to the upper part.

Figure 2.7: Glass flask containing the polymers immersed in a mixture of water and ethanol.

The polymers were extracted from the moulds and immersed in the flask, which was filled to about half the volume. Then, the heating blanket was switched on to bring the liquid to the boiling point. The temperature helps the diffusion of the liquid molecules inside the polymer chains, which act as a solvent of the possible remaining unreacted molecules. A coil condenser was

placed over the flask in order to prevent it from running out of liquid and burning the samples. This condenser was connected to a closed recirculating system of water, which was running the water through a tank with ice sheets. The whole assembly of the washing system can be observed in Fig. 2.8. Some glass pellets were also introduced in the flask for homogenising the boiling process and avoiding turbulences in the bubble formation.

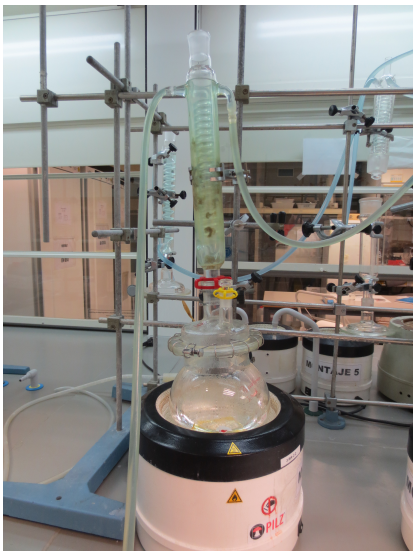

Figure 2.8: Glass flask with the coil vapour condenser connected to a refrigerant recirculation system.

The openings of both the flask and the condenser were joined with a trap and the heating blanket placed with a safety margin for security reasons. Two washings were performed per sample, during 6-8 hours each one. The mixture of water and ethanol was changed every time.

Drying, Punching and Swelling

Once the gels are washed and free of harmful remaining molecules, these need to be dried to remove the swollen solvent. First, the samples were put within an extraction cabinet for 24 hours, where the liquid evaporated into the air. After that, a more powerful extraction procedure was carried out to ensure the complete drying. This consisted in a thermal plate enclosed with a glass bell and connected to a vacuum bomb that extracted the air from inside the chamber. It acted as a desiccator, as shown in Fig. 2.9.

The samples were put in Petri dishes and placed over the thermal plate, which was set to 50 °C to increase the evaporation ratio. Then, the desiccator was closed by means of the glass cover and the pump switched on. This system is able to work in either continuous or discontinuous vacuum, i.e, keeping the vacuum after switching off the pump by means of a stopcock. In this case, the continuous extraction was conducted for an hour, after which the stopcock was closed. This discontinuous vacuum was kept for another hour, time during which the solvent evaporated and condensed in the glass cover. After this time, the stopcock was opened and the vacuum broken, so that the desiccator was opened and cleaned to remove the mixture condensed vapours. Subsequently, the vacuum procedure was repeated several times until the gels were completely dry. Next step was the material die-cutting, in order to obtain a great number of samples of the same material. Thus, samples were matched in size by means of a hammer and a die cutter of a diameter of 7 mm that can be seen in Fig. 2.10.

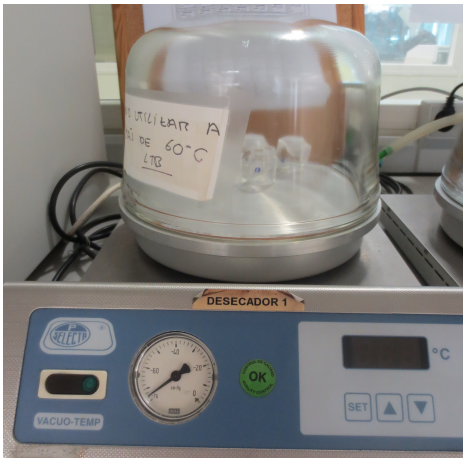

Figure 2.9: Desiccator with a glass cover and thermal plate with adjustable temperature.

It should be mentioned that the PAM gels are not easy to die-cut at room temperature, since their glass transition temperature is under that of the room when they are dry. Accordingly, they were die-cut before drying them in the desiccator. Finally, the cross-linked polymers were swollen by immersing them in 20 mL vials with the desired liquid. The swelling is not instantaneous, so it was required to leave them for 24 hours to reach the equilibrium. The weight of the gels was measured before and after swelling, in a way that the swelling index could be calculated for each case.

(a) Hammer and die cutter (b) Die-cut samples

Figure 2.10: Hammer and die cutter with a diameter of 7 mm and the die-cut samples before swelling.

2.3 Experimental Design

2.3.1 Characterisation of the Relative Permittivity

Open-Ended Coaxial System

The dielectric measurements of the samples were conducted by means of the open-ended coaxial method [54, 55]. It consisted of a VNA connected to a coaxial probe through a coaxial cable. The setup was slightly modified over the course of the experiments, 3 different VNAs and 2 coaxial probes were used in total:

- Vector Network Analysers
  - Keysight ENA E5072A. Frequency range from 30 kHz to 8.5 GHz.
  - Keysight N9918A FieldFox Handheld Microwave Analyzer. Frequency range from 30 kHz to 26.5 GHz.
  - Keysight Technologies N5247A PNA-X. Frequency range from 10 MHz to 67 GHz.
- Open-Ended Coaxial Probes
  - Keysight 85070E slim-form probe. Frequency range from 500 MHz and 50 GHz.
  - SPEAG DAK-1.2E. Frequency range from 5 to 67 GHz.

This method consists of an indirect measurement of the relative permittivity based on the reflection coefficient (S_{11}) of the Material Under Test (MUT) when an electromagnetic signal strikes it. The principle is founded on the effect that waves suffer in a change of medium, explained in Section 1.1 and depicted in Fig. 1.2. The S_{11} parameter contains information about the amplitude and phase of the reflected wave from the material. From the original signal sent, it can be mathematically conversed to the relative permittivity that causes this particular reflection [56]. The VNA is the responsible for generating the incident signal and comparing it with the received one afterwards. The coaxial probe, along with the cable, is the transmission medium up to the material, and it must be perfectly characterised in order to remove its influence over the original signal. The whole characterisation system is mounted as shown in Fig. 2.11.

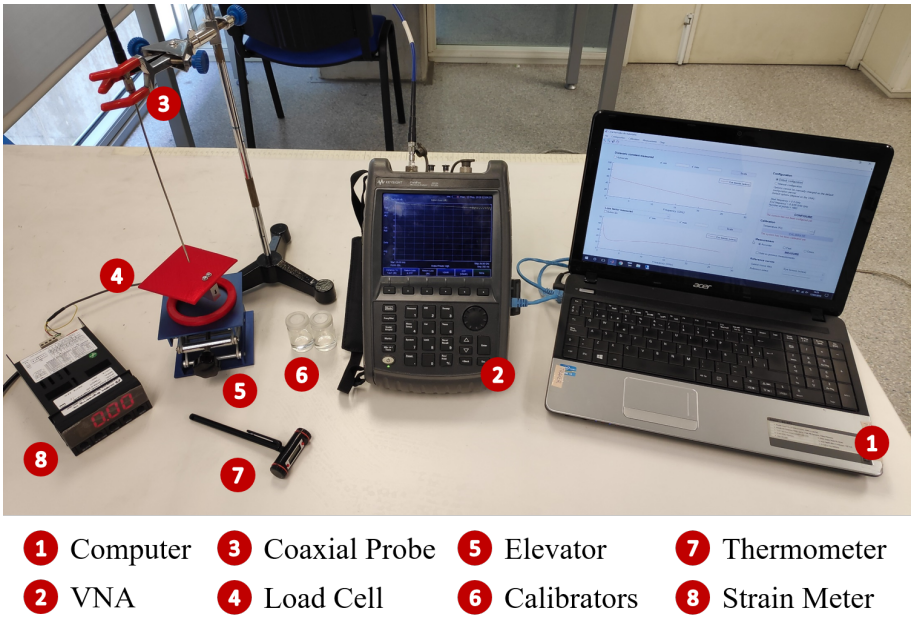

Figure 2.11: Setup of the characterisation system of the relative permittivity through the open-ended coaxial method.

A computer was also connected to the VNA, which managed the configuration parameters and executed the measurements. It was also in charge of processing the data and perform its transformation to the relative permittivity. The open-ended coaxial method owns several advantages such as the wide

bandwidth that is able to analyse in each measurement in an easy and quick way. Besides, it is a non-destructive characterisation method, suitable for liquids and semisolids, which are precisely the materials to be analysed. The indications to be taken for achieving good results are to ensure that the material is isotropic, non-magnetic, homogeneous, with a flat surface and there are no bubble or air gaps between the coaxial end and the MUT. Another limitation is the size of the samples, which need to be big enough (around half centimetre), specially for the lowest frequencies. After performing the calibration it is mandatory that there is no movement in any element of the setup. Any little change would affect the measurements and calibration should be carried out again. Thus, the cable and the probe were fixed with a clamp support and only the sample was moved with a mechanical elevator (see Fig. 2.11).

Calibration

This method requires some calibrators with well-known dielectric properties in order to compute the relative permittivity. The calibration of the system also removes the influence of all the connectors, cables and the probe. These references are usually the air (open circuit), a short circuit and the water. In this work, the methanol has been also incorporated as a calibrator, since it has been proven that its addition improves the accuracy of the dielectric measurements of materials with similar values to those of the body tissues [57]. Methanol has a dielectric constant comprised between the value of water and air, so it is like an intermediate calibrator. The closer the values of the calibrators are to the target the better the accuracy the system will reach. It is important to know that the relation of the reflection coefficient is not linear, but it is not equally accurate depending on the reflection value. Indeed, the resolution of the method is worse for high dielectric constants, whereas the range of values where reflection can vary without affecting that much the dielectric constant is at low values. This fact makes it more necessary to include calibrators with high values to increase the accuracy in this particular range of values. At high values, little changes in the reflection coefficient will lead to greater variations in the dielectric constant.

The computer connected to the VNA had a software that defined the measuring parameters (frequency range, power, intermediate frequency bandwidth, number of points, etc.) and processed the results. It was also responsible for the calibration procedure, asking for the different materials. Taking into account that temperature is a factor that influences the relative permittivity (see Section 1.2), it must be indicated to the software to specify the relative permittivity of the calibrators. These need to be at the same temperature so they were stored at room temperature in the same place where the measurements

were carried out. After defining the control parameters, the software asks for the calibrators sequentially, so they are measured in various steps. In the case of the liquids, the probe must be immersed to approximately half the height of the vial, as in Fig. 2.12.

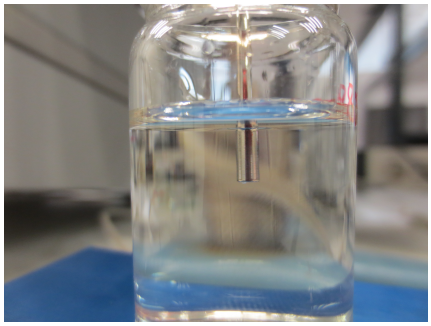

Figure 2.12: Immersion of the coaxial probe within the MUT.

The lack of any little bubble between the coaxial end and the liquid is very important. The air has a relative permittivity similar to that of the vacuum, so if signal come into contact with the air the apparent value will be reduced drastically. The method that was followed to avoid bubbles was to gently tap the probe once it was immersed, or taking it out and put it back in when necessary. After each calibrator, the probe must be cleaned with deionised water and dried to avoid contamination of the liquids. Calibration must be done periodically, since there are factors such as the thermal drift that affects the VNA. Indeed, it is recommended to turn on the equipment at least one hour before using it.

Measurement Procedure

Liquid materials were measured in the same way as calibrators, i.e., the probe was immersed in the vial up to half the height (Fig. 2.12). Samples were characterised at 24 °C, which was the room temperature, and there was a climate control that ensured that it was kept constant. This is necessary for ensuring the repeatability of the measurements. Three different samples were prepared for each composition in order to avoid any human error during the preparation of the mixtures. Three measurements per sample were conducted for averaging the values. Anyway, variation between measurements of the same sample was negligible. The other kind of material that was characterised were the gels, which behave like a semisolid material. In this case, the gels were not measured inside the vials, where they were swollen up, since the liquid

would be in contact with the tip of the probe and it would interfere with the measurement. Gel samples were taken out from the vials and placed in a glass sample holder, on which the measurements were made directly, as can be observed in Fig. 2.13.

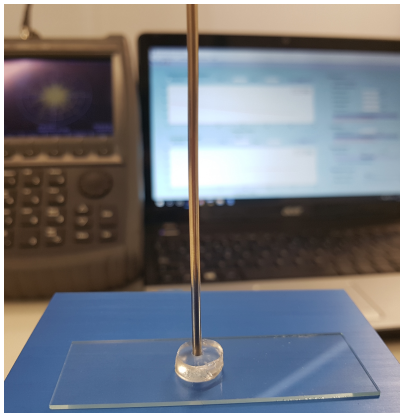

Figure 2.13: Measurement of a semisolid material with the open-ended coaxial probe.

The gel samples were taken with tweezers carefully to avoid breaking or squeezing them. As stated above, there is a required minimum size of the samples to ensure suitable measurements. The samples size was approximately 5 mm in depth and 1 cm in diameter, which has been reported to be a suitable sensing volume for dielectric measurements with this probe [58]. Taking into account that semisolids have an elastic behaviour, they deform when pressure is applied. This deformation can alter the results due to the fitting of probe to the mouldable surface. A too low pressure would lead to non-appropriate contact and air gaps within the gel. On the other side, an excessive force would pull the liquid out of the gel or could break it. For that reason, this kind of measurements were conducted by adding a load cell (Omega, LCAE-3KG) under the sample to monitor the applied force at all times, as suggested in [59]. This sensor was also useful to ensure repeatability of the measurements, which were carried out under 1.5 N of strength. This force yielded consistent results without breaking the gels. The force monitoring system was completed with a 3D-printed plastic support and a strain gauge meter (Omega, DP25B-S-230), both required to supplement the setup, which remained as in Fig. 2.14.

It should be ensured that the measure is taken from the gel and not the liquid. Because of that, both the end of the probe and the gel surface were dried with paper before any measurement. The pressure was prevented from being very high precisely to avoid leakage of liquid. The variation of the values

of this kind of materials is higher than that of produced in the liquids case, which is practically negligible. Ten measurements were taken from the gels, all in different positions, with the aim of obtaining the average and standard deviation.

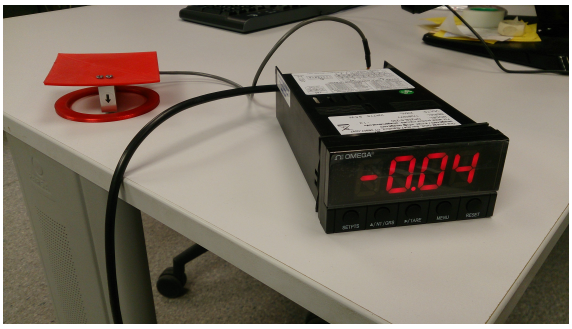

Figure 2.14: Single point load cell (left) connected to the strain meter (right), which shows the strength applied to the red surface in newton.

2.3.2 Degradation Analysis

The most feasible alternative for fabricating solid phantoms that was considered is the 3D printing of tissues as containers and then fill them with liquid phantoms. The most common current 3D printing systems are based on Fused Deposition Modelling (FDM), which consist in the extrusion of thermoplastic polymers. One should consider the chemical resistance of the polymers that are currently used in FDM if they are going to hold solvents for long periods. The most used ones are the Acrylonitrile Butadiene Styrene (ABS), although there are more polymers employed in FDM such as Polylactic Acid (PLA), Polyethylene Terephthalate (PET), PVA, Polycaprolactone (PCL) or Polypropylene (PP), among others. The PVA was immediately discarded because of its solubility in water, considering that it will probably be present in any phantom. From the others, the chosen ones for performing degradation tests were the PLA, ABS and PP, i.e., the most used ones along with the most chemically resistant, also to compare.

The analysis consisted of manufacturing specimens with these polymers and immersing them in a representative mixture of the composition of the liquid phantoms. After the immersion for a particular time, they would be analysed by means of a tensile test. Since this is a destructive assay, different samples for each time period were made. The samples were left in the mixtures for the following time periods: 1 week, 2 weeks, 1 month, 2 months, 4 months,

6 months and 9 months. Five samples per material and immersion time were made.

Fabrication of the Polymer Specimens

Different specimens where made for each material in order to immerse them in a equivalent medium and perform the further analyses. For that, it was required to start from the polymers in the form of pellets and so conform them according to the needs of characterisation. PLA and PP were already available in this form, but ABS was not. However, a commercial filament for 3D printing of this polymer was accessible instead. The solution was to transform the filament into pellets by using a pelletiser machine, which is shown in Fig. 2.15.

Figure 2.15: Pelletiser machine.

Afterwards, these pellets were shaped into a thin film, considering that the main characterisation analysis for assessing the degradation was going to be the tensile test. A thickness within a range of 200-300 μm was selected for the test in order to be able to analyse the influence of the medium over the materials. This shape format was achieved by means of a hydraulic press with heating plates, concretely the one shown in Fig. 2.16.

The conditions to achieve the aforementioned thickness were the following ones: ABS pellets were placed over one metallic sheet (one part of the mould), arranged around the central zone and without covering the whole surface be-

cause of the clear expansion. Then, the other sheet of the mould (another metallic sheet) was put on the pellets, in a way that these were enclosed between the two layers. This mould was placed over the bottom plate of the hydraulic press.

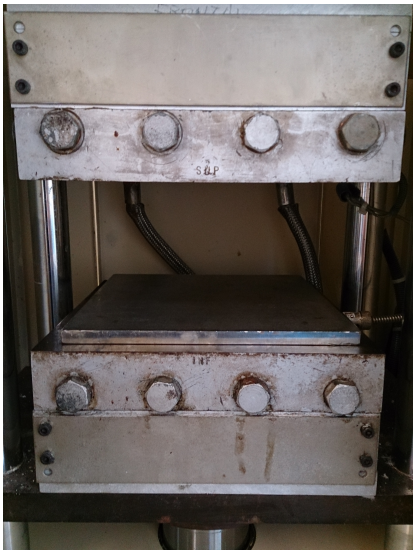

Figure 2.16: Hydraulic press with heating plates where the polymer specimens were shaped.

Then, the temperature of the press was set to 150 °C and it was left to reach that value before applying any pressure. Once the temperature was enough, a three-step pressure program was followed. First, 50 bar were applied for 1 min; then, pressure was increased up to 100 bar during 1.5 min; and finally, 200 bar were set for 2.5 extra minutes. After this, the mould was removed from the inside of the press and cold water was poured onto its surface to cool it. PLA and PP were shaped in a similar but easier way. In this case, the pressure was equally applied during all the time, which was 50 bar for 2 minutes in both cases. The difference lay in the temperature, 160 °C for PLA and 150 °C for PP. After making the film of the three materials, they were cut in pieces of 4×1 cm^2. The final result of these specimens can be observed in Fig. 2.17.

Test Methodology

The shape and the size of the aforementioned specimens were chosen in that way for the tensile testing. These had one centimetre per side for the subjection with the grips and the remaining dimensions were twice as long as they were

wide, i.e., 2×1 cm^2 of gage area. The assays were carried out with a mechanical testing machine (Adamel Lhomargy DY34), which subjected the specimens to tensile stress until fracture. The full setup can be observed in Fig. 2.18.

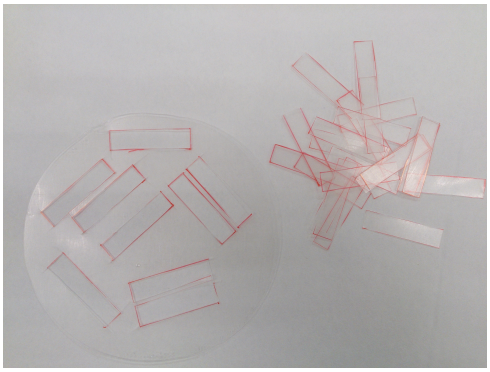

Figure 2.17: PLA specimens of a 4×1 cm^2 area and 200-300 μm of thickness.

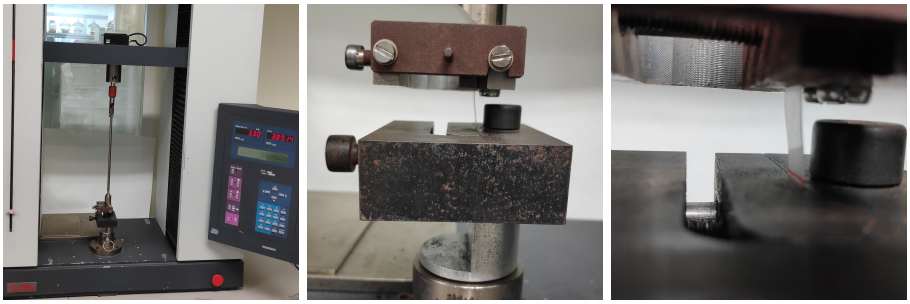

(a) Testing machine (b) Grips (c) Specimen

Figure 2.18: Tensile testing setup with serrated grips for subjecting the specimens.

A computer controlled the movement of the arms from the tensile machine and processed the data. The speed was set at 10 mm/min, and the initial position was chosen to ensure a distance between grips of 2 cm. The machine started its movement until reaching the fracture point, after which it returned to the initial position for the next specimen. The measured data was the force required to deform the sample along its longitudinal axis. This was conversed to the stress that suffered the specimen from its dimensions.

Chapter 3

Phantom Engineering

The first objective of this thesis was the study of the influence of different chemicals that could be suitable in the phantom preparation. Then, once the suitable compounds were selected, it would be useful to obtain the relationship between their concentration and the final relative permittivity of the mixture. The scope of this chapter is to establish the compounds that will take part in the phantoms formulations, according to their physical state and working frequency band. On the one hand, some chemicals can be suitable for large bandwidth but expensive or difficult to prepare. These would be included when the requirements of bandwidth are mandatory. On the other hand, if the band is narrow as in the current medical bands, probably a cheaper a easy-to-prepare phantom is the best choice. Thus, the candidates will be classified for different purposes by taking their possibilities into account.

3.1 Basic Common Compounds

Initially, the most common compounds used in literature, i.e., water, sucrose and salt, were studied in order to check their limitations. The measuring system was the one described in Section 2.3 and depicted in 2.11, including the Keysight ENA E5072A VNA and the Keysight 85070E slim-form probe. The operation frequency was comprised between 500 MHz and 8.5 GHz, measuring 1601 points per sample at each frequency sweep, i.e, the resolution was 5 MHz. The output power was set at 10 dBm and the IF bandwidth to 1 kHz. Five samples per composition were prepared and measured in order to average the results. Compositions were made of water with increasing concentration of sucrose and salt (sodium chloride). Concretely, the sucrose was added in weight percentages of 0, 17, 34 and 51%, whereas the salt was included in percentages

from 0 up to 5%, in steps of 0.5%. These percentages were combined between them for analysing if the effect was the same.

Analysis of the Influence of Sucrose and Salt

First of the samples was water without sucrose with an increasing amount of NaCl (see Fig. 3.1). Then, here it is possible to analyse the influence of the salt itself in aqueous solutions. This influence is different in the real (dielectric constant) and the imaginary part (loss factor) of the relative permittivity. In the real part, the addition of salt progressively reduces its value without changing its slope or trend. It just shifts the curves downwards. This means that the relaxation frequency is not affected by the addition of salt. Ions are also not polarised by orientation, so they actually reduce the concentration of polarised molecules per volume unit, i.e., there is less proportion of water molecules. Concerning the imaginary part, this is precisely the one where ions are key until certain frequency (see Fig. 1.7). Salt ions increase the conductivity of the solution, and so the loss factor, since both are directly related (see Section 1.2). Particularly, it increases the loss factor at the lowest frequencies. From 5 GHz approximately, free charges are not capable of following the fast variation of the external field, so its contribution to the polarisation disappears.

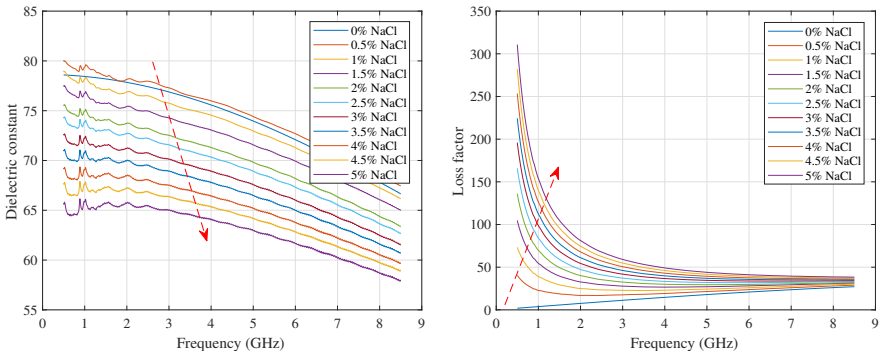

(a) Dielectric constant

(b) Loss factor

Figure 3.1: Relative permittivity of water with 0% sucrose with different concentrations of NaCl.

The next graphs depict the results for the measurement of the relative permittivity of water with a 17% (Fig. 3.2) and 34% (Fig. 3.3) of sucrose with the range of concentrations of salt. The effect of the salt is the same as in the previous case, it does not alter the trend of the curves of the dielectric constant.

The concentration of ions increase the loss factor at frequencies under 5 GHz, though. Sucrose addition has a qualitatively different effect. It also reduces the values of the curves, but changing their trends as well. This means that the value of the dielectric constant drops faster when sucrose is present. In fact, the shape of the curve changes progressively from concave (Fig. 3.1) to a convex one (Fig. 3.4).

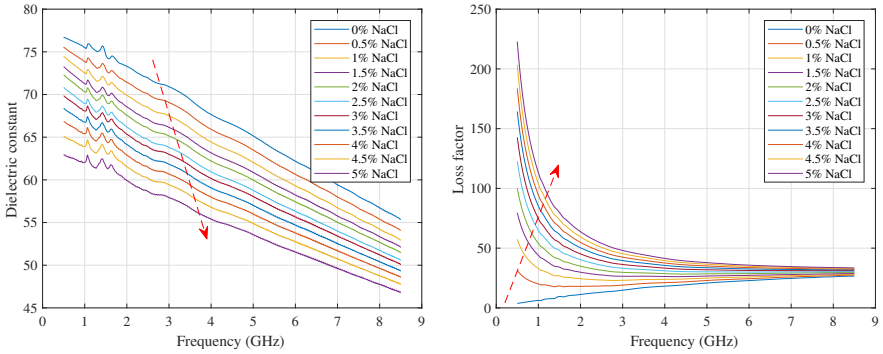

(a) Dielectric constant (b) Loss factor

Figure 3.2: Relative permittivity of water with 17% sucrose with different concentrations of NaCl.

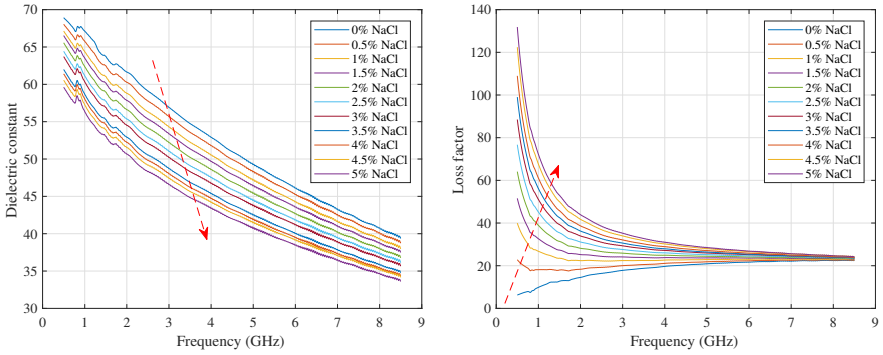

(a) Dielectric constant (b) Loss factor

Figure 3.3: Relative permittivity of water with 34% sucrose with different concentrations of NaCl.

The last results of this measurement batch were based on an aqueous solution with a 51% of sucrose, which is shown in Fig. 3.4. The aforementioned effects are repeated here, with a dielectric constant that decreases quicker than before. In brief, the addition of salt increases the loss factor with barely changing the dielectric constant, whereas sucrose decreases the dielectric constant (with its slope) without changing the losses too much.

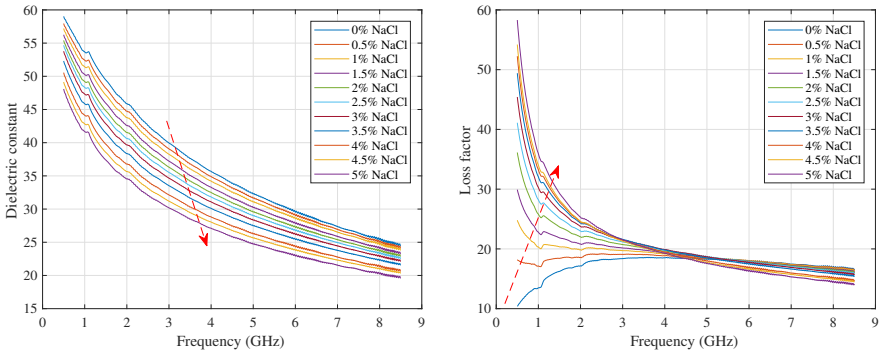

(a) Dielectric constant

(b) Loss factor

Figure 3.4: Relative permittivity of water with 51% sucrose with different concentrations of NaCl.

The change in the trend of the dielectric constant is high, and it is caused by the big size of the sucrose molecules compared to the others, which limit the orientation of water dipoles. On the contrary, salt ions are small enough to not bother the movement of the orientating molecules. This remarkable change in the trend of the dielectric constant causes the unsuitability of this molecule to be used in wideband phantoms, since tissues own steeper slopes. Moreover, the addition of salt does not improve (or worsen) the slope of water, which is not similar to that of the tissues neither. It also increases the loss factor too much for the low frequency band, which would risen the propagation losses in a communication scenario. However, these compounds could be fruitful in narrow bands, where there is not a notable change for values of permittivity along frequency. This can be done through a mathematical model that is able to predict the required composition for a particular relative permittivity.

Cole-Cole Fitting

The previous results can be fitted to a simple-pole Cole-Cole model, which is widely used in the literature for modelling the dielectric properties of body

tissues. The number of poles is related with the dispersion regions of the relative permittivity of the tissues that appear within the analysed frequency range (see Appendix A). It is often appreciated in the changes of trend graphs of the dielectric constant. The formula that models the relative permittivity is Eq. 3.1:

$$\varepsilon_r' - j\varepsilon_r'' = \varepsilon_\infty + \frac{\varepsilon_s - \varepsilon_\infty}{1 + (j\omega\tau)^{1-\alpha}} + \frac{\sigma_s}{j\omega\varepsilon_0} \tag{3.1}$$

where ε_∞ is the dielectric constant at infinite frequency, ε_0 is the static dielectric constant (frequency 0 Hz), ω is the angular frequency in rad/s, τ is the relaxation time in s^{-1}, α is the exponential parameter, and σ_s is the static conductivity in S/m. This amount of unknowns results in an overdetermined system with multiple solutions. Thus, in order to simplify the fitting, the ε_∞ parameter can be taken from reference data of the water [60]. The rest of coefficients can be calculated through a mathematical software, by solving a least squares problem with the Levenberg-Marquardt algorithm. The different curves from above were fit with this algorithm, each one with its own parameters. Then, the relationship between these parameters and the concentration of salt and sucrose can be parametrised with polynomials, which remain as Eq. 3.2, 3.3, 3.4, 3.5 and 3.6:

$$\varepsilon_\infty = 5.89 \tag{3.2}$$

$$\begin{aligned} \triangle\varepsilon = \varepsilon_s - \varepsilon_\infty = &(405.69 \cdot c_{Sucrose} - 307.09) \cdot c_{NaCl} \\ &- 27.405 \cdot c_{Sucrose} + 75.53 \end{aligned} \tag{3.3}$$

$$\begin{aligned} \tau(ps) = &(319,525 \cdot c_{Sucrose}^3 - 153,143 \cdot c_{Sucrose}^2 + 14,467 \cdot c_{Sucrose} \\ &+ 158.84) \cdot c_{NaCl}^2 + (753.53 \cdot c_{Sucrose}^2 - 1.6545 \cdot c_{Sucrose} \\ &- 23.15) \cdot c_{NaCl} + 430.89 \cdot c_{Sucrose}^3 - 136.86 \cdot c_{Sucrose}^2 \\ &+ 24.823 \cdot c_{Sucrose} + 8.2933 \end{aligned} \tag{3.4}$$

$$\begin{aligned} \alpha = &(81.587 \cdot c_{Sucrose} - 43.035) \cdot c_{NaCl}^2 + (0.4214 \cdot c_{Sucrose} \\ &+ 2.0407) \cdot c_{NaCl} - 0.6678 \cdot c_{Sucrose}^2 + 0.9347 \cdot c_{Sucrose} \\ &- 0.0023 \end{aligned} \tag{3.5}$$

$$\sigma_s(S/m) = -280.71 \cdot c_{Sucrose} + 166.31 \tag{3.6}$$

Formulas for 2.4 GHz

Previous equations enable the possibility of replicating the curves shown above or predicting new ones for solutions that have not been previously prepared.

From those, or using the results, new relations can be obtained for a chosen frequency, like the 2.4 GHz, which is the most used one from the ISM bands, due to its non-licensed nature. A single frequency can be considered in the case of narrowband technologies, since the values of the relative permittivity barely change in a few megahertz of difference. Therefore, the values of the permittivity at 2.4 GHz are analysed here to find their evolution with the concentration of sucrose and salt. Two mathematical relations are needed to describe the relative permittivity, one for each part, and they are obtained separately. The analysis of the variation the dielectric constant is shown in Fig. 3.5a, where the values at 2.4 GHz are linearised for each sucrose series. All values show a linear behaviour with the increase of salt, obtaining a coefficient of determination of at least a 98.95% in the worst case. Then, the equations for the dielectric constant can be expressed as in Eq. 3.7 by studying the slope and y-intercept of their trend in function of sucrose and salt.

$$\varepsilon_r^*(c_{NaCl}, c_{Sucrose}) = \overbrace{m_1(c_{Sucrose})}^{\text{slope}} \cdot c_{NaCl} + \overbrace{b_1(c_{Sucrose})}^{\text{y-intercept}} \tag{3.7}$$

These coefficients are dependent on the sucrose concentration, and they change with respect to the sucrose concentration as in Fig. 3.5b. They are fitted again, but this time with a quadratic regression for the case of the y-intercept, with a coefficient of determination of 99.97%. The slope is fitted to a linear regression, achieving a coefficient of determination of 92.44%.

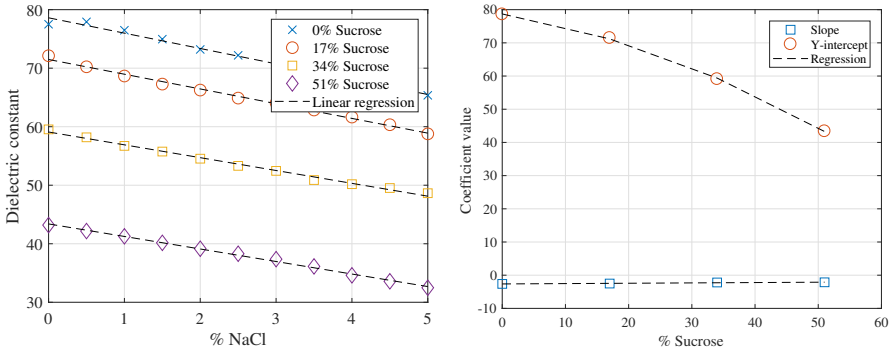

(a) Dielectric constant from sucrose series

(b) Slope and y-intercept from (a)

Figure 3.5: Evolution of the dielectric constant at 2.4 GHz according to the concentration of salt and sucrose in aqueous solutions.

Combining the obtained regressions, as described in Eq. 3.7, one can reach Eq. 3.8, where ε'_r is the dielectric constant, c_{NaCl} is the concentration of salt, and $c_{Sucrose}$ is the concentration of sucrose, both in weight percentage. The left side of the equation is the relation that describes the slope of Fig. 3.5a, which is obtained in the regression of Fig. 3.5b. The right side of Eq. 3.8 is obtained through the quadratic regression of 3.5b, being added to the general equation as in Eq. 3.7.

$$\varepsilon'_r(c_{NaCl}, c_{Sucrose}) = \overbrace{(0.01 \cdot c_{Sucrose} - 2.633)}^{\text{slope}} \cdot c_{NaCl} \overbrace{-0.007 \cdot c_{Sucrose}^2 - 0.316 \cdot c_{Sucrose} + 78.704}^{\text{y-intercept}} \tag{3.8}$$

The analysis of the loss factor for the series of aqueous solutions of sucrose and salt at 2.4 GHz is depicted in Fig. 3.6a, whose values are fitted to a linear regression as well, with a coefficient of determination of a 90.7% in the worst case. This means that the imaginary part of the relative permittivity of these solutions can be also represented with a relation similar to Eq. 3.7. As in the previous case, the slope and the y-intercept for curves of the different sucrose series are analysed in Fig. 3.6b. Both coefficients follow a linear trend and can be fitted with this kind of regression, achieving a 99.9% of determination for the slope and a 97.8% for the y-intercept.

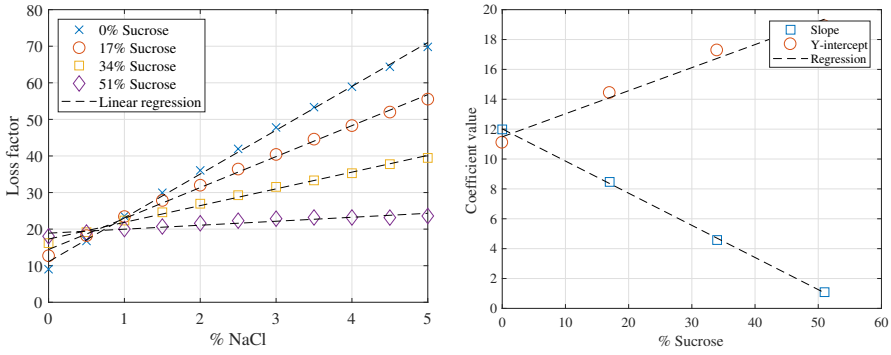

(a) Loss factor from sucrose series

(b) Slope and y-intercept from (a)

Figure 3.6: Evolution of the loss factor at 2.4 GHz according to the concentration of salt and sucrose in aqueous solutions.

The general formula that describes the loss factor according to the concentration of sucrose and salt is shown in Eq. 3.9. This is obtained by substituting the regressions from Fig. 3.6b in Eq. 3.7.

$$\varepsilon_r''(c_{NaCl}, c_{Sucrose}) = \overbrace{(-0.215 \cdot c_{Sucrose} + 12.015)}^{\text{slope}} \cdot c_{NaCl} \overbrace{+0.154 \cdot c_{Sucrose} + 11.485}^{\text{y-intercept}} \tag{3.9}$$

With the help of Eq. 3.8 and 3.9, the dielectric constant and loss factor of an aqueous solution of sucrose and sodium chloride can be predicted at 2.4 GHz. Conversely, setting the desired values of those parameters one can obtain the chemical formulation of the solution to prepare in order to achieve the corresponding phantoms.

3.2 Materials Selection for Liquid Phantoms

As explained in Section 1.2, the main polarisation mechanisms at the frequencies of interest is the orientation (see Fig. 1.7). Chemicals with a good orientation capability will be those with higher dielectric properties. The molecules that own these feature are those with asymmetric distribution of charges around their atoms, i.e., polar molecules. Water is one of them, and it is precisely the main compound of most of the tissues, so it will be included as the baseline for phantoms and combined with other polar liquids. The procedure for selecting the most suitable polar compounds for achieving wideband phantoms was to prepare aqueous mixtures of polar liquids to analyse the behaviour of their dielectric properties with frequency. The polar liquids that were reviewed are common chemicals in laboratories such as acetic acid, acetone or ethanol, which were chosen as a first step because of their easy availability. Others like N,N-dimethylformamide, nitromethane, N,N-dimethylacetamide, or pyridine could be useful as well because of their promising dielectric properties [61], but they were not studied because of their toxicity or difficulty of finding them. The samples were prepared and measured with the open-ended coaxial method, using the Keysight 85070E slim-form probe and the Keysight N9918A FieldFox Handheld Microwave Analyzer, which cover a bandwidth wider than in the previous section, i.e., the scanning range was comprised between 500 MHz and 18 GHz. The number of points was 1601 again, so this time the resolution frequency was 10.9375 MHz. The IF bandwidth was set to 3 kHz and the output power was -3 dBm. The calibration procedure and the measurement methodology was that explained in Section 2.3. Since they are liquids, the handling

was performed with a pasteur pipette, which was used to pour them into the vials. The samples were made of a half the weight of a polar compound and then filled up to 20 grams with deionised water. Next, the content of the vials was stirred for 15 minutes to ensure a complete dissolution and mixture. As before, there were prepared three samples per composition in order to minimise the experimental errors. Moreover, the calibration process was repeated every five scans. Fig. 3.7 shows the results of the relative permittivity of the different samples that were prepared with polar liquids, in comparison to the values of the muscle tissue, as an example of the normal behaviour of tissues with high water content.

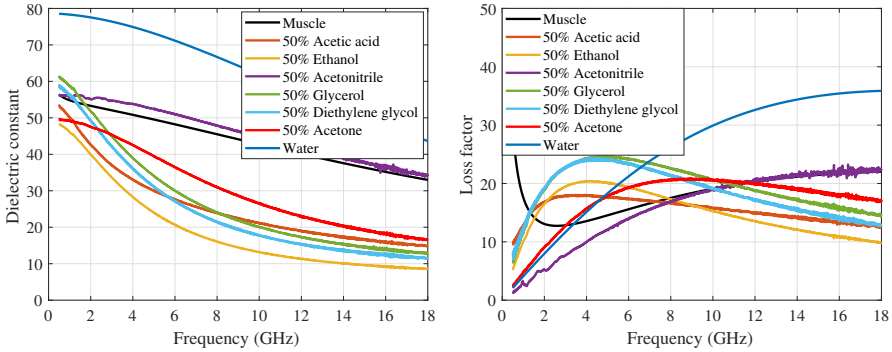

(a) Dielectric constant

(b) Loss factor

Figure 3.7: Relative permittivity of water, 50% aqueous mixtures of different polar liquids, and that of the muscle tissue according to Gabriel [3].

All the mixtures cause a decrease in the dielectric constant from that of the water within the frequency range. This means that the water molecule is the one with the highest orientation polarisation, and this is due to its geometry. Despite it is not the molecule with the highest dipole moments, its geometry and bond angles allow it to create hydrogen bonds with up to four additional water molecules of the surroundings (see Fig. 3.8). These act as dipole moments that also alter the external electrical field, so they define the relative permittivity of the material.

The drawback of most of these mixtures is the fact that they show a remarkable drop of the values in the dielectric constant with frequency. This is related with the relaxation frequency, i.e., due to the impossibility of the molecules to orientate towards the applied electrical field at the same speed at which it changes. Tissues normally own a gentle slope of the dielectric constant within the microwave band, since relaxation is progressive, not abrupt like res-

onance (see Fig. 1.7). Even more important is the difference in the loss factor, which grows considerably around 4 GHz and exceeds the muscle reference values (Fig. 3.7). This is related with the relaxation mechanism, which always produces a rise in the losses when a polarisation mechanism disappears. After this growth, the value of the loss factor falls again and deviates again from the behaviour of the tissue.

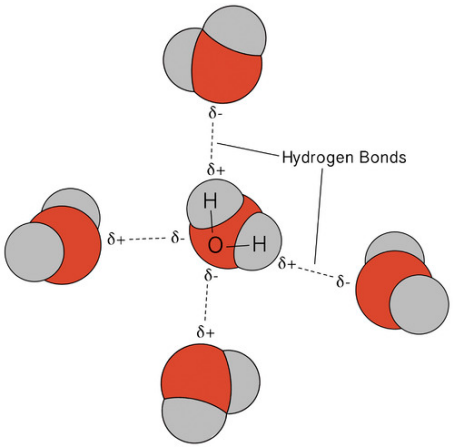

Figure 3.8: Hydrogen bonds of a single water molecule with four other water molecules. Reprinted from [62], licensed under CC BY-NC 3.0.

Nevertheless, there is a candidate that fits the behaviour of the muscle really well. It is the acetonitrile, which exhibits a stable dielectric constant with frequency and a maximum in the loss factor at higher frequencies than the other candidates. This behaviour is due to the high relaxation frequency of acetonitrile, 45.734 GHz, which is much larger than other candidates like ethanol, 976.41 MHz [61]. The higher this frequency is, the further to the right part of the graph the loss pick shifts. Regarding the frequency range from 500 MHz to 9 GHz, where the trend of the loss factor does not match that of the muscle, this region is highly influenced by the ionic polarisation (see Fig. 1.7). A salt that increases the conductivity of the mixture would improve the matching at this frequency range. Sodium chloride is the habitual salt in these cases [21, 63], since it is the most accessible and cheap one. However, in order to find if there is a better option to include as salt in the mixtures, three solutions with a 2.5% of different salts were prepared: sodium chloride (NaCl), potassium chloride (KCl) and sodium bromide (NaBr). The values of the loss factor of these salts are compared between them and with deionised water in Fig. 3.9.

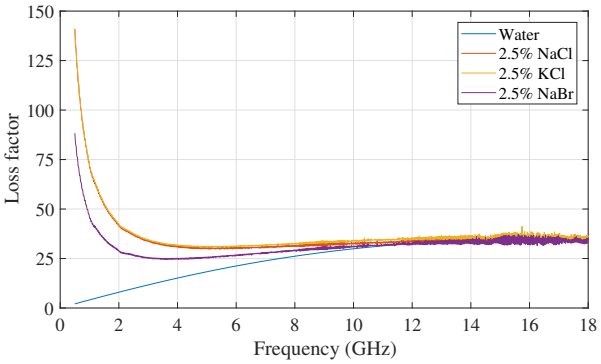

Figure 3.9: Loss factor of aqueous solutions with a 2.5% of sodium chloride (NaCl), potassium chloride (KCl) and sodium bromide (NaBr) compared with deionised water.

It can be observed that the chosen salt is not crucial for adjusting the loss factor to the trend of the tissues. All salts produce a huge increment at the lowest frequencies and own the same trend, i.e., the relaxation frequency of the ionic polarisation is not affected by the kind of salt. The increment in the loss factor is higher than that pursued in every curve, and the curves of potassium chloride and sodium chloride almost overlap in the graph. Because of all this, the sodium chloride seems the best option to be used in phantoms, since it raises heavily the loss factor with a minimum quantity and it is the most easily available salt.

Analysis of the Influence of Acetonitrile

Once the acetonitrile is selected as the suitable candidate for preparing the liquid phantoms, an analysis of its influence on mixtures with water, as in the case of the basic compounds above explained. Then, several series of acetonitrile at different compositions were prepared, specifically mixtures of 30, 40, 50 and 60%. Each of the series was replicated with a different concentration of NaCl, from 0 to 5% or until saturation point in those cases where it was not possible to add more salt. First of these series is the one corresponding to the 30% of acetonitrile, which is shown in Fig. 3.10.

The influence of sodium chloride is really similar to the cases with sucrose (e.g., Fig. 3.1). The dielectric constant is reduced progressively with the addition of salt, without changing its slope and proportionally at the measured frequencies. This can be explained by the size of the ions, which are so small that do not interfere with the rotation of the polar molecules.

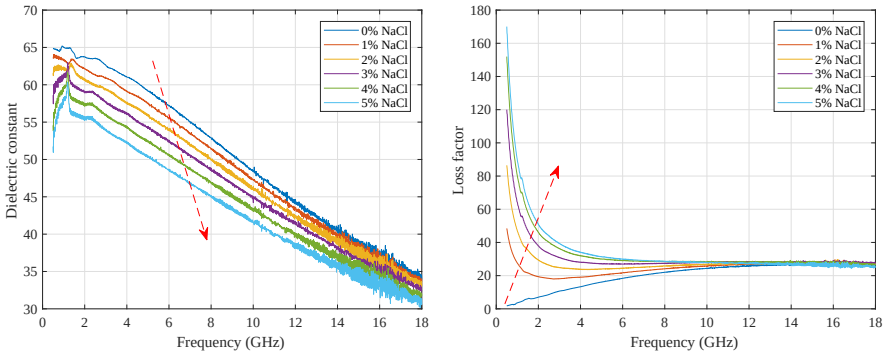

(a) Dielectric constant

(b) Loss factor

Figure 3.10: Relative permittivity of 30% acetonitrile mixtures with different concentrations of NaCl.

Then, the relaxation frequency is not altered by the ion concentration. As before, the reduction of the value is due to the less polarised water particles per unit volume. Regarding the loss factor, the effect is more or less the same as well. The conductivity provided by the ions cause the exponential shape at the lowest frequencies of the loss factor, which disappears after around 10 GHz, after the relaxation process of the ionic polarisation.

The following series are depicted in Fig. 3.11, where acetonitrile is mixed with water at a proportion of 40%. The dielectric constant just falls a few units with respect to the previous combinations, and the effects are almost the same. As in all the previous cases, the salt decreases the real part without changing the behaviour or trend of the curve with frequency. Again, the loss factor grows exponentially at frequencies below 10 GHz.

In Fig. 3.12, the importance of the acetonitrile addition is better observed. It shows the relative permittivity of a 50% composition of acetonitrile in water with increasing amounts of salt. The dielectric constant gets more stable values with frequency as acetonitrile is added (note the y-axis). The higher relaxation frequency of acetonitrile compared to water induces this effect, which will be significant in order to mimic the behaviour of body tissues (see Fig. 3.7). One can notice from the previous series, and here it is confirmed, that the permissible salt concentration is inversely proportional to that of acetonitrile. In this case, the maximum dissolved quantity of NaCl was 2%. Once the saturation point is overtaken, the mixture splits in two immiscible phases, in a way that it is no longer a homogeneous liquid. At this point, it cannot be used as a phantom, so these mixtures are discarded from the measurements.

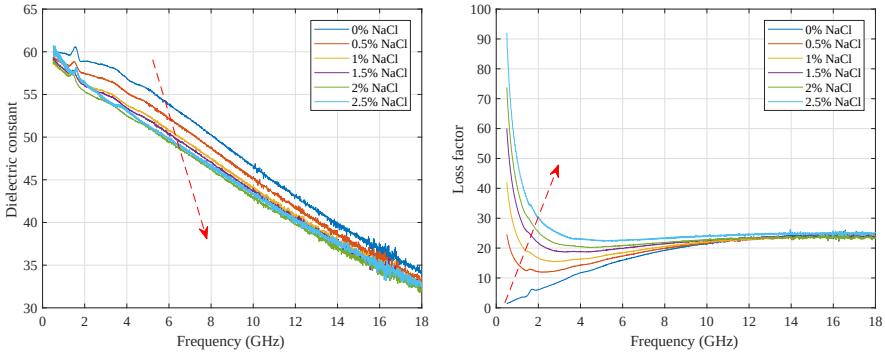

(a) Dielectric constant (b) Loss factor

Figure 3.11: Relative permittivity of 40% acetonitrile mixtures with different concentrations of NaCl.

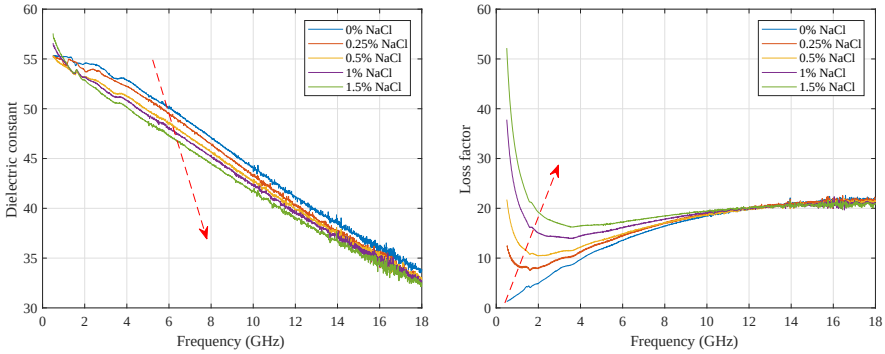

(a) Dielectric constant (b) Loss factor

Figure 3.12: Relative permittivity of 50% acetonitrile mixtures with different concentrations of NaCl.

The most concentrated mixture of acetonitrile was the 60% in water, which is given in Fig. 3.13. Once again, the values of the dielectric constant present a gentle slope with frequency, more stable this time than in the previous cases with less concentration of acetonitrile. Another effect that must be mentioned is the effect in the overall loss factor that the increase of acetonitrile produces, which is reducing it at all the frequencies. At the lowest frequencies (below 10 GHz), salt can be used to counteract this effect. However, from this point,

the only way to change the loss factor is to vary the concentration of the polar liquids. It should be also noticed that the increase in the loss factor at frequencies below around 2 GHz is great because of the exponential shape of the curves. Little changes in the salt concentration lead to huge variations in the values, so adjusting the loss factor at those frequencies could be challenging.

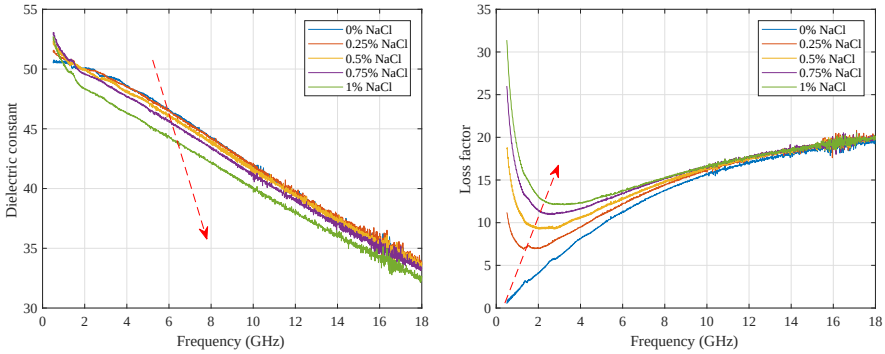

(a) Dielectric constant

(b) Loss factor

Figure 3.13: Relative permittivity of 60% acetonitrile mixtures with different concentrations of NaCl.

In short, the addition of acetonitrile causes an increase of the relaxation frequency of the mixture that has an important effect over the relative permittivity. The real part, i.e., the dielectric constant, suffers a progressive reduction of its values within the entire frequency range while it reduces also the slope of the curve. The lowest values of the curve are due to the lower polarisation capability of acetonitrile molecules compared to that of the water. The increase in the relaxation frequency will be key for the creation of wideband phantoms. It changes also the behaviour in the loss factor, which is also reduced in the whole measured bandwidth due to the shift of its maximum to higher frequencies (outside the measuring frequency range). These systematised results are useful for interpolating the results of the graphs so that it is possible to estimate the required composition for a particular phantom at certain frequency.

3.3 Liquid Phantoms Tailoring

Formulas for 2.4 GHz

Like in Section 3.1, one of the purposes of the previous analysis was the development of different formulas that model the behaviour of the relative permittivity

with the concentration of the used compounds. These mixtures are supposed to be suitable for wideband phantoms, since they imitate the trend of their values with frequency. However, these can be useful for narrow bands, like ISM, as well. The key is in the fact that other compounds such as the sugar, increase the loss factor precisely at frequencies around 2-4 GHz, which fall under this mentioned band. Then, the losses are higher than those of the body tissues by using these compounds. The advantage of acetonitrile is that the shift of the peak in the loss factor leads to a decrease in most of the analysed frequencies, including the main medical bands (see Section 1.1).

Taking advantage of these possibilities in the narrow band, one could obtain phantoms with better accuracy by using acetonitrile and sodium chloride instead of other basic compounds like sucrose. Considering that the most used unlicensed narrow band is the 2.4 ISM one, this was selected for creating the equations. As previously, the real part was the first to be analysed, in series of different acetonitrile concentrations (Fig. 3.14a). The y-axis shows the dielectric constant of the different series, which are fitted with linear regressions, achieving a determination coefficient of at least 93.09%. The pursued information from this graph is the slope of the influence of the salt. Since the first three series own almost the same slope, an average of these ones is chosen for the equation. The slope for the series containing 60% of acetonitrile is neglected due to the deviation with respect to the rest of them, probably because of the reduced interval of salt concentrations. The average of the slope for the three other series was -1.46.

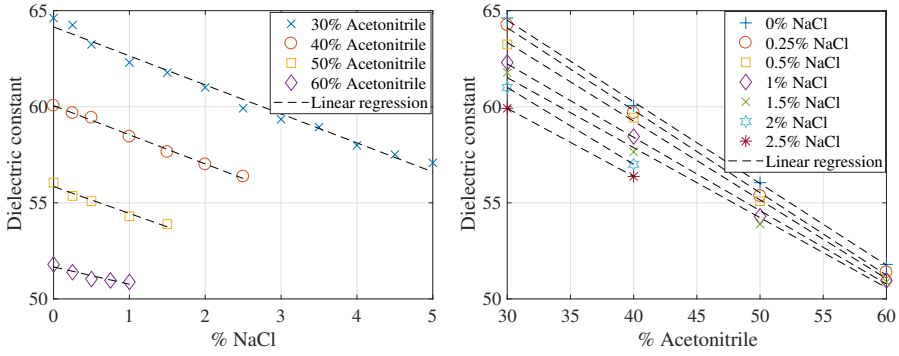

(a) Dielectric constant from acetonitrile series (b) Dielectric constant from salt series

Figure 3.14: Evolution of the dielectric constant at 2.4 GHz according to the concentration of acetonitrile and salt in aqueous solutions.

After that, the influence of the acetonitrile for each concentration of salt is analysed in Fig. 3.14b. Thus, the values of the dielectric constant are drawn in different series of NaCl, which change with the concentration of acetonitrile (x-axis). The values are fitted to a linear regression, with a determination coefficient of 99.86% in the worst case. This time, the selected slopes were the cases of 0, 0.25 and 0.5% NaCl, those with the least deviation between them. Besides, phantoms are supposed to own a salt concentration in the order of these values, so a better approximation in this range is desirable. The average slope for the three first slopes was -0.421. These relationships are reflected in Eq. 3.10, where the y-intercept corresponds to that of the series with 0% of salt, i.e., the case without acetonitrile or NaCl.

$$\varepsilon'_r(c_{ACN}, c_{NaCl}) = \overbrace{-0.421}^{\text{slope}} \cdot c_{ACN} \overbrace{-1.46 \cdot c_{NaCl} + 77.24}^{\text{y-intercept}} \tag{3.10}$$

The imaginary part is more complex to obtain due to the absence of a linear trend with the values. The curves of the linearisation of the the loss factor values are depicted in Fig. 3.15a. The series show the values with the salt constant and changing the acetonitrile concentration. Once again, the data are adjusted to a linear trend each series, with a coefficient of determination of at least 98.79%.

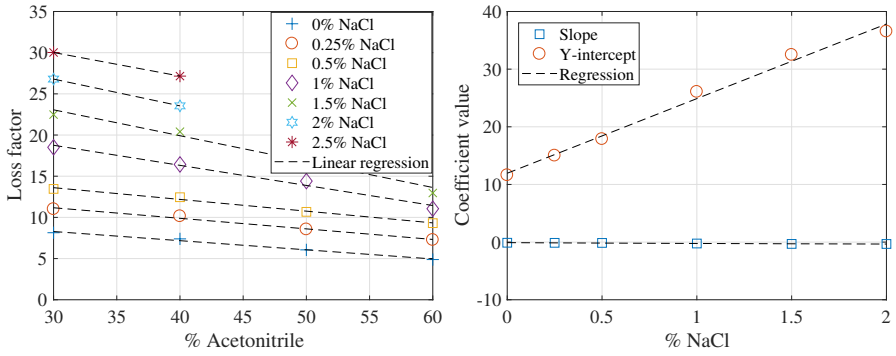

(a) Loss factor from salt series

(b) Slope and y-intercept from (a)

Figure 3.15: Evolution of the loss factor at 2.4 GHz according to the concentration of acetonitrile and salt in aqueous solutions.

One can see that the slope gets steeper when the salt concentration is increased. This means that it is not possible to take the average value of the slope and assume that the the influence of acetonitrile is independent of the

salt concentration. Because of that, the evolution slope and the y-intercept of Fig. 3.15a is analysed according to the salt concentration in the mixture. Results are shown in Fig. 3.15b, with a linear trend in the case of the y-intercept and a polynomial variation of degree 2 in the case of the slope.

The equations obtained through the linearisation of these values are useful for the general equations of the loss factor at 2.4 GHz (Eq. 3.11). This formula is the sum of the relationship of the y-intercept and the function of the slope multiplied by the acetonitrile concentration.

$$\varepsilon_r''(c_{ACN}, c_{NaCl}) = \overbrace{-4.39 \cdot c_{NaCl}^2 - 1.04 \cdot c_{NaCl} - 0.46}^{\text{slope}} \cdot c_{ACN} \overbrace{+72.07 \cdot c_{NaCl} + 11.72}^{\text{y-intercept}} \tag{3.11}$$

These equations will be used to obtain the recipe for mimicking different tissues in the 2.4 GHz ISM band. The calculated values will not be exact, since the equations own an error intrinsic to the approximations. One should consider that the regressions were calculated without taking into account the high concentrations of salt with the aim of improving the least concentrated ones. This is something that will be checked, and they will be considered valid if the achieved error with the actual values of the tissues is negligible.

Formulas for Ultrawideband

Until now, the presented formulas were intended to design phantoms that cover narrow bandwidths, since the relative permittivity was modelled according to the composition of the mixture at one single frequency. Then, in these phantoms, it was assumed that the bandwidth is so small that there is not an appreciable variation of the permittivity between two different frequencies. The problem with wideband phantoms that cover such distant frequencies, e.g. UWB (3.1-10.6 GHz), is the fact that the values of the relative permittivity change several units along that band. However, the phantom must imitate all the values at their corresponding frequencies, i.e., it should imitate the initial and final values as well as the trend. This time is not enough with two equations with two unknowns each and one single solution with the suitable concentration of the studied compounds. One option for wide bands could be to develop a model that parametrise a curve depending on the concentrations of the aforementioned compounds. However, this is quite complex and would not be more suitable than other simpler solutions. The trend of the dielectric constant of tissues is quite plain with frequency, i.e., they follow a linear trend

within the studied frequency range. One can consider these values like a line in order to simplify the resolution of the problem. Then, with just two points, the system can be characterised in the whole frequency band. Besides, the acetonitrile flatten the curves of the relative permittivity, so this approximation is suitable in this case as well. The choice was to select two frequencies near to the limits of UWB. The chosen ones are 4 and 8 GHz, which are near the limit points, i.e., 3.1 and 10.6 GHz. The procedure for obtaining the equations for those frequencies is the same that has been explained in sections 3.1 and 3.3 for 2.4 GHz. In this case, four equations are obtained, two for each frequency: Eq. 3.12 and 3.13 for 4 GHz, and Eq. 3.14 and 3.15 for 8 GHz.

$$\varepsilon'_r(c_{ACN}, c_{NaCl}) = \overbrace{-1.61}^{\text{slope}} \cdot c_{ACN} \overbrace{-9.60 \cdot c_{NaCl} + 74.12}^{\text{y-intercept}} \tag{3.12}$$

$$\varepsilon''_r(c_{ACN}, c_{NaCl}) = \overbrace{-0.76}^{\text{slope}} \cdot c_{ACN} \overbrace{+25.74 \cdot c_{NaCl} + 19.07}^{\text{y-intercept}} \tag{3.13}$$

$$\varepsilon'_r(c_{ACN}, c_{NaCl}) = \overbrace{-1.14}^{\text{slope}} \cdot c_{ACN} \overbrace{-8.9 \cdot c_{NaCl} + 62.52}^{\text{y-intercept}} \tag{3.14}$$

$$\varepsilon''_r(c_{ACN}, c_{NaCl}) = \overbrace{-1.23}^{\text{slope}} \cdot c_{ACN} \overbrace{+8.36 \cdot c_{NaCl} + 31.81}^{\text{y-intercept}} \tag{3.15}$$

All the previous four equations have to be solved in order to find out the required composition of acetonitrile and salt for mimicking the relative permittivity of a particular tissue. A system with four equations and two unknowns cannot be actually solved, so the solution for one frequency can be calculated and checked if the value match with the other frequency. Another way to calculate the result is to use a non-linear solving method with stopping conditions, in which the software tries to find out the optimal solution or the one that most approaches. The software starts iterations until it meets the conditions, either the pursued values or the stopping ones. If it is not possible to solve the system of equations for both frequencies, one can consider to obtain a better approximation in one of them in prejudice of the other. This may be useful for phantoms that are intended to work just on the low or high part of the frequency band.

3.4 Material Selection for Gel Phantoms

The reason for choosing semisolid phantoms instead of solid ones is the fact that they own the required consistence or stiffness to keep the shape of the mimicked tissue while they are able to hold huge amount of liquid. In fact, gels composition is mostly water-based, normally with around a 0.5-5% in weight of a polymer, like gelatin or agar. Natural polymers were initially discarded due to their poor durability and inability to be formed in the presence of solvents different from water. Although it is highly desirable that a gel storage the maximum amount of liquid, these drawbacks makes them bad candidates to be used as synthetic models. The solution proposed here is a synthetic polymer, like PAM or PHEA, which owns the ability to be swollen with a solvent according to their chemical affinity (see Section 2.1). Both of them storage large amounts of water when they are immersed, but they can also absorb different solvents or mixtures. The solution that emerge here is the possibility to make the gels absorb the phantoms made by the compounds that have been selected in Section 3.2, or at least with a variation in the percentages of these mixtures. Hence, a study of how these swell with the candidate mixtures needs to be pursued for subsequently choosing the most suitable polymer to create the gels.

Swelling Degree

As seen in Section 2.1, the way of characterising the percentage of liquid that a gel contains is the swelling index, which can be calculated with Eq. 2.1. The two aforementioned polymers, i.e., PHEA and PAM, were characterised in a swelling test in which these were immersed in water and in a 50% acetonitrile aqueous mixture until equilibrium (constant weight). For this experiment, five samples were used in order to calculate the average swelling degree and its standard deviation, whose results are shown in Fig. 3.16. As explained previously, apart from the chemical affinity, there are other factors that affect the swelling degree. One of the most important ones is the cross-linking degree, which can be tailored in an easier way than the chemical structure of the polymer. The methodology of synthesis of the gel included the choice of the cross-linking degree (see Section 2.2). The results from the gels shown below correspond to several cross-linking degrees, concretely from the minimum percentage that ensured non-solving up to 2%.

The PAM gel has an extraordinary capacity to absorb water inside, much higher than that of PHEA (see Fig. 3.16). However, the latter owns a better affinity with the acetonitrile mixtures, which are the pursued ones because of their promising characteristics for imitating the trend of the dielectric prop-

erties of tissues with frequency. This fact makes PHEA more suitable for gel phantoms. The following graph includes the results for the average swelling index from the gels at different cross-linking degrees, so the large deviation in the case of PAM is not representative of the variability between samples, but the range of values that the gel achieves by changing the cross-linker percentage. The disaggregated results for the PHEA gels are depicted in Fig. 3.17, where the values are separated according to the cross-linking degree of each sample group.

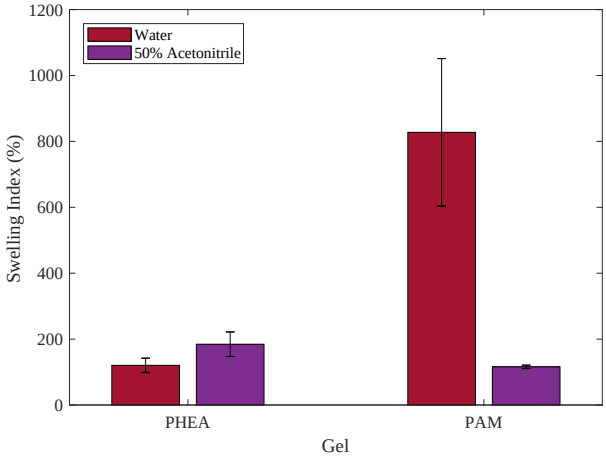

Figure 3.16: Average swelling index and standard deviation of the PHEA and PAM gels, swollen in water and in a 50% acetonitrile aqueous mixture.

One can appreciate the trend of the swelling degree with the cross-linking degree, which is descending with the increase of the latter. This was the expected behaviour of the gels, since a greater number of joining points in the network leads to smaller reticles so that the network is able to storage a lower volume. This influence is not as pronounced as the nature of the gel itself. For instance, the values attained with PAM cannot be obtained with PHEA even with the lowest cross-linker concentration. However, the tailoring capabilities that this offers can be really useful for obtaining the desired values of relative permittivity. For instance, the swelling index of PHEA, 0.2% cross-linked and swollen in water, can be obtained with the acetonitrile mixture (which normally has better swelling) by increasing the cross-linking concentration up to 2%. The fact that they both own the same amount of liquid does not mean they have the same relative permittivity.

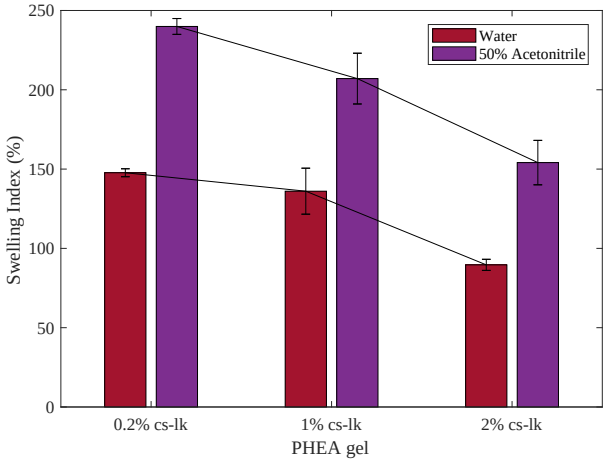

Figure 3.17: Average swelling index and standard deviation of PHEA gels, with different cross-linking degrees (percentages), when swollen in water and in a 50% acetonitrile aqueous mixture.

The key will be the slope or trend of the values with frequency, and that is changed by the acetonitrile concentration. Changing the amount of liquid that the gel is able to hold will only shift the values upwards or downwards in the graphs.

Mechanical Properties

As mentioned above, the purpose of choosing a synthetic gel instead of a natural one, apart from absorbing solvents different from water, is the better mechanical properties of the first ones. This is key in phantoms due to the requirements of keeping the shape of the tissue by themselves without any container. Thus, the mechanical properties need to be enough to ensure that the models stand on its own without breaking with ease. For this reason, the mechanical properties of PHEA were studied here by means of a compression test. This type of test was chosen because it was considered the most representative of the forces to which the models will be subjected, since they will have to bear their own weight. The studied variable was the break point, i.e., the strength that the sample is able to withstand. The first study is the comparison between the PHEA gel, cross-linked 1%, and two natural polymers that are commonly used for preparing phantoms: κ-carrageenan and agar. The three gels contained water inside, depending on the corresponding swelling degree of each one, being the naturals those with a greater moisture content. The results of the test for

ten replicates per material are depicted in Fig. 3.18, represented in a box-and-whisker diagram to show the variability of the measurements.

The resistance of the PHEA synthetic polymer is much greater than that of the other two polymers. The average ultimate strength is more than four times better in the case of PHEA with respect of κ-carrageenan, and around ten times better than that of the agar, the most used polymer in the literature. These results demonstrate the suitability of synthetic polymers for long-term models. Taking into account that the synthetic gels are made with different cross-linking degrees, which affect some physical properties like the swelling index, one could think that the strength they are able to bear also changes with this parameter. Moreover, the swelling mixture may play an important role in the mechanical properties. Because of that, the PHEA gel was studied with different cross-linking degrees and swollen in two different liquids, water and a 50% acetonitrile aqueous mixture, based on the candidate mixtures that will be used for imitating the human tissues. The results of these tests are shown in Fig. 3.19, also in a box-and-whisker diagram.

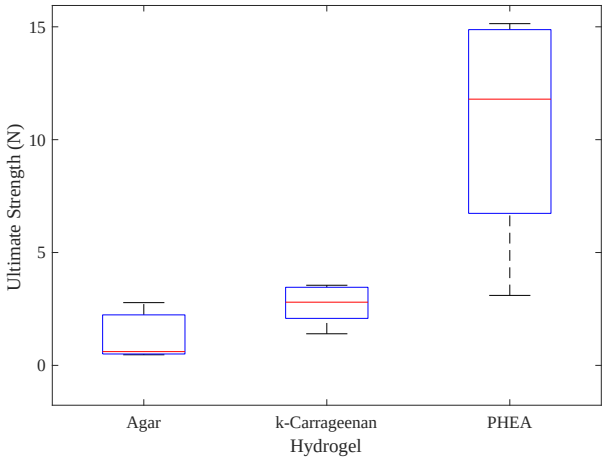

Figure 3.18: Box-and-whisker diagram of the ultimate strength for gels made of agar, κ-carrageenan and PHEA in water.

These results show that there is no significant difference among the results of the different sample. That means that the percentage of cross-linker added during the polymerisation or the liquid mixture in which the gel has been swollen is not relevant for the resistance of the final phantom. Thus, the amount of liquid that the polymer network holds can be controlled without hardly altering the strength that the final gel supports. Even thought the range of

values is very large, as can be appreciated with the whiskers of the diagram, the average ultimate strength is pretty high in all cases.

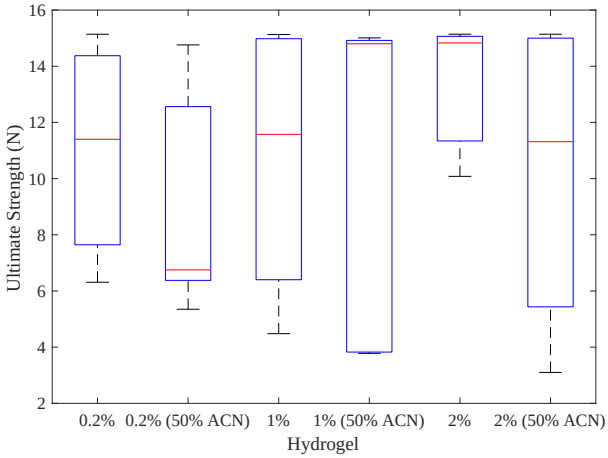

Figure 3.19: Box-and-whisker diagram of the ultimate strength for PHEA gels, swollen in water and in a 50% acetonitrile aqueous mixture, with different cross-linking degrees (percentages).

3.5 Gel Phantoms Design

Once seen that the cross-linking degree defines the swelling properties, it is time to analyse how the dielectric properties are affected by this behaviour, since the amount of liquid that the gel holds is directly related with the relative permittivity. In a mixture of materials with no interaction between them, the resulting effective relative permittivity is an intermediate between the values of both materials, according to the percentages each one represents. In the case of gels, it can be considered that there is the polymer network on the one hand, and the mixture on the other hand. The more the amount of liquid retains the network, the more similar to the mixture the effective permittivity will be. This effect can be used to tailor the range of values in which the dielectric properties fall. The manner to control this parameter will be the cross-linking degree, which increase decreases the swelling index. The effect of this variation can be observed in Fig. 3.20, where the relative permittivity of PHEA for three different cross-linking concentrations is plotted for comparison. The bars in the graph depict the standard error of the measurements.

The least swollen gels, i.e., those with a greater cross-linker percentage, show the lowest values of relative permittivity, in both the dielectric constant and the loss factor. The other way to achieve this reduction in the values is the addition of acetonitrile in the swelling mixture, whose permittivity is lower than that of water. However, this addition would lead to the increase of the amount of liquid that the polymer absorbs, and it makes the effective permittivity of the gel closer to that of the liquid. On the one hand, the acetonitrile mixtures reduce the relative permittivity, but on the other hand, a greater amount of liquid inside the network increases it, so both effects are compensated in a certain way. At low acetonitrile concentrations, the values are higher than water due to the increase in the swelling degree, that is later counteracted with the low permittivity of acetonitrile. This effect can be appreciated in Fig. 3.21, where the gel with a concentration of acetonitrile of 30% has higher loss values than water, but these drop considerably when this concentration is increased.

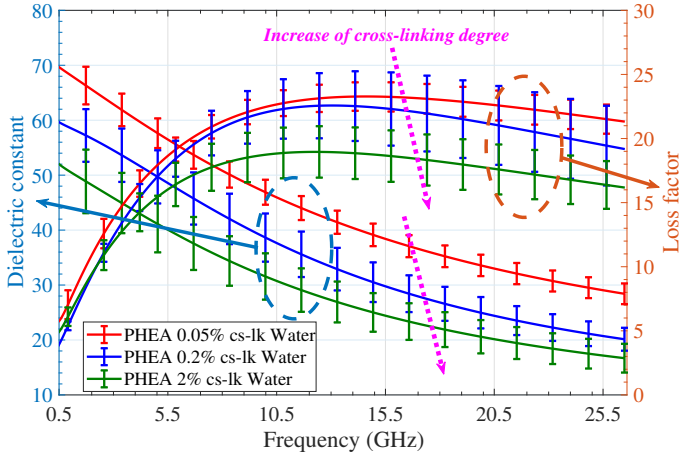

Figure 3.20: Relative permittivity of the PHEA gel, swollen in water, with different percentages of cross-linker.

These both parameters, the cross-linking degree and the percentage of acetonitrile in the mixture, can be combined for achieving the different target values and imitate the tissues on demand. However, there is a substantial difference between both methods. While increasing the acetonitrile concentration changes the slope of the dielectric constant because of its higher relaxation frequency (see Section 3.2), the increase of the cross-linking degree basically reduces the amount of liquid in the gel, and so the ratio with respect to the polymer. The latest just reduces the values of both parts of the relative per-

mittivity. Since these materials are based on hydrogels, these are more likely to imitate soft tissues.

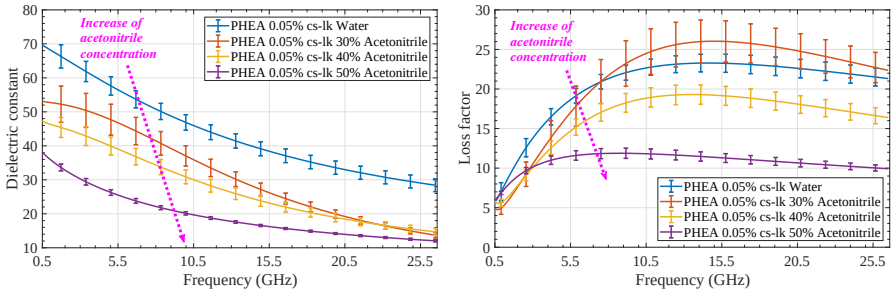

(a) Dielectric constant

(b) Loss factor

Figure 3.21: Relative permittivity of the PHEA gel, with a fixed cross-linking degree of 0.05%, swollen in different acetonitrile aqueous mixtures.

3.6 Printing Materials

The suggested solution for the case of the solid phantoms was to print the shape of the corresponding tissues with 3D FDM and then fill them with the liquid phantoms. Thus, a degradation test for the most common printed polymers was needed in order to check their suitability for this purpose. These were immersed in the degradation medium for different time periods, after which their mechanical properties were analysed. A 50% acetonitrile, 9% ethanol and 1% NaCl aqueous mixture was chosen as representative of the liquid phantoms. The polymers under study were the ABS, PLA and PP. The first two are the most commonly printed polymers through the FDM technique, whereas PP was chosen as reference of a non-degradable polymer, since it is very chemically resistant.

After being submerged for the time indicated, they were taken out of the vials and subjected to the tensile test. The results obtained by the equipment are of the type of those shown in Fig. 3.22, where those of a PP specimen are included as an example. The graph shows a typical stress-strain diagram where one can extract several interesting data, such as the elastic modulus (energy to elastically deform the material), the yield strength (after which there is non-reversible deformation), the ultimate strength (maximum stress the material withstand) or the fracture point. The value considered here are the ultimate strength (E), which is the maximum stress that the material can

withstand. The purpose was to examine if this value decreased after the sample was in contact with the degradation medium. The results for the three different polymers, before being immersed or suffer any degradation, are those shown in Fig. 3.23. One can see that their resistance is quite similar, with the PLA having the greatest variability.

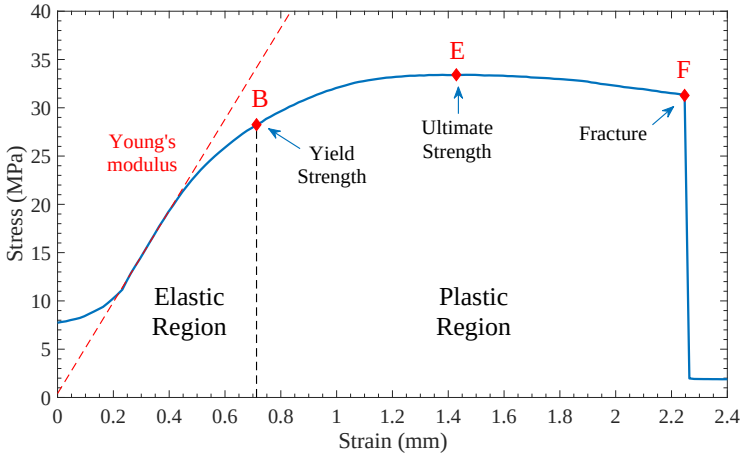

Figure 3.22: Stress-strain curve of a PP specimen after being immersed in the degradation mixture for 9 months.

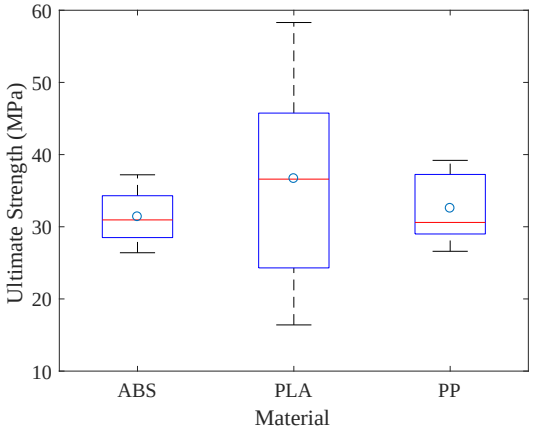

Figure 3.23: Box-and-whisker diagram of the ultimate strength for ABS, PLA and PP.

The ABS specimens were partially dissolved and softened after a few hours in the mixture, so that they lost their original shape. Thus, ABS was discarded for any further mechanical test or for printing the solid models. Furthermore, PLA samples were reduced in dimensions by around 15% after the first week and remained constant the rest of the time. PP specimens kept their shape intact during the whole degradation time, as expected. The results for the ultimate strength of the specimens of PLA and PP after the degradation procedure are those shown in Fig. 3.24 and 3.25.

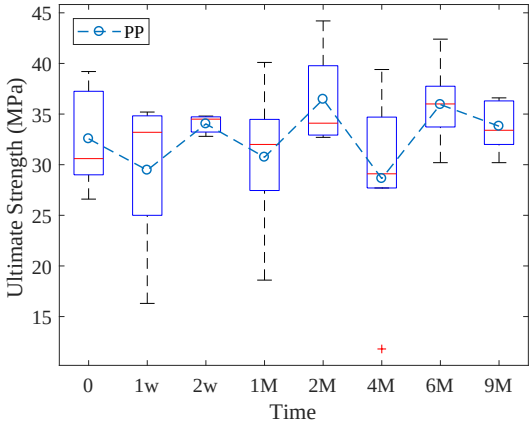

Figure 3.24: Box-and-whisker diagram of the ultimate strength for PP specimens, after being immersed in the degradation mixture for the indicated time.

There is not a significant variation in the PP properties after the 9 months that the degradation test lasted. On the contrary, results from the PLA show a drastic drop of its mechanical properties after the second month being in contact with the liquid. This means that the life time of a solid model with these features would be these two months. However, the initial size reduction should be taken into account before considering using this material for the tissue shape.

In conclusion, none of the most common 3D printing materials have been proven to be suitable to function as shell for the solid models. The ABS polymer didn't stand more than a few hours, whereas the PLA suffered a reduction in its size, unlike PP, which perfectly maintained its mechanical properties. However, PLA may be used for the models if one considers the reduction in the initial design. This material could storage the liquid phantoms continuously for at

least 2 months. Although if the container was filled and emptied after each experiment, it could last much longer.

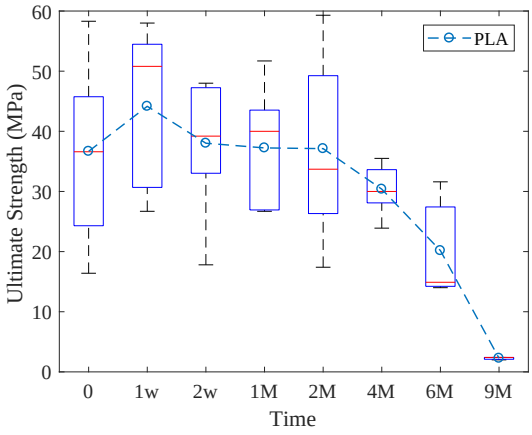

Figure 3.25: Box-and-whisker diagram of the ultimate strength for PLA specimens, after being immersed in the degradation mixture for the indicated time.

Chapter 4

Tissue Phantoms

The main purpose of this thesis is the development of synthetic models of the human body tissues in terms of their dielectric properties. In Chapter 3, an analysis of different materials that can be included in the phantoms composition has been pursued. Besides, the influence of the different compounds within the range of frequencies of interest was established. The formulas obtained then, were supposed to be useful in order to predict the required composition of the liquid mixtures. They are used in this section to calculate the weight percentages of the candidate compounds, either for narrow or wideband phantoms. The basic compounds are used just in the narrowband case due to their limitations for mimicking the trend of the dielectric properties of the tissues with frequency. The polar compounds are used in both, the narrow and the wide bands, since they own better tailoring capabilities.

4.1 Narrowband Models

4.1.1 Industrial, Scientific and Medical Band

Narrowband phantoms are, in theory, easier to create than the wideband ones, since they can be approximated to just one frequency, assuming that the dielectric properties barely change within the band boundaries. One of the most important bands, not just for the biomedical uses, but also for general purposes, is the non-licensed 2.4 GHz ISM band. Because of its relevance, this is inside the scope of the target phantoms, which may be useful in exposure or interference studies in everyday technologies as widespread as WiFi. As previously described in Section 3.1, the basic compounds used here, and in many of the reference works, are sucrose and salt. The salt is the sodium chloride,

which is used for rising the loss factor at the lowest frequencies of the studied band. It also causes a reduction of the dielectric constant at every frequency, since it does not change the relaxation frequency. However, sucrose is a better candidate to adjust the dielectric properties, because the salt increases losses too much, and the imaginary part is even more important than the real one regarding the influence in wireless communications. Certainly, what can be achieved with both compounds is highly limited. The range of values for the dielectric constant that can be achieved with those compounds at 2.4 GHz is comprised around 35 and 80 approximately. Human tissues own dielectric values lower than water, so it is necessary to add these compounds to reduce these. Making use of Eq. 3.8 and 3.9, which model the dielectric properties of aqueous mixtures with sucrose and salt, one can obtain the compositions listed in Table 4.1.

Table 4.1: Phantoms made of aqueous solutions of sucrose and salt for the 2.4 GHz ISM band compared to tissues values from Gabriel [3].

Tissue	**Composition**	**Dielectric constant**		**Loss factor**	
		Gabriel	**Phantom**	**Gabriel**	**Phantom**
Heart	39.2% Sucrose, 0% NaCl	54.92	53.13	16.60	16.92
Muscle	41.53% Sucrose, 0% NaCl	52.79	50.97	12.77	17.17
Pancreas	36.52% Sucrose, 0% NaCl	57.27	55.59	14.44	17.02
Liver	51.16% Sucrose, 0% NaCl	43.12	38.39	12.38	16.87
Colon	40.25% Sucrose, 0% NaCl	53.97	52.59	14.98	17.25

The tissues that were intended to replicate are the heart, muscle, pancreas, liver and colon, preparing the solutions of sucrose and salt with the calculated required composition. The results of the measurements of the dielectric properties are shown in Table 4.1. In no case was it possible to imitate the real and the imaginary part of the target simultaneously. Besides, the salt is not required in any case, since the loss factor is high enough in all cases. In fact, it should be reduced in most of them, but this is not possible with these kinds of solutions. Only the case of the heart is acceptable, with just two units less in the dielectric constant. The other approximations have higher deviations, mainly in the imaginary part. Even though the deviations in the real part are reasonable, those from the loss factor are not admissible, e.g., a 36.24% in the case of liver or a 34.46% for the muscle. Except from the heart, the rest of

the phantoms own deviations greater than 10% in the loss factor. This large deviation, even it is easier to adjust at one single frequency, is due to the physical impossibility to adjust the relative permittivity by using sucrose and salt exclusively.

Accordingly, there are also equations for the acetonitrile aqueous mixtures, which have been proved in Section 3.3 to be suitable for narrow bands as well, due to their tailoring possibilities. Their suitability lies especially in their ability to reduce the loss factor at 2.4 GHz, unlike the compounds that approach the peak of the loss factor to this frequency. The formulas that were obtained in the previous chapter for the 2.4 GHz ISM band are Eq. 3.10 and 3.11. In the same way as in the case of the basic compounds, these equations are used with the non-linear solving method with stopping conditions to calculate the required composition of acetonitrile and salt in the aqueous mixture (Table 4.2).

Table 4.2: Phantoms made of acetonitrile mixtures for the 2.4 GHz ISM band compared to tissues values from Gabriel [3].

Tissue	**Composition**	**Dielectric constant**		**Loss factor**	
		Gabriel	**Phantom**	**Gabriel**	**Phantom**
Heart	48.56% Acetonitrile, 1.24% NaCl	54.92	54.24	16.60	16.83
Muscle	55.05% Acetonitrile, 0.86% NaCl	52.79	51.94	12.77	12.78
Pancreas	44.48% Acetonitrile, 0.84% NaCl	57.27	56.54	14.44	14.39
Liver	50% Acetonitrile, 17.5% Ethanol, 1% NaCl	43.12	43.97	12.38	12.54
Colon	51.46% Acetonitrile, 1.08% NaCl	53.97	53.31	14.98	15.03
Cartilage	45% Acetonitrile, 30% Ethanol, 1.25% NaCl	38.88	38.39	12.86	12.95
Tongue	55.04% Acetonitrile, 0.92% NaCl	52.70	51.99	13.23	13.45

One only has to compare the results between the two previous tables to realise that the accuracy achieved with the polar compounds formulation, also valid for wide bands, is much better than that of attained with the basic compounds. The decision on which will be the suitable phantom for a particular experiment lies on requirements that one can have. For instance, the heart basic phantom can be valid in some situations and it is easier and more cost effective than the acetonitrile mixtures.

4.2 Ultrawideband Liquid Phantoms

Taking advantage of the analysis carried out in Section 3.3, one can make the empirical attempts to develop the wideband phantoms. The pursued tissues are mainly those of the torso due to their relevance in WBAN applications. The reference values used in order to replicate the dielectric values are those of Gabriel's work [3]. The equations obtained in the aforementioned section are deigned for 4 and 8 GHz, which are near the boundaries of UWB. As mentioned along the development of those equations, the dielectric constant of most of the tissues can be approximated to a line within the studied frequency range. Thus, it can be modelled with two points, which have been chosen to be these two frequencies. The equations that have been used for achieving the liquid phantoms for UWB are Eq. 3.12, 3.13, 3.14 and 3.15. These equations, and the samples that are prepared through them, are designed for 24 °C, but they are compared with the relative permittivity of the tissues at body temperature. Then, these phantoms will imitate the tissues within a real environment in which the human body is present in the communications.

Hereinafter, the wideband liquid phantoms that were synthesised are presented. In Fig. 4.1, there is the **muscle** phantom, which is probably the most important target to imitate due to its relevance in all kinds of tests. The required composition of this mixture is 54.98% acetonitrile and 1.07% NaCl. In this graph, one of the most used muscle phantoms is depicted as well [10], which has a very different trend with respect to the body tissues.

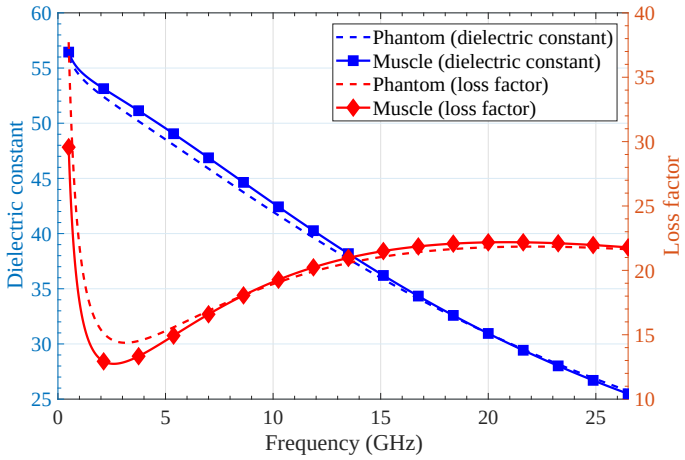

Figure 4.1: Relative permittivity of the liquid mixture of 54.98% acetonitrile and 1.07% NaCl, compared to the muscle values according to Gabriel [3].

One can see in the figure that the match is quite sound within UWB, i.e., from 3.1 to 10.6 GHz, but also beyond these frequencies. The trend is similar to that of the actual tissue, so it can be stated that it is suitable for mimicking the muscle in electromagnetic tests. Another important tissue, which is precisely key for pacemakers is the **heart**, and it is depicted in Fig. 4.2.

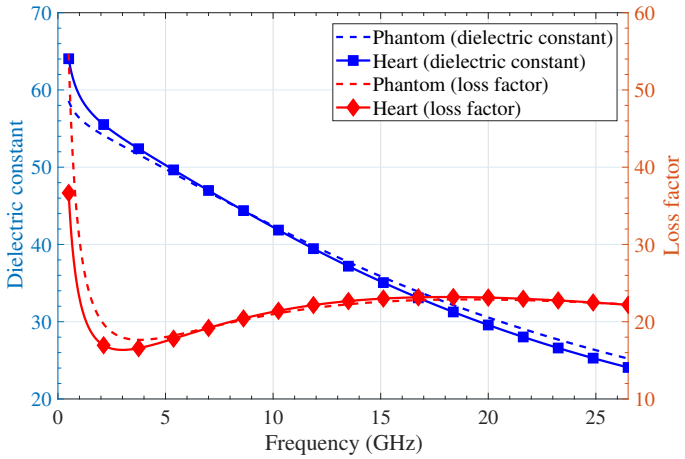

Figure 4.2: Relative permittivity of the liquid mixture of 49.94% acetonitrile and 1.58% of NaCl, compared to the heart values according to Gabriel [3].

This is another tissue with a high water content, so the composition is similar to the previous one. The difference lies in the fact that it owns a steeper slope than in the case of the muscle. The values of the heart tissue are higher than those of the muscle, that is why it requires less concentration of acetonitrile. The final composition is 49.94% of acetonitrile and 1.58% of NaCl, which is the calculated one from the equations. The increase of acetonitrile causes a reduction in the slope, so it deviates a bit from that of the reference tissue. It is not possible to change the slope of the dielectric constant by using only these three compounds because of their nature. The next tissue that was possible to adjust in a very approximate way was the **pancreas**, which is achieved by including 44.49% acetonitrile and 1.09% NaCl. The relative permittivity of this tissue is shown in Fig. 4.3.

Both parts of the relative permittivity have a similar trend and close values to those of the reference. The phantoms or tissues shown so far present similar compositions, with high values of relative permittivity, and all of them have great amount of water.

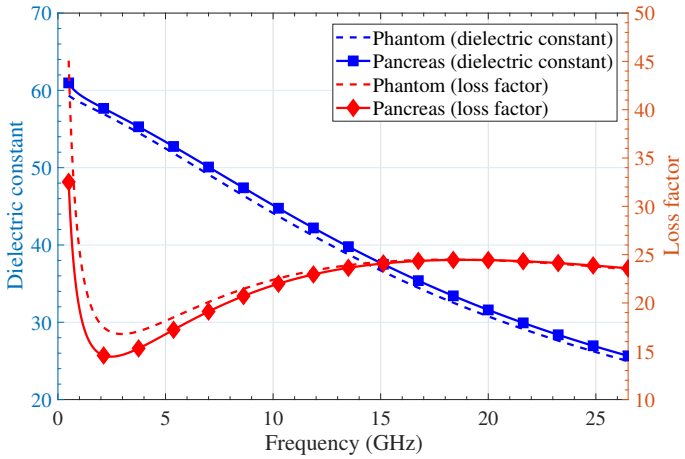

Figure 4.3: Relative permittivity of the liquid mixture of 44.49% acetonitrile and 1.09% NaCl, compared to the pancreas values according to Gabriel [3].

The problem of the addition of acetonitrile is that when the concentration is too high, the trend is excessively flat due to the high relaxation frequency, moving away from the natural one of tissues. One solution for these cases where the slope needs to be increased is the addition of a third polar compound with a lower relaxation frequency. This extra component can be ethanol, which has a relaxation frequency of 976.41 MHz [61], and is miscible in water and acetonitrile, so they can be combined. It allows the preparation of phantoms with lower values of relative permittivity, since its dielectric constant is around 6 at 3 GHz, and it is quite stable with frequency. One example of the results that can be obtained with this combination is the **colon** phantom, in which just a 2.5% of ethanol is enough to improve the slope ant match that of the actual tissue. The calculated composition with the equations was 52.29% acetonitrile and 1.42% NaCl, from which ethanol was added until reaching a final composition of 48.5% acetonitrile, 2.5% ethanol and 1.165% NaCl. The dielectric properties of the phantom of the colon tissue are depicted in Fig. 4.4 compared to the reference values.

The procedure to obtain this phantom was to first calculate the composition without ethanol, with the equations, and then add progressively ethanol until reaching the required trend of the dielectric constant. The influence of the ethanol gets a slope similar to that of the reference tissue without changing values of the relative permittivity substantially. Adding greater amounts of ethanol would lead to lower values of the dielectric constant that are not

possible to achieve by using only acetonitrile, water and NaCl. However, its influence is not considered in the equations used above so, it has to be manually adjusted. This requirement of trial and error testing limits the equations to orientation purposes, since a high concentration of ethanol changes the permittivity a lot.

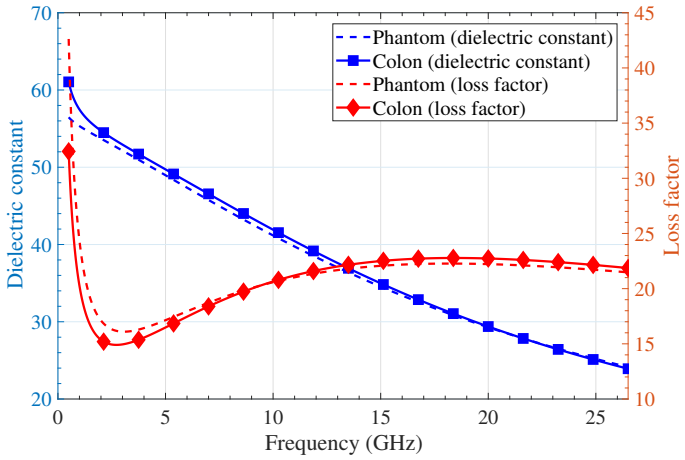

Figure 4.4: Relative permittivity of the liquid mixture of 48.5% acetonitrile, 2.5% ethanol and 1.165% NaCl, compared to the colon values according to Gabriel [3].

In summary, acetonitrile and ethanol reduce the dielectric constant of the water at every frequency, but the ethanol in a greater way. Regarding its slope, the acetonitrile decreases it whereas the ethanol increase it, so they have opposite behaviours. Regarding the loss factor, on the one hand, acetonitrile decreases it at within the whole studied frequency range and flatten the curve. On the other hand, ethanol increases the loss factor and shift the peak of losses to the studied band, that is why one cannot include a huge percentage of ethanol without bringing this peak to the frequencies of interest.

Next result is the **liver** phantom, which was achieved by this trial and error approach from the calculated composition, including the ethanol in its formulation. The required concentrations in this case is 51% acetonitrile, 17% ethanol and 0.95% NaCl. The graphs of both parts of the relative permittivity are depicted in Fig. 4.5. Ethanol helps here to lower the values of the dielectric constant that would require high concentrations of acetonitrile. Besides, it matches perfectly the trend of the liver tissue. Trying to imitate this tissue just with the acetonitrile is not possible because of the trend, which would be too flat with respect to the actual tissue.

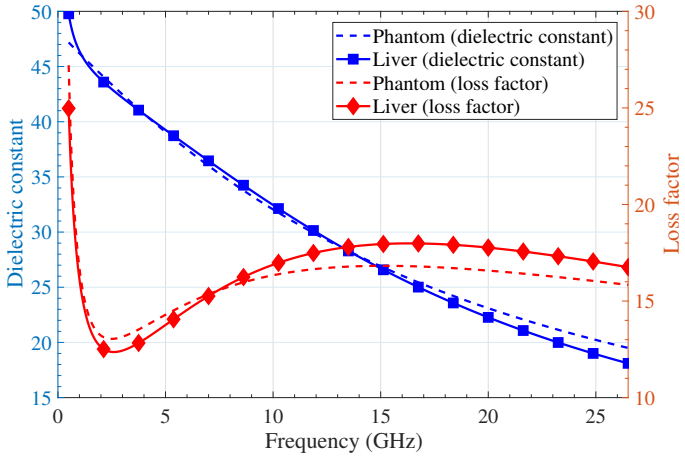

Figure 4.5: Relative permittivity of the liquid mixture of 51% acetonitrile, 17% ethanol and 0.95% NaCl, compared to the liver values according to Gabriel [3].

Another tissue that requires an important amount of ethanol to reach its values is the **cartilage**, which despite being one high water content tissue owns lower values than the average of the region. On this occasion, the required composition is 41% acetonitrile, 30% ethanol and 1% NaCl, whose values are shown in Fig. 4.6.

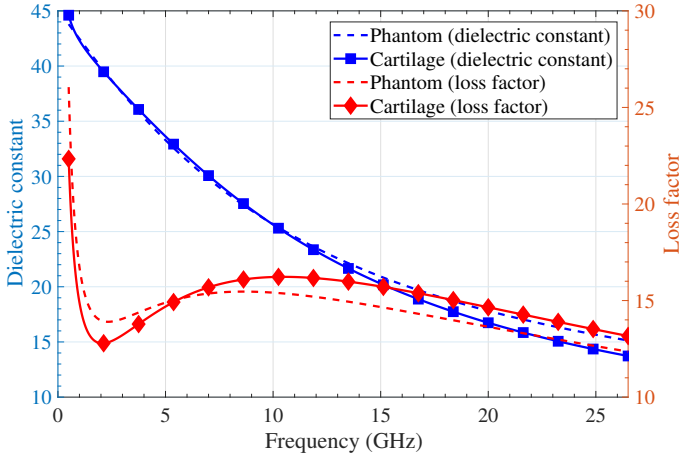

Figure 4.6: Relative permittivity of the liquid mixture of 41% acetonitrile, 30% ethanol and 1% NaCl, compared to the cartilage values according to Gabriel [3].

This tissue has a loss factor quite similar to that of the liver (see Fig. 4.5), but different values in the dielectric constant. Thanks to the addition of ethanol it is possible to keep the loss factor within the range of values and also the trend with frequency, and at the same time shift the values of the real part to the lower values of cartilage. The **skin** is another tissue that is also under the average value of dielectric constant from high water tissues. Then, ethanol is also required here to imitate these values. Concerning the skin tissue, Gabriel's report [3] includes two types: dry and wet. The difference remains in the fact that the first one was measured after excision and loss of moisture and the latter after immersion in water [9]. The one achieved here is the wet one, which is closer to the tissues with high water content. The results of this phantom are shown in Fig. 4.7.

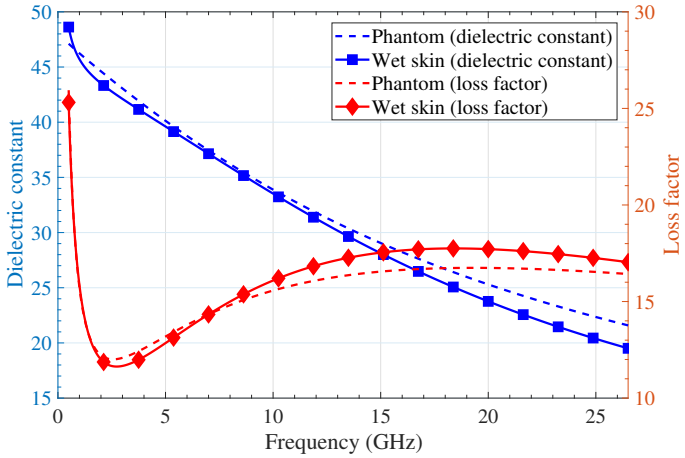

Figure 4.7: Relative permittivity of the liquid mixture of 57% acetonitrile, 13% ethanol and 0.9% NaCl, compared to the wet skin values according to Gabriel [3].

The composition to achieve this phantom is 57% acetonitrile, 13% ethanol and 0.9% NaCl. The ethanol adjusts the trend of the dielectric constant until matching the actual one from reference. The **grey matter** also has lower values that are a bit far away from the average ones, and needs the addition of a significant amount of ethanol, but not as much as in the previous tissue. This phantom is prepared with 50% acetonitrile, 10% ethanol and 1% NaCl, and it is depicted in Fig. 4.8.

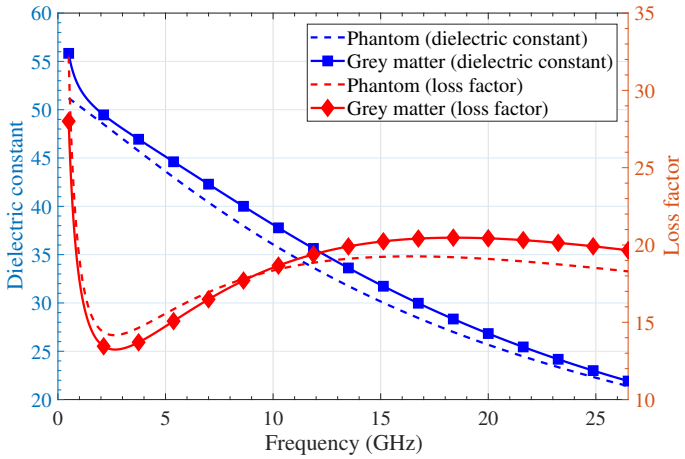

Figure 4.8: Relative permittivity of the liquid mixture of 50% acetonitrile, 10% ethanol and 1% NaCl, compared to the grey matter values according to Gabriel [3].

Besides, there are the tissues that just need a little amount of ethanol to tune the slope of the real part of the relative permittivity. This is the case of the **kidney** and **cornea**, both with just 1% of ethanol on their formulations. The kidney phantom is made with a composition of 50% acetonitrile, 1% ethanol and 1.5% NaCl, and it is depicted in Fig. 4.9. The cornea phantom is shown in Fig. 4.10, with 49% acetonitrile, 1% ethanol and 1.5% NaCl.

Both phantoms, cornea and kidney, differ only in 1% of acetonitrile in their composition, since both have similar dielectric properties. Sometimes, the tissues with a high water content are so similar in terms of dielectric properties that their composition almost match. However, the tailoring capabilities of these polar mixtures is high that can be fine-tuned with precision. Finally, the tissue with the highest dielectric values from those pursued was the **blood**, whose results are drawn in Fig. 4.11.

This is not actually a tissue, but is key in the effect that the body can produce over the electromagnetic signals, especially in some areas like the heart, which is crucial in pacemakers. It does not require, thus, a significant amount of acetonitrile in the composition, which remains with 40% acetonitrile and 1.25% NaCl. The compositions of all the phantoms presented so far are summarised in Table 4.3, together with their deviation from the reference values from [3] in RMSE. Coming back to the state of the art (see Section 1.4), particularly in Table 1.1, one can compare the deviation of the suggested phantoms here and those reported in the literature for similar frequency bands.

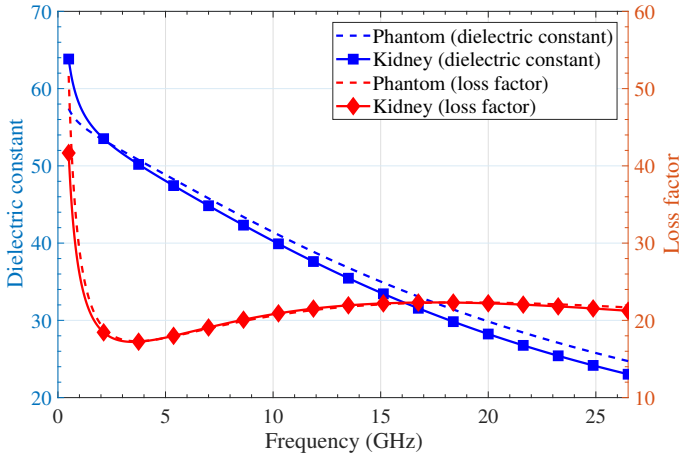

Figure 4.9: Relative permittivity of the liquid mixture of 50% acetonitrile, 1% ethanol and 1.5% NaCl, compared to the kidney values according to Gabriel [3].

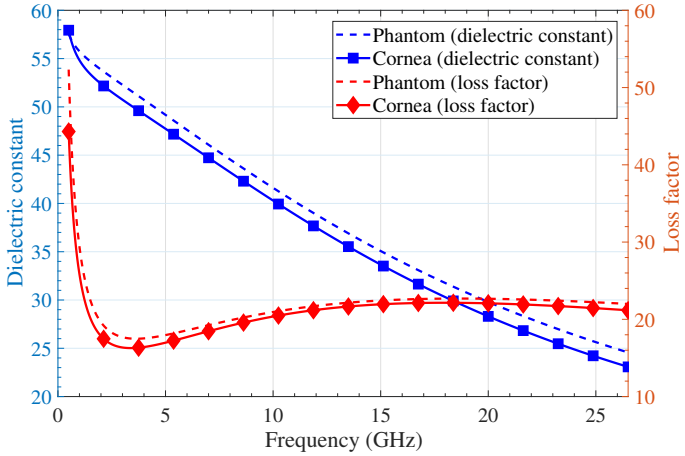

Figure 4.10: Relative permittivity of the liquid mixture of 49% acetonitrile, 1% ethanol and 1.5% NaCl, compared to the cornea values according to Gabriel [3].

The accuracy obtained with the proposed model of mixtures, with polar compounds and sodium chloride for the loss factor at low frequencies, is high in all cases. Comparing the RMSE values with those obtained from the literature, one can observe that these are generally lower. There are some cases where one of the parts (real or imaginary) is better to the detriment of the other one.

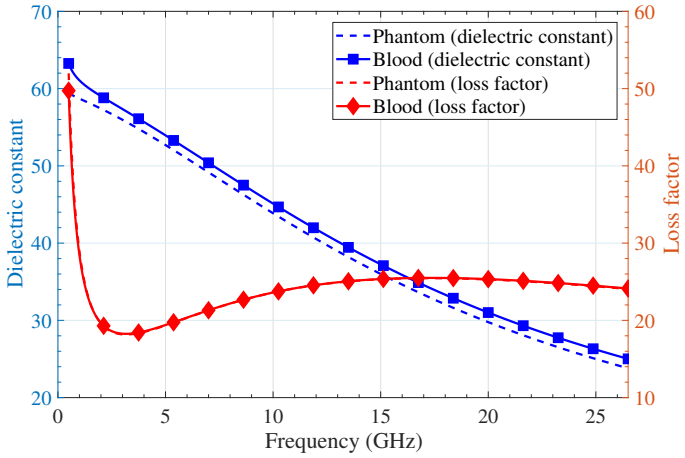

Figure 4.11: Relative permittivity of the liquid mixture of 40% acetonitrile and 1.25% NaCl, compared to the blood values according to Gabriel [3].

This does not happen with the phantoms presented in Table 1.1, where the deviation is well balanced between both of them. In addition to that, the number of mimicked tissues has been enlarged, since there are tissues that have not been presented until now, at least for this frequency band. Certainly, the number of tissues can be further enlarged, but the scope of this thesis was the torso or abdominal region due to its relevance in the propagation medium. Of course, one has to consider that the region that these models are able to imitate is limited to the high water content tissues, since the values are generally high. Other tissues like the fat or bone require different kind of compounds, with less polarisation capabilities, like polymers or big molecules (see Section 1.2).

These low water content tissues are equally important for some applications, and cannot be placed outside the scope of this thesis. This issue is properly addressed in [18], where authors suggest emulsions made of water and oil to adjust the dielectric properties. As already explained, water is a molecule with high polarisation features, just the opposite as oil, which is composed of all kinds of hydrocarbons, mostly with long chains, like polymers. Then, the proportion between these two compounds is adjusted according to the target values. Water is added with the aim of increasing the relative permittivity of the phantom, and oil to decrease it. The problem with these compounds is the fact that they are not miscible between them because of their different nature (water is polar and oil is non-polar).

Table 4.3: Phantoms composition along with their corresponding RMSE values for real (Re) and imaginary (Im) part, compared with the reference values from Gabriel's report [3].

Tissue	**Phantom composition**	**RMSE (Re/Im)**
Muscle	54.98% Acetonitrile, 1.07% NaCl	1.17/1.6
Pancreas	44.49% Acetonitrile, 1.09% NaCl	1.25/1.86
Liver	51% Acetonitrile, 17% Ethanol, 0.95% NaCl	0.9/1.11
Colon	48.5% Acetonitrile, 2.5% Ethanol, 1.165% NaCl	1.07/1.42
Kidney	50% Acetonitrile, 1% Ethanol, 1.5% NaCl	1.77/1.34
Grey matter	50% Acetonitrile, 10% Ethanol, 1% NaCl	1.7/1.34
Cornea	49% Acetonitrile, 1% Ethanol, 1.5% NaCl	1.64/1.45
Blood	40% Acetonitrile, 1.25% NaCl	1.59/0.82
Wet skin	57% Acetonitrile, 13% Ethanol, 0.9% NaCl	1.3/0.88
Cartilage	41% Acetonitrile, 30% Ethanol, 1% NaCl	0.91/1.02
Heart	49.94% Acetonitrile, 1.58% NaCl	1.4/2.26

The solution the authors take is to solidify the mixture by adding gelatin and formaldehyde in a way that the phantom remains more stable in time and does not split in two phases. However, most of the in-body characterisation tests require liquid phantoms in order to place and move freely the antennas inside the phantom and analyse different positions. Because of that, taking the main components of the aforementioned phantom, a liquid version can be obtained, changing the gelling agent by a surfactant, the Triton X-100 (Sigma-Aldrich). It allows the mixture of water and oil with just adding a 1% in

the composition and stirring it during some minutes. After some trials, the recipe was left in two emulsions of 80% and 86% of oil in water, which imitate the infiltrated and non-infiltrated fat respectively. The results of the dielectric measurements, as well as the comparison with the reference values is shown in Fig. 4.12.

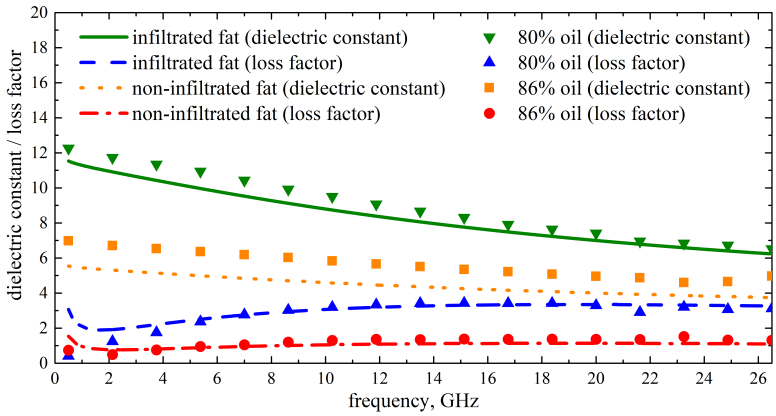

Figure 4.12: Relative permittivity of the proposed emulsions for imitating the infiltrated and non-infiltrated fat according to Gabriel [3].

Results presented in Fig. 4.12 are in good agreement with those of the reference. The MSE values were calculated for these phantoms in order to make a comparison with the accuracy of the reported one in [21], where the authors prepared a semisolid fat phantom based on the composition of [18]. In this work, they present a phantom of non-infiltrated fat, from 0.2 to 20 GHz, with MSE values of 0.21 and 0.29 S^2/m^2 for the real and imaginary parts, respectively. The results for the suggested liquid fat phantoms here are 0.42 and 0.14 S^2/m^2 for the infiltrated fat, and 1.32 and 0.7 S^2/m^2 for the non-infiltrated one. One can appreciate that the errors are low and similar in both cases, so it is possible to choose between a liquid or a gel type and preserve the good approximation in the dielectric values. The advantage of the liquid phantom is the fact that it is more suitable for in-body propagation studies. However, one has to take into account that the durability of these phantoms, either emulsion or gelatin type, is not going to be good for long times. In spite of adding the surfactant, the time is limited to some hours, and the same for the semisolid phantom, which loses liquid and ends up breaking, not to mention how its properties will change. Nevertheless, these phantoms can be made relatively easily and are inexpensive.

In conclusion, the liquid models presented here have been proven to be excellent to replicate the dielectric properties of several tissues within a wide bandwidth. Besides, the accuracy of most of the phantoms is increased with regard of that of the literature, or at least improves the bandwidth they achieve. Thus, these phantoms can be used for testing any kind of microwave application in current and future technologies that make use of different large and simultaneous bands. They cover a great number of frequencies that are being considered for the upcoming mobile communications.

4.3 Ultrawideband Synthetic Gels

The guidelines given in Section 3.5 were followed in order to obtain the dielectric properties of several tissues within the studied frequency range. Those specially pursued were the soft tissues, since they are the most relevant in the main propagation scenarios. The tissues from the outermost layers were also a target because of the exposure assessment tests. All of them have an important moisture content, so the values to imitate will be high as well. Thus, the liquid content of the phantom gels is supposed to be elevated. One has to take into account that gels are susceptible to moisture loss though diffusion into air, and this would change drastically their dielectric properties. Thus, it is highly advisable to cover them even with a thin plastic film when they are not being used or swell them up again before any reuse if they are exposed. These gels can be dried and swollen again reversibly without degradation because of their synthetic nature. Besides, they own a high durability in time, up to several months or even years. Listed below are the candidate gels for several tissues that have been mimicked according to Gabriel's reference [3]. As explained in Section 2.3, semisolid materials are difficult to measure with the open-ended coaxial method. Their deformation capacity affects the measured relative permittivity of the material with this technique. Because of that, the measured values are not so stable as with the liquids, in which only the two curves depict the actual relative permittivity. In this case, the variability of the values must be considered and shown with the measurements. The curves, subsequently, are here accompanied by a shaded are that represents their standard deviation.

The measurements were carried out from 0.5 to 26.5 GHz, which was the full measurement range of the setup, again the Keysight N9918A FieldFox Handheld VNA and the Keysight 85070E slim-form probe. However, it can be noticed that there is a significant difference between the values from the gels and those of the reference under around 2 GHz. Hence, it was considered that the phantoms are actually valid from this frequency up to the limit. They could be improved within this particular region by adding a salt to the swelling mixture,

taking into account that this would probably affect the swelling index due to the water activity (see Section 2.1). The highest part of the frequency spectrum does follow the trend of the reference, which suggests that these phantoms may match the dielectric properties of the tissues at further frequencies.

Regarding the tissue phantoms, it was found that a concentration of 1% of cross-linker in the initial polymerisation solution was suitable to imitate tissues with a mid-range water content. The first tissue to be imitated was the cerebellum, which was achieved with 1% cross-linked PHEA, swollen in a 40% acetonitrile aqueous mixture, whose results can be seen in Fig. 4.13. The same type of gel, but this time swollen in a 60% acetonitrile mixture. This increase in the acetonitrile concentration is useful to reduce the values of the dielectric constant to the levels of the skin tissue, which is a relevant tissue for exposure assessment tests, mainly at high frequencies where the penetration depth is low. The comparison between this gel and the real tissue values can be observed in Fig. 4.14. The slope is better rendered with this last phantom, even though the values are a bit lower than those of the reference.

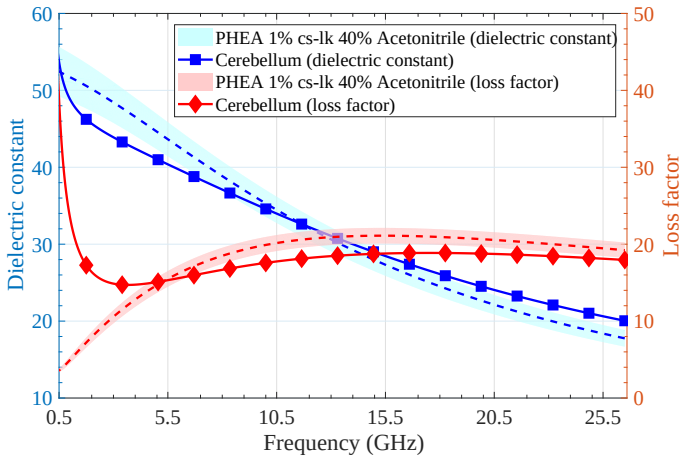

Figure 4.13: Relative permittivity of the PHEA gel, with a cross-linking degree of 1%, swollen in a 40% acetonitrile aqueous mixture, compared to the cerebellum values according to Gabriel [3].

A bit different case is the liver, which has a more pronounced slope in the dielectric constant than the previous tissues. Herein, the addition of acetonitrile is meaningless, since it causes the opposite effect to the slope, and water should be used instead. It will affect the swelling degree, which will be smaller with water (see Fig. 3.16), and so the values of the relative permittivity.

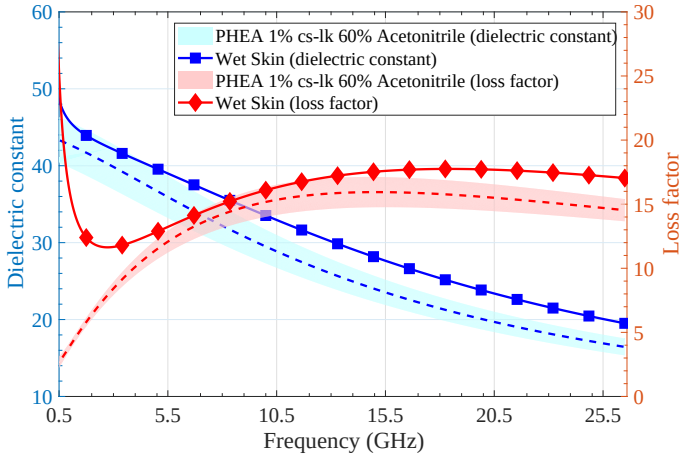

Figure 4.14: Relative permittivity of the PHEA gel, with a cross-linking degree of 1%, swollen in a 60% acetonitrile aqueous mixture, compared to the wet skin values according to Gabriel [3].

The increase in water concentration leads to a steeper slope, whose maximum will be limited precisely by that of the water. Once the slope of the dielectric constant has matched the target one, i.e., that of the reference, the best way to get closer to the values is to change the cross-linking degree, which does not affect the trend of the values with frequency. The liver phantom, together with its reference values, can be appreciated in Fig. 4.15. It has been attained with a PHEA gel, cross-linked at 1% and swollen in water.

There is another way to create a steeper slope in the dielectric constant of the gels that require high values, which is to reduce the cross-linker concentration so that the network absorbs more liquid and then reduce the values and slope by adding acetonitrile. An example of this approach can be found in Fig. 4.16, where the tendon tissue has been imitated with a PHEA gel, cross-linked at 0.2% and swollen with a 60% acetonitrile mixture. This tissue may be useful for researchers that study the heat impact over the tendon in ankle wearables.

It is also possible to reduce more the cross-linking degree in order to increase the liquid content of the gels and then imitate tissues with higher water content. The lowest concentration of cross-linker that can be used to ensure that a non-soluble network is obtained, was 0.05%, and the phantom with the highest target values from those pursued was the colon, whose results are shown in Fig. 4.17, where water is the only swelling liquid. The attained values are even higher than those of the colon, but the trend is replicated properly.

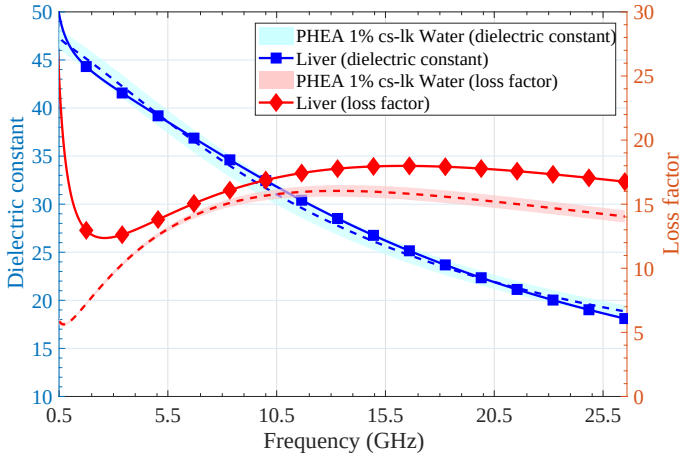

Figure 4.15: Relative permittivity of the PHEA gel, with a cross-linking degree of 1%, swollen in water, compared to the liver values according to Gabriel [3].

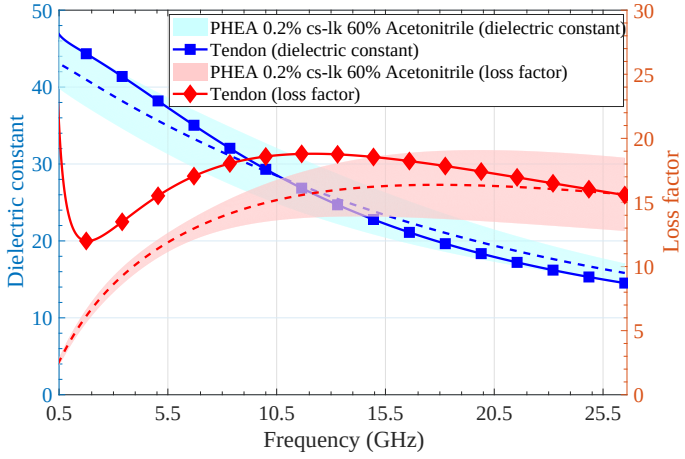

Figure 4.16: Relative permittivity of the PHEA gel, with a cross-linking degree of 0.2%, swollen in a 60% acetonitrile aqueous mixture, compared to the tendon values according to Gabriel [3].

One feature that may be seen like a drawback of these gels is the fact that they hold less water than the natural ones. They have worse mechanical properties because of that, certainly. However, these synthetic gels achieve levels of liquid content that are sufficient to imitate soft tissues.

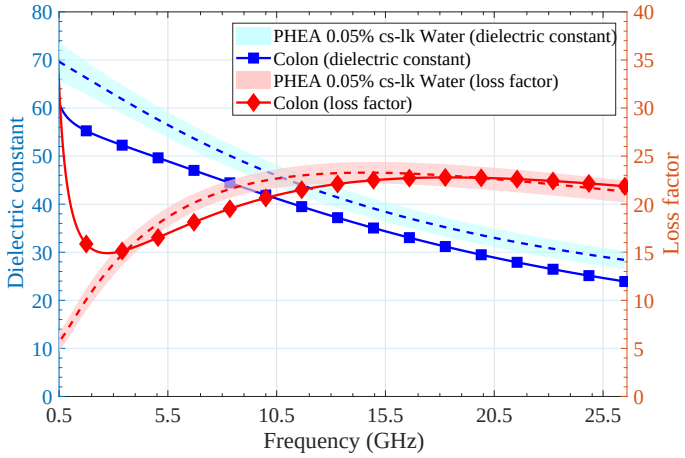

Figure 4.17: Relative permittivity of the PHEA gel, with a cross-linking degree of 0.05%, swollen in water, compared to the colon values according to Gabriel [3].

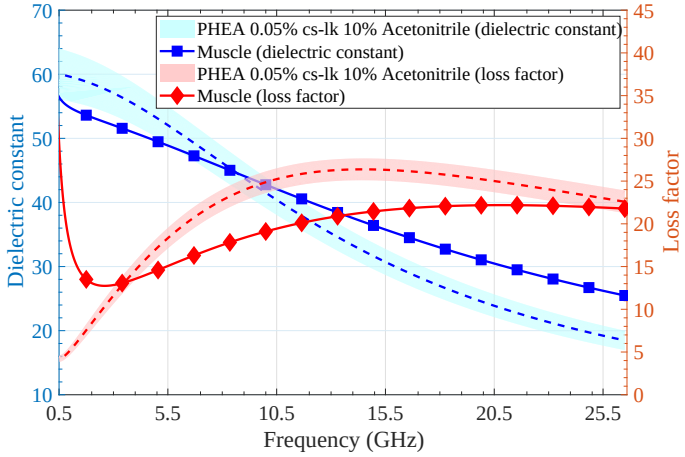

Figure 4.18: Relative permittivity of the PHEA gel, with a cross-linking degree of 0.05%, swollen in a 10% acetonitrile aqueous mixture, compared to the muscle values according to Gabriel [3].

The muscle tissue is quite similar to the colon, with a similar range of values. However, they have different values of loss factor, which is around ten units lower in the case of the muscle. Keeping the values of the dielectric constant while the loss factor is changed is not an easy task, considering that

both parameters are not independent, i.e., they are related. Taking this into account, the muscle phantom requires to lose a bit of accuracy regarding the slope in the dielectric constant with the aim of improving the matching in the loss factor. This effect can be obtained by using the same cross-linked gel than before, but this time by adding acetonitrile in the swelling mixture. The results of this gel are shown in Fig. 4.18, where the PHEA is swollen in a 10% acetonitrile mixture and is compared to the values of the muscle tissue.

Another tissue that can be crucial because of its relevance in the ear is the cartilage. It is mainly exposed to the radiation of mobile phones, so surely this is an issue that will be assessed. Cartilage can be mimicked with these kinds of gels by including a 40% of acetonitrile in the mixture, so that a good approximation is obtained, both in terms of values and trend of the dielectric properties. The results from this gel can be observed in Fig. 4.19.

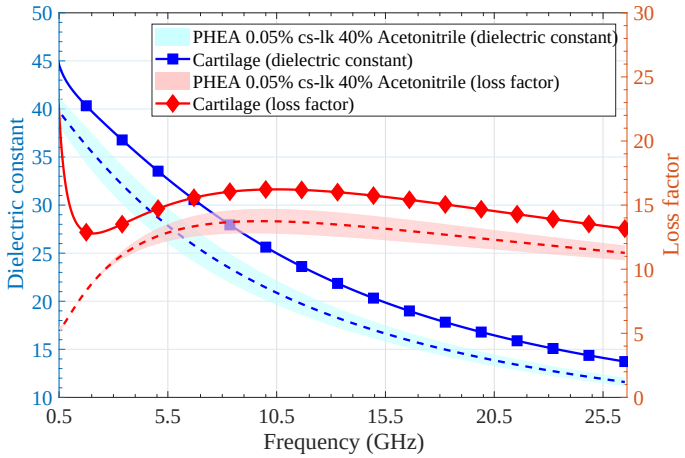

Figure 4.19: Relative permittivity of the PHEA gel, with a cross-linking degree of 0.05%, swollen in a 40% acetonitrile aqueous mixture, compared to the cartilage values according to Gabriel [3].

The last tissue phantom is the nerve, which is depicted in Fig. 4.20. The gel that better reproduces the dielectric properties of this tissue is the PHEA, cross-linked at 0.05% and swollen with a 50% acetonitrile aqueous mixture. The relevance of this tissue could be found in the fact that it is the main component of the nervous system. Researchers may be interested in assessing the influence of the continuous exposure of this body region to the electromagnetic radiation.

All the phantoms shown above have been measured in the whole frequency range regardless the applications or the bands they are supposed to work in, since this feature can change with time because of technology. There are com-

munication scenarios that have evolved over time. For instance, currently the in-body propagation channel does not exceed the 800 MHz band, but this will probably change with the UWB technology. The compositions for all the mentioned phantoms as well as their RMSE values (from 2 up to 26.5 GHz) are summarised in Table 4.4.

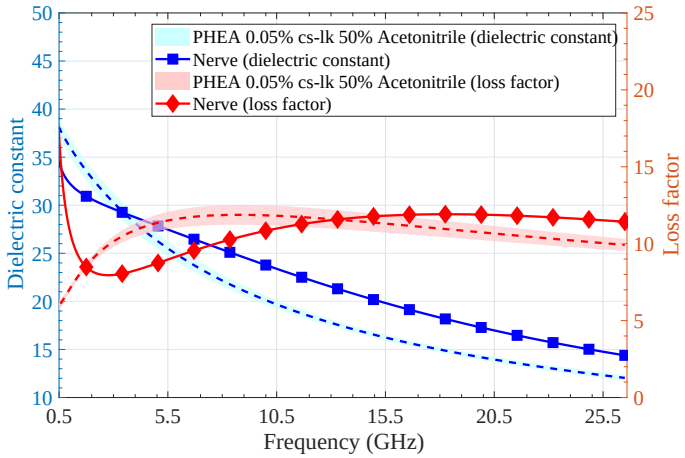

Figure 4.20: Relative permittivity of the PHEA gel, with a cross-linking degree of 0.05%, swollen in a 50% acetonitrile aqueous mixture, compared to the nerve values according to Gabriel [3].

These values can be useful to make a comparison between the results obtained here and those from the literature that have a similar frequency range and report the deviation from the reference. As an example, the skin reported in [21] has a RMSE of 2.62 for the real part and 2.44 for the imaginary one. The accuracy of this reference is better in the real part than the one presented here, but this is at the expense of the narrower bandwidth (until 20 GHz) and the weaker mechanical properties because of the gelatin composition. Another model of this tissue is also presented in [26], where Garrett and Fear achieve a 10% of relative error in the real part and 21% in the imaginary one, in the best case. Both deviations are larger than the ones suggested here, even though the skin phantom presented there reaches just up to 10 GHz. Other authors prepare a liver phantom in [27], where they attain a RMSE of 8.55 for the dielectric constant and 5.49 for the loss factor, quite worse than those presented here in both cases.

Table 4.4: Composition of the synthetic gel phantoms along with their corresponding RMSE values for real and imaginary part, compared with the reference values from Gabriel's report [3].

Tissue	Phantom composition	RMSE (Re/Im)
Cerebellum	PHEA with 1% of cross-linker swollen in a 40% acetonitrile aqueous mixture	2.23/2.32
Wet Skin	PHEA with 1% of cross-linker swollen in a 60% acetonitrile aqueous mixture	3.63/1.97
Liver	PHEA with 1% of cross-linker swollen in water	0.55/2.12
Tendon	PHEA with 0.2% of cross-linker swollen in a 60% acetonitrile aqueous mixture	1.63/2.84
Colon	PHEA with 0.05% of cross-linker swollen in water	5.59/1.26
Muscle	PHEA with 0.05% of cross-linker swollen in a 10% acetonitrile aqueous mixture	5.00/3.97
Cartilage	PHEA with 0.05% of cross-linker swollen in a 40% acetonitrile aqueous mixture	3.62/2.35
Nerve	PHEA with 0.05% of cross-linker swollen in a 50% acetonitrile aqueous mixture	3.01/1.46

Besides, the reported phantom is more solid rather than semisolid. Moreover, a muscle phantoms is presented in [21], with a better approximation than the one reported here, which is a RMSE of 4.6 in the case of the real part and 2.49 in the imaginary one. However, this phantom owns a loose structure, again because of the gelatin material.

In conclusion, the gels presented here have the novelty of being tailorable to control the liquid content and absorb different mixtures in addition to the water. This fact allows the use of acetonitrile in the swelling mixture, which has been proven in Section 4.2 to be suitable for mimicking body tissues in large bandwidths. The possibility to control the swelling degree by means of the cross-linker concentration can make them absorb from high percentages of liquid to a little water content, in a way that it could be used for tissue such as bones or fat. Another important feature from these gels is their mechanical resistance, which is much better than natural polymers, and more stable chemically in general. As explained above, like any kind of gel, there is a

matter transfer between the air and the liquid that causes dehydration. This phenomenon may be avoided by covering the gel with a thin plastic film of a few microns of thickness. Anyway, these can be reversibly dried and swollen again, so in case of evaporation of the content they can be immersed in the liquid mixture. The combination of the different gels, mimicking different tissues, can bring researchers the choice to study the propagation or assess the exposure in complex heterogeneous environments that replicate the human body in an accurate way. Their main advantage is the fact they imitate several tissues in a wide frequency band, so that they can be used to assess different technologies at once in laboratory tests.

4.4 5G New Radio Frequency Range 2

The phantoms suggested in the previous section are focused on the frequency bands of the current mobile communications services, but not on the upcoming 5G systems. Some of the bands that will be used in this new technology are placed at high frequencies, in which the propagation losses increase and the influence of the body is greater than in the current bands. Taking into account the health concerns, the International Commission on Non-Ionizing Radiation Protection (ICNIRP) establishes the guidelines of the exposure limits that should not be exceeded in terms of absorbed radiation [64]. There are tests that deal with accomplishing these limits by measuring the energy absorbed by a particular region of the body when it is exposed to certain devices. The parameter that quantifies this exposure is normally the SAR [4], which is given in W/kg and averaged for 1 or 10 gram of a body tissue. Manufacturers are called upon to meet the regulations considering the incident power density. Most of the phantoms that are designed and sold for these particular tests are narrowband or own weak approximations (see Table 1.1), since finding a suitable material to imitate large bandwidths is challenging. The problem with current SAR measurements is that there is no possibility to assess the effect of multiple technologies working at once or multi-carrier communications, since the phantom needs to be changed for each single frequency. Regarding the frequencies above 26.5 GHz, these are now covered by the phantoms presented in Table 4.3 with a great accuracy. The standard for upcoming technologies such as 5G communications is considering the use of higher frequencies to increase the channel capacity, specifically from 24.25 to 86 GHz [65]. There is a requirement here for phantoms that cover these candidate mm-wave bands. There are some phantoms that have been suggested for these particular bands, but they still do not cover the whole band [12, 34]. At these frequencies, the penetration depth of the electromagnetic waves is really low, almost negligible,

so the skin arises as the key tissue to consider in order to assess the influence of the body on the propagation mechanisms. Some authors have suggested the gelatin as a good candidate to imitate the dielectric properties of the skin at those high frequencies [66], but their matching should be improved.

Considering what has been commented in Section 1.2 regarding the polar compounds, alcohols have been selected this time to adjust the dielectric properties of the liquid mixtures. Since they are polar compounds like water, they are miscible and can produce homogeneous liquids, unlike the emulsions suggested above with the oil and water. Three simple alcohols are suggested here: methanol, ethanol and 1-propanol, to be combined with water and between them in order to assess their interaction. The choice of these compounds is due to their availability in any kind of laboratory and their simple preparation procedures. This time, the setup for the dielectric measurements consists of the Keysight Technologies N5247A PNA-X and the SPEAG DAK-1.2E probe, allowing a measurement bandwidth from 5 up to 67 GHz. The gamma dispersion region, which is related to the polarisation of water molecules within the tissues, is overpassed at these frequencies. After this point, the trend of the dielectric properties of the body tissues becomes more stable with frequency, i.e., the values do not change as much with frequency. This should facilitate imitating the trend of the tissues within the studied band. C. Gabriel, the author of the compilation of the dielectric properties of the body tissues [9], suggests in [3] that a good option to imitate the skin is to make the average between the dry and wet. The explanation for this is the fact that the dry skin is not well measured due to poor contact of the probe with it due to its roughness. On the contrary, the wet skin contains an oversized amount of moisture that may lead to values greater than the actual ones.

In this case, as the skin imitates the properties of a whole region of the body, the whole body indeed, the values of the relative permittivity should not be pursued as an exact value, because of the heterogeneity of the body. Tissue values actually differ from one specimen to another, and also with other factors such as the age. When researchers consider these variations, they usually assume 10% of variability. In the following results, there is a shadowed region that depicts this variability from the average values of the skin. Some of the results from the mixtures of methanol and 1-propanol are shown in Fig. 4.21 and 4.22, particularly the series from 5 to 15% of concentration.

The results from both graphs are really similar, so one can conclude that their influence over the relative permittivity is close too. However, 1-propanol yields a behaviour more similar to that of the skin than methanol. In summary, 1-propanol leads to a greater reduction of the values of both parts of the relative permittivity from the initial ones for water than methanol.

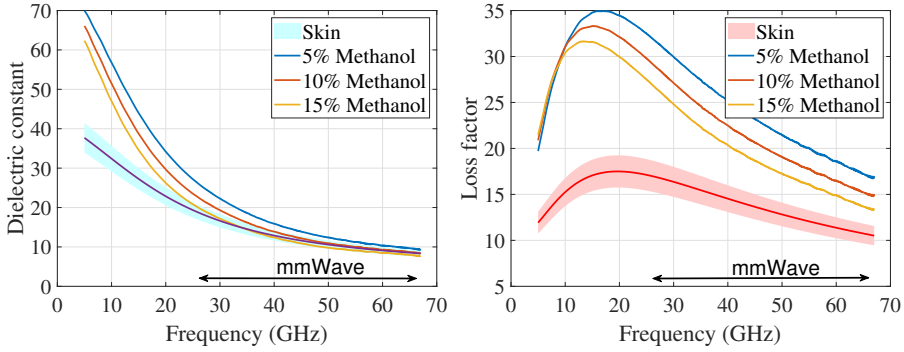

(a) Dielectric constant

(b) Loss factor

Figure 4.21: Relative permittivity of methanol aqueous mixtures together with the average values of the dry and wet skin according to Gabriel [3].

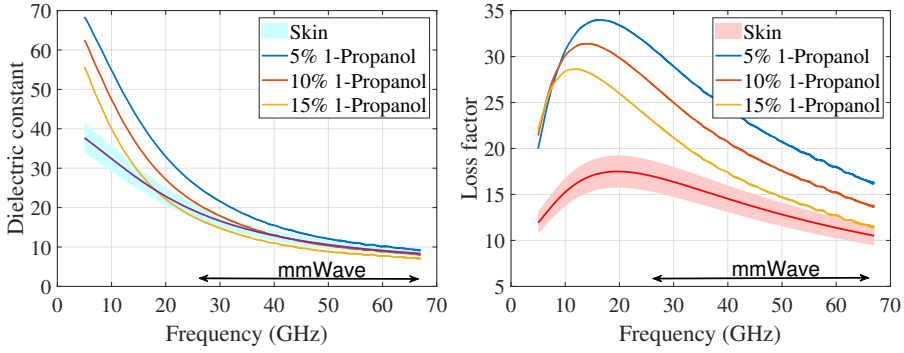

(a) Dielectric constant

(b) Loss factor

Figure 4.22: Relative permittivity of 1-propanol aqueous mixtures together with the average values of the dry and wet skin according to Gabriel [3].

Besides, it changes more the relaxation frequency of water, which is noticed in the movement of the peak in the loss factor to lower frequencies. The reason for the higher change in the relaxation frequency is the size of the molecule, since 1-propanol molecules are bigger than methanol ones. This fact causes higher polarisation capabilities in the case of methanol molecules and worse for 1-propanol, which slows down the frequency at which the molecules are not able to follow the field movements.

The results of Fig. 4.22 show the best approximation that was achieved by these kinds of alcohols, and fall near the boundaries of the shadowed region of the acceptable values of the skin. Ethanol showed also results that are quite similar to 1-propanol, since both only have one carbon difference in chain length. Regarding the combination of different alcohols in the same mixture, the trend is very similar to that provide by just increasing the concentration of the initial alcohol. This means that the main effect produced by any of the alcohols is to hinder the free rotation of the water molecules due to the presence of these large molecules. This effect can be observed in both parts of the relative permittivity: while the real part is decreased and the slope made steeper, the imaginary part mainly changes the peak to a lower frequency. It results in a trade-off between the lower limit of the region in the real part and the upper limit of the region in the imaginary one.

4.4.1 Data Modelling with Mixing Rules

Taking into account that there is a large number of possible combinations between the different alcohols, it is not possible to prepare all of them until getting the perfect match. Because of that, a method to estimate the dielectric properties of a alcoholic aqueous mixture given its composition is pursued. The goal is to obtain a mathematical model, i.e., equations, which relate these properties with the concentrations, like in the acetonitrile mixtures or the basic compounds.

The problem here is the fact that there are three different alcohols that can be mixed and all of them have a significant effect in both parts of the relative permittivity, not like in the aforementioned mixtures, where the salt effect was mainly appreciated in the loss factor and there was not a significant interaction between it and the polar compound. There are some approaches in the literature to address this issue, with a set of equations that theoretically estimate the dielectric properties of a mixture taking into account the particular relative permittivity of each component and its volume fraction in the final mixture. The resolution method consists of starting from a background, which is the main compound in the mixture, and then adding the different inclusions that appear in the material. Apart from the volume fraction, one has to take into account the shape and orientation of these inclusions, since this affects how the medium or material polarises. This is the purpose of Eq. 4.1, 4.2, 4.3, 4.4 and 4.5.

$$\text{Linear} \Rightarrow \underline{\varepsilon}_L(\omega) = \sum_{n=1}^{N} \nu_n \underline{\varepsilon}_n(\omega) \tag{4.1}$$

$$\text{Electrolyte} \Rightarrow \underline{\varepsilon}_{Electrolyte}(\omega) = \underline{\varepsilon}_{Water}(\omega) + \frac{\kappa_{Ion}}{j\omega\varepsilon_0} \tag{4.2}$$

$$\text{Inverse Linear} \Rightarrow \frac{1}{\underline{\varepsilon}_{IL}(\omega)} = \sum_{n=1}^{N} \frac{\nu_n}{\underline{\varepsilon}_n(\omega)} \tag{4.3}$$

$$\text{Maxwell-Garnett 3D} \Rightarrow \underline{\varepsilon}_{MG3D}(\omega) = \underline{\varepsilon}_B(\omega) + 3\nu_I \underline{\varepsilon}_B(\omega) \frac{\underline{\varepsilon}_I(\omega) - \underline{\varepsilon}_B(\omega)}{\underline{\varepsilon}_I(\omega) + 2\underline{\varepsilon}_B(\omega) - \nu_I(\underline{\varepsilon}_I(\omega) - \underline{\varepsilon}_B(\omega))} \tag{4.4}$$

$$\text{Maxwell-Garnett 2D} \Rightarrow \underline{\varepsilon}_{MG3D}(\omega) = \underline{\varepsilon}_B(\omega) + 2\nu_I \underline{\varepsilon}_B(\omega) \frac{\underline{\varepsilon}_B(\omega) - \underline{\varepsilon}_I(\omega)}{\underline{\varepsilon}_B(\omega) + \underline{\varepsilon}_I(\omega) + \nu_I(\underline{\varepsilon}_B(\omega) - \underline{\varepsilon}_I(\omega))} \tag{4.5}$$

Each equation models a different kind of inclusion, so its choice is key in order to get an accurate calculation of the relative permittivity. The linear model makes uses of Eq. 4.1 to calculate the volume-weighted average. It is the simplest one, and it should be used when the polarisation of the applied electric field extends parallel to the flat boundary surfaces of all the materials of a layered model. Eq. 4.2 is designed for the electrolytes such as the salts, which provide the mixtures with conductivity in the form of free ions. There is also the inverse linear model, represented in the Eq. 4.3, where the materials are supposed to own parallel boundary surfaces that are, in this case, perpendicular to the electric field vector. The Maxwell-Garnett 3D model assumes inclusions with the shape of spheres in a homogeneous background, whose influence is estimated by Eq. 4.4. Finally, the Maxwell-Garnett 2D model is made for infinitely long and parallel cylindrical inclusions whose axes are perpendicular to the external electric field. This particular case is modelled according to Eq. 4.5.

In all the aforementioned equations, ν_I is the volume fraction of the inclusions, ε_I is the relative permittivity of the inclusion in question, ε_B is that of the background, ω is the angular frequency in rad/s, and κ is the conductivity in S/m. These equations are used here with the aim of modelling the alcoholic aqueous mixtures described above. The first trials are made with the simplest mixtures, i.e., those ones with just one alcohol in the composition and with a low concentration. Regardless the type of inclusion, all the equations from the mixing rules are used except from the electrolyte model (Eq. 4.2), since there is no salt here. Water, as the predominant compound, is used as the background

for every mixture. The measured values from the prepared alcoholic mixtures are compared to those obtained with the different models in order to assess with is the more suitable one. A visual comparison can be made in Fig. 4.23, where the results from the 5% methanol mixture are shown as an example. The numerical comparison can be made in Table 4.5, where the RMSE values for the different compositions and models are gathered together.

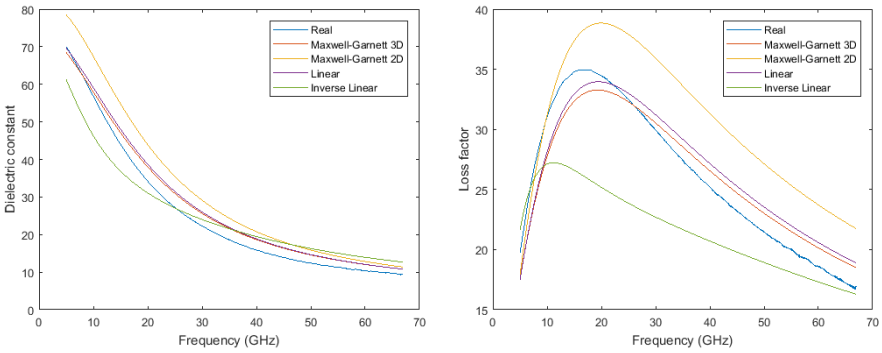

(a) Dielectric constant

(b) Loss factor

Figure 4.23: Comparison between the measured relative permittivity of 5% methanol aqueous mixtures and the predicted one by using the equations from the mixing rules.

The obtained results cannot be considered suitable to choose this approach as valid for modelling the dielectric properties of the alcoholic mixtures. The deviation can be clearly appreciated in Fig. 4.23, where with just 5% of methanol addition none of the models imitate the actual trend of the measured values. This deviation can be better observed in the loss factor, being the linear and the Maxwell-Garnett 3D models the ones that better fit the real values. Numerically, one can also observe in Table 4.5 that these are the best models in all cases. The Maxwell-Garnett 3D model (Eq. 4.4) is the one that yields better results, although the linear one (Eq. 4.1) presents similar results with a much simpler resolution. The problem is that despite the fact that there were not alcohol combination or high concentrations considered, the RMSE values are high, so the models are not actually useful. The reason for those deviations can be found in the assumption of lack of interaction between the molecules in the mixture. Polar molecules own strong interactions due to the presence of dipoles, which create internal fields that change the way how they orientate. In conclusion, this model is not useful to predict the properties of mixtures made of compounds with strong interactions inside. An empirical model may be used instead for this purpose.

Table 4.5: RMSE values of the deviation of the values achieved by the different equations of the mixing rules from the real measured values.

Alcohol	Maxwell-Garnett 3D		Maxwell-Garnett 2D		Linear		Inverse Linear	
	ε_r'	ε_r''	ε_r'	ε_r''	ε_r'	ε_r''	ε_r'	ε_r''
Methanol								
5%	2.65	1.71	6.87	5.03	3.04	1.90	4.99	5.47
10%	3.88	2.45	12.41	9.48	4.65	2.88	6.96	7.98
15%	4.52	2.77	17.14	13.38	5.60	3.38	7.80	9.26
Ethanol								
5%	4.20	2.88	8.92	5.89	4.69	3.03	7.97	8.60
10%	6.15	4.42	15.78	11.30	7.16	4.87	9.55	10.89
15%	7.19	5.18	21.48	15.99	8.64	5.93	9.54	11.32
1-Propanol								
5%	2.91	1.99	8.28	6.21	3.50	2.26	10.86	13.56
10%	4.87	3.45	15.54	12.16	6.05	4.12	12.16	16.07
15%	6.16	4.35	21.80	17.52	7.83	5.44	11.43	15.76

4.4.2 Cole-Cole Fitting

As explained in Appendix A, the Cole-Cole model (Eq. 3.1) is the most widespread one to fit the data of the dielectric properties from tissues. These properties are supposed to follow the behaviour of the body tissues, so they should be equally valid.

$$\varepsilon_r' - j\varepsilon_r'' = \varepsilon_\infty + \frac{\varepsilon_s - \varepsilon_\infty}{1 + (j\omega\tau)^{1-\alpha}} + \frac{\sigma_s}{j\omega\varepsilon_0} \qquad \text{(3.1 revisited)}$$

Following the same procedure than in Section 3.1, the data from the experimental results can be fitted by means of a least squares problem solver through a software tool. In this case, two variables are fixed, ε_∞ and $\alpha = 0$, since it is an overdetermined system and and the more equations would not add up. The other parameters of the Cole-Cole model are described according to the concentration for each alcohol. The result is a set of linear equations, which are grouped by parameter type in Eq. 4.6, 4.7 and 4.8.

$$\triangle\varepsilon = \varepsilon_s - \varepsilon_\infty = \begin{cases} 73.149 - 0.6981 \cdot c_{Methanol} & \text{if methanol} \\ 75.321 - 1.0469 \cdot c_{Ethanol} & \text{if ethanol} \\ 73.28 - 1.1484 \cdot c_{Propanol} & \text{if 1-propanol} \end{cases} \qquad (4.6)$$

$$\tau(ps) = \begin{cases} 8.7057 + 0.1764 \cdot c_{Methanol} & \text{if methanol} \\ 8.9836 + 0.2857 \cdot c_{Ethanol} & \text{if ethanol} \\ 8.2397 + 0.2713 \cdot c_{Propanol} & \text{if 1-propanol} \end{cases} \tag{4.7}$$

$$\sigma_s(S/m) = \begin{cases} 8.7057 + 0.1764 \cdot c_{Methanol} & \text{if methanol} \\ 8.9836 + 0.2857 \cdot c_{Ethanol} & \text{if ethanol} \\ 8.2397 + 0.2713 \cdot c_{Propanol} & \text{if 1-propanol} \end{cases} \tag{4.8}$$

The accuracy of this model can be compared to the previous one of the mixing rules by means of the RMSE values. In Table 4.6, the accuracy of this model for the same compositions as in Table 4.5 are presented. The way to calculate these values is the same in both tables, where the values of the alcohol concentrations have been introduced in the equations and these have been compared to those of the real measurements. One can appreciate that the values from Table 4.6 is greater in all cases, so it can be concluded that an empirical model is better to fit the dielectric properties of mixtures with polar compounds in which there is interaction between the dipolar moments.

Table 4.6: RMSE values of the deviation produced with the Cole-Cole experimental models.

Alcohol	**Ethanol**		**Methanol**		**1-Propanol**	
	ε_r'	ε_r''	ε_r'	ε_r''	ε_r'	ε_r''
5%	0.43	0.50	0.30	0.40	0.35	0.36
10%	0.50	0.41	0.47	0.36	0.36	0.43
15%	0.48	0.58	0.47	0.54	0.38	0.53

4.4.3 Gelling of the Mixtures

In Chapter 2, it is mentioned that natural polymers are not able to form gels when the concentration of water is low, or with the presence of some kinds of solvents. This is not the case of the alcoholic mixtures presented above, which can be gelled with those kinds of polymers. After preparing the liquid mixtures, it was also considered the possibility of manufacturing gels from the same compositions. The advantage of these compounds, as there is not the need of the synthetic polymers, is that they can be gelled with adding just a small percentage of a natural polymer. The choice was κ-carrageenan, which is widely used as a food additive in the industry and own good mechanical properties, better than those of agar (see Fig. 3.18), another important gelling

agent. Dissolving κ-carrageenan in water requires ions present in the solution to modify its conformation, as can be observed in Fig. 2.2. In this case, 1% of $CaCl_2$ is added to the liquid mixture together with κ-carrageenan powder. Beside, like other gel with physical cross-linking mechanisms (see Table 2.1), it requires to be heated up to 90°C to improve the diffusion of the polymer chains and then left to cool down with a film that slightly allows the air recirculation. After following this procedure to prepare the gel version of the previous liquid mixtures, some of the results are shown in Fig. 4.24.

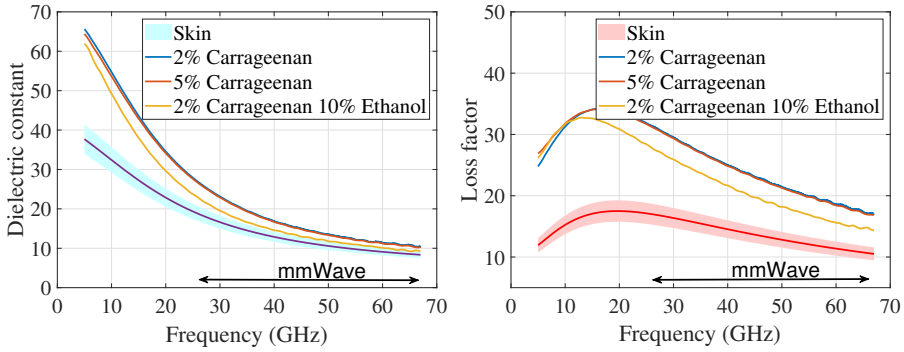

(a) Dielectric constant

(b) Loss factor

Figure 4.24: Relative permittivity of the κ-carrageenan gels.

Results show that the influence of the gelling additives are not significant over the dielectric properties of the mixture. After several tests, it was observed that the percentage of κ-carrageenan powder can be also increased up to 5% of the final concentration to improve the tailor the mechanical properties, and even so, the dielectric properties are kept practically unalterable. The influence of the alcohol in the mixture was also maintained regardless the liquid or gel state. All the alcoholic mixtures, with their combinations, were possible to be prepared, so the most suitable liquid solution for mimicking a certain tissue could be also achieved. It would keep the target dielectric properties intact.

In summary, the alcoholic samples have been measured in a wideband frequency range that contains the highest frequencies that are being considered for the 5G new radio spectrum. The target tissue has been the skin due to the fact that the penetration depth is really low at those frequencies and this would be the tissue of relevance. The approximation to the skin tissue still needs to be improved. That is why an attempt to model the influence of the different alcohols in the aqueous mixtures with the so-called mixing rules has

been pursued. It has been proven that the application of these equations is not suitable to predict the dielectric properties of a mixture when there is a high interaction between the constituent molecules. Thus, an empirical approach that makes use of the Cole-Cole fitting model has been analysed instead. This model achieves better results than the theoretical equations from the mixing rules in all the cases. Finally, the obtained mixtures have been made semisolid with the addition of κ-carrageenan powder and $CaCl_2$ in the composition. The gels provide promising results in terms of stiffness and keep the dielectric properties of the original liquid mixtures.

Chapter 5

Applications in Biomedical Engineering

The phantoms that have been developed in this thesis are a tool for researchers or manufacturers in order to replace the use of animals or humans in all types of testing. Although the core of the thesis is not to explain the real application scenarios, this chapter is aimed at demonstrating the applicability of the proposed phantoms. Thus, a series of experiments that make use of phantoms for different purposes have been carried out. These tests include the assessment of the influence of the body tissues over the radiocommunications links, the evaluation of the health effect of the microwave devices for exposure regulations or the validation of a tumour diagnosis system based on the differences in the dielectric properties.

5.1 Effect of the Arm on the Antenna Matching of a Wearable

The antenna matching determines how this device transmits the electromagnetic waves to the environment as well as its radiation pattern. This matching is highly influenced by the surroundings of the antenna in terms of relative permittivity. That is why the medium where an antenna is supposed to work must be considered from the initial stages. A poor matching may cause the loss of a wireless link and the impossibility to carry out an application. An example of the devices that usually change the surrounding medium are the wearables, which are placed in different parts of the body. The most common ones are the smartwatches or bands, which are carried in the wrist during the

whole day. These are usually connected, either to a smartphone or another external device. Hence, they include antennas that make them able to send and receive data as efficiently as possible. Moreover, considering that the battery life of these devices is a crucial issue. The optimisation of the device in order to improve the matching of the antenna helps to achieve this wireless link with the minimum consumption. The design of these devices can be performed with software that includes human body models for virtual simulations. After that optimisation, the prototypes are manufactured and they are usually tested in test benches like the one shown in Fig. 5.1.

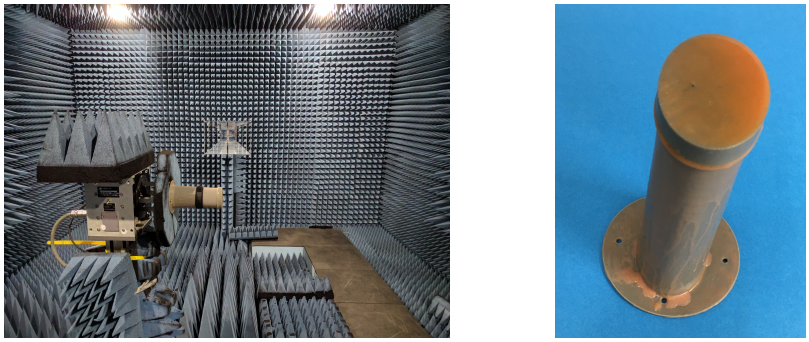

(a) Wearable circling the phantom

(b) Arm phantom

Figure 5.1: Study of the influence of the arm over the performance of a wearable in an anechoic chamber.

In this example, the radiation pattern as well as the matching of the antenna are studied in a controlled environment inside an anechoic chamber to avoid undesired microwave signals. It consists in a wearable designed to be carried in the wrist of patients in a hospital for localisation purposes. The technology that this device uses to communicate with external nodes is Bluetooth, so it uses the 2.4 GHz ISM band. A 3D-printed cylinder acts as the arm of a patient, which includes the muscle narrowband phantom described in Table 4.2 so that the dielectric properties of the arm are approximated. The main purpose of this test is to validate if the matching frequency is kept at 2.4 GHz or it is shifted to another frequency, in which case it would not work well. This change is really important because the bandwidth the device uses is quite narrow, and the energy consumption must be minimised, so any little change is key. The behaviour of the antenna in the virtual scenario, i.e., the software, and that of the experimental test can differ in some way. For instance, Fig. 5.2 shows a comparison between the reflection parameter (S_{11}) of the wearable in the design software and the measured one with the experimental phantom.

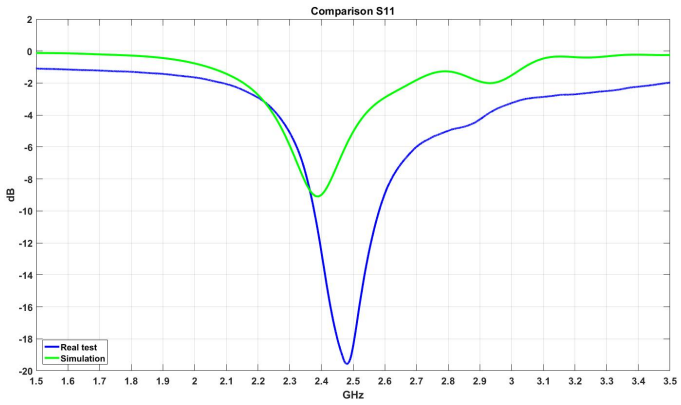

Figure 5.2: Comparison between the simulated and measured reflection parameter (S_{11}) of the wearable antenna in contact with an arm phantom.

One can observe that although the matching frequency is centred at 2.4 GHz in the simulations, it is actually closer to 2.5 GHz in the experimental setup. This can be a problem regarding the performance of the device that should be taken into account in the optimisation of the antenna.

5.2 Assessment of Specific Absorption Rate

The SAR values are one of the most important parameters that a wireless device must consider before being released to the market. Regulations are becoming more restrictive in this sense because of the population concern and due to the fact that the presence of these devices is increasing exponentially. Mobile devices, or others that make use of wireless communications, are tested with standardised dipoles and probes whose radiation pattern and behaviour is well known. The assembling is depicted in Fig. 5.3, where the dipole is changed by the device under test and the container chosen with the shape of the part of the body of interest. The absorbed power is measured by a specific probe that is able to analyse the electric fields inside the liquid and average the results for an established volume of tissue. This volume is usually represented by a 10 gram cube, taking into account the average density of the tissue. The phantoms used in these kinds of tests are narrowband, for a one single frequency, so the advantage of having wideband phantoms that cover all the frequencies of interest is the possibility of measure different frequencies without changing the liquid or measure several frequencies at once. In fact, this is an issue that will

be considered in the near future, since people are exposed to many frequencies at the time, and their contribution should be added. Thus, a SAR test was carried out by taking advantage of the new wideband solutions presented in Chapter 4, as an example of how these measurements work.

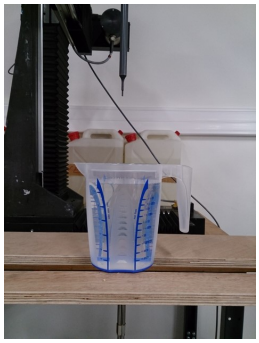

(a) Probe and phantom

(b) Dipole antenna

Figure 5.3: Setup for the SAR measurements, where the phantom container is fixed with the dipole under it, and the probe is moved by a 3D positioner system.

The setup was composed of a cylinder 10 cm in diameter and 20 cm in height (Fig. 5.3), which was filled with the 2.4 GHz ISM phantom of the muscle reported in Table 4.2. The measurement system consisted in a SAR probe (SPEAG, DAE 3 mini EX3DV4) connected to a computer that was running an acquisition software. The transmitting devices were three dipole antennas of 900, 1800 and 2450 MHz, which were connected to a signal generator (Rohde & Schwartz, SMB 100A, frequency range: 100 kHz-12.75 GHz). The SAR probe was calibrated for the dielectric parameters of the muscle. Before performing the tests, the output power of the antennas was determined. First of all, the reflection coefficient (S_{11}) was measured for each antenna with a VNA (Rohde & Schwartz, ZNB 20, frequency range: 100 kHz-20 GHz). For that, the VNA was calibrated with match, open and short loads, and then the S_{11} parameter was measured by placing each antenna 1 cm under the container filled with phantom (Fig. 5.3). Then, the output power of the signal generator at the terminal connection before the antennas was measured with a power meter (NRVS). To do this, the signal generator was set to work at 18 dBm with a continuous sinusoidal signal. The values were 16.77, 16.17 and 15.91 dBm at 900, 1800 and 2450 MHz, respectively. The SAR probe was located in the centre of the cylinder, 5 mm above the bottom, and it was automatically moved by a 3D positioner (SPEAG, DASY 3 mini system). The position with the maximum peak of absorbed power (W/kg) was established by performing

a first scan of a 5×5 cm^2 square over the bottom of the phantom. The results from this scan are shown in Fig. 5.4. This point was the centre of the 10 gram cube where the measurements took place. The resolution points were specified by the monitoring software according to the standard.

The SAR measurements were carried out for the three different aforementioned frequencies individually, but using the same phantom in all of them. Although the phantom is designed for the 2.4 GHz ISM band, these kind of mixtures have been proven to imitate the body tissues within a wide frequency range. Thus, it is better to use a phantom designed for 2.4 GHz rather than a UWB phantom that has been adjusted from 3 GHz, since the first one is nearer to the frequencies measured here. The dielectric parameters of this phantom were the following ones: 54.363 and 20.04 at 900 MHz, 52.63 and 13.983 at 1800 MHz, 51.935 and 12.78 at 2450 MHz, for the real and imaginary part, respectively. These measurements are usually performed with a sucrose solution that is adjusted for each single frequency and has to be changed after each measurement. This time, the SAR values were obtained for the three frequencies by changing just the dipole and keeping the mixture in the container with the same conditions.

The measurements were carried out at different z planes, i.e., the probe was moved up vertically to make each layer. As the measurement moves away from the bottom plane, i.e., the surface near the dipole, the absorbed power is lower. This can be observed in Fig. 5.5, where the results for the top layer of the 10 gram cube are shown. The SAR values have been reduced by almost half with respect to those of Fig. 5.4. One can see that the SAR values are higher as the frequency increases in the concerned area. However, this area gets smaller when the frequency rises due to the greater propagation losses. The peaks for the 10 gram averaged tissue were 6.65 W/kg at 900 MHz, 20.19 W/kg at 1800 MHz, and 19.85 W/kg at 2450 MHz.

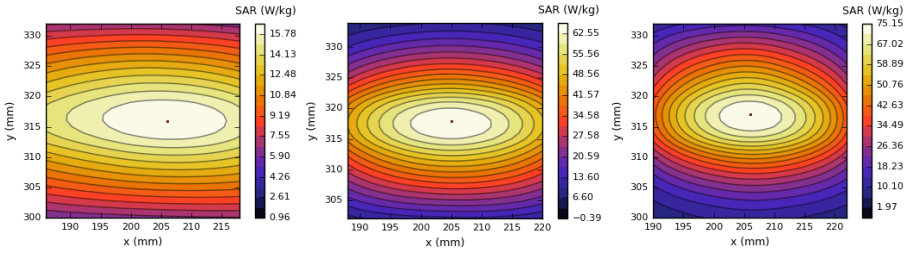

(a) 900 MHz (b) 1800 MHz (c) 2450 MHz

Figure 5.4: Specific Absorption Rate over the bottom of a 10 gram cube of muscle tissue by using the muscle phantom.

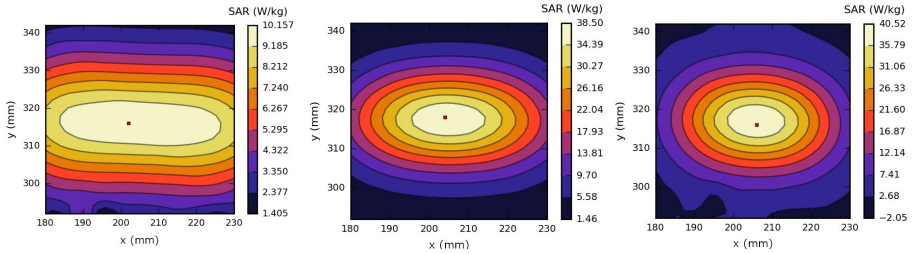

(a) 900 MHz (b) 1800 MHz (c) 2450 MHz

Figure 5.5: Specific Absorption Rate over the top of a 10 gram cube of muscle tissue by using the muscle phantom.

5.3 Channel Characterisation at Ultrawideband Frequencies

As explained in Section 1.1, the current bands used in biomedical communications are narrowband and at low frequencies because of the high losses that produce the body tissues [67]. These bands are limited in terms of bandwidth, which makes them unsuitable for modern communications that require higher data rates in applications such as high quality video transmission. Because of that, there are researchers working in the use of alternative bands and technologies, e.g., UWB (3.1-10.6 GHz), which is only intended for external WBAN communications and may be used also in intracorporal communications [68].

The most striking example is the capsule endoscopy due to the requirement of video transmission. Nowadays, the images are recorded and watched afterwards or in real time with poor quality. The way to decide if a particular band can be used in a particular scenario is to characterise the channel with the aim of assess the losses that the transmitted signal suffers. This means to study the ratio of received power depending on the distance between antennas and the depth that can be reached by keeping a reliable communication link inside the tissue. This characterisation cannot always be carried out in humans, which are the final scenario where these devices will work, so body phantoms emerge as the best way to substitute them. In Section 1.4 some of the phantoms that are used for this purpose were described, along with their limitations. The most critical one was the frequencies they usually cover, which makes not possible to test technologies, like UWB, with high accuracy. Thanks to the liquid wideband phantoms obtained in 4.2, a new field of possibilities opens up, which also allow the antennas to be moved freely around the mimicked tissue. This

is precisely what is done in [69], where the channel characterisation is studied for different WBAN scenarios as well as a correlation model.

The simulated scenarios were, on the one hand, the in-body to in-body case, and on the other hand, an in-body to on-body transmission. The measurement setup consisted of the Keysight ENA E5072A VNA, connected to a computer that controlled the equipment and processed the results. Two different antennas were used for the measurements, both designed for UWB transmission and reception [70], which are shown in Fig. 5.6.

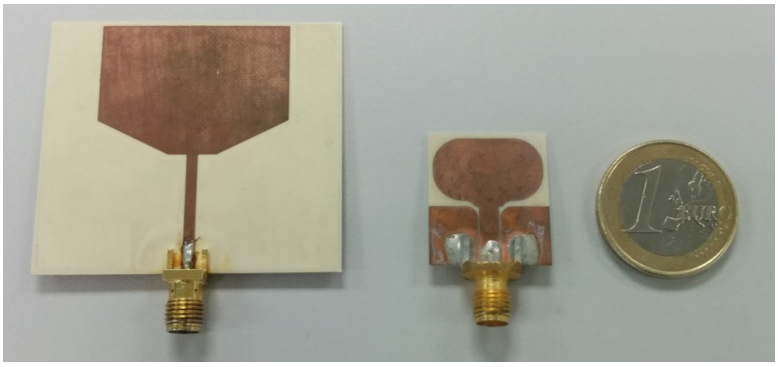

Figure 5.6: UWB antennas used in the studied scenarios. Large antenna (left), for the on-body location, and miniaturised antenna (right), for the in-body location. Reprinted from [69], © 2016, IEEE.

The antenna from the left size (the biggest one), is designed to be near the body but not totally surrounded, i.e., it is intended to work on the body surface. The other antenna (the smallest), is designed by taking into account the relative permittivity of the muscle, like an average of the gastrointestinal region. The latter is the one that would send the data from the inside to the outside, to be collected by the other antenna. In this case, the body torso is represented by a square container, filled with the wideband muscle phantom (see Fig. 4.1). The full setup is shown in Fig. 5.7. A 3D positioner was in charge of the movement of the small antenna. This was automatically moved by the computer software, which also controlled the VNA and acquire the data.

For the in-body to on-body scenario, the large antenna was fixed over the surface in one of the walls from the container, whereas the small one was attached to the 3D positioner. The experiment consisted in a set of measurements, taken within a virtual xyz mesh of $19 \times 19 \times 3$ cm^3, where the external antenna was also changed to several positions after each measurement sweep. In the in-body to in-body scenario, the large antenna was placed inside the

phantom and the small antenna was moved in a smaller xyz mesh, this time of $11 \times 11 \times 2$ cm^3.

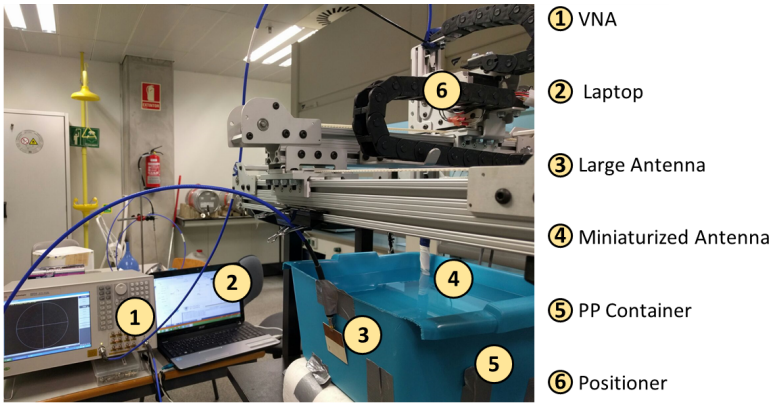

Figure 5.7: Experimental measurement setup particularised for the in-body to on-body scenario. Reprinted from [69], © 2016, IEEE.

The measurements were used to obtain the path loss models for each scenario. In this case, the in-body to in-body scenario was better fitted to a linear trend, whereas the in-body to on-body scenario was adjusted to a logarithmic model. The measurement points as well as the obtained models for both scenarios are depicted in Fig. 5.8. The path loss values are quite high due to the fact that the last frequencies of UWB own high losses. Then, more recent research has been performed, using the same phantoms and setup, with further analyses.

Phantoms can be used in further experiments taking into account different techniques that improve the transmission. For instance, in [71], authors characterise the UWB channel from its different subbands, which could be used for the codification of the data based on multiple carrier frequencies. Moreover, other features such as the diversity of the channel can be assessed, which is investigated in [69], where the correlation coefficients in the transmission at different positions was calculated. Representing the values on a position map, it results in a graph that remains like in Fig. 5.9.

The particular scenario of the graph is the in-body to on-body one, at two different z planes. It can be concluded that the correlation decreases significantly as the distance increases in both x and z axes. Thus, the channel can be considered to be uncorrelated in transmitting positions that are separated more than 5 cm in each axis. This means that the use of more than one antenna would benefit the transmission in terms of improvement of the

data rate or the accuracy in the localisation of the internal device. This would fit perfectly with a belt that had several antennas separated from each other that would locate an ingested endoscopic capsule. These results may be useful for the implementation of different techniques such as time reversal, suggested in [72], where the same phantoms are used. These techniques are intended to improve the reception of the signal in a challenging environment for the wireless transmission.

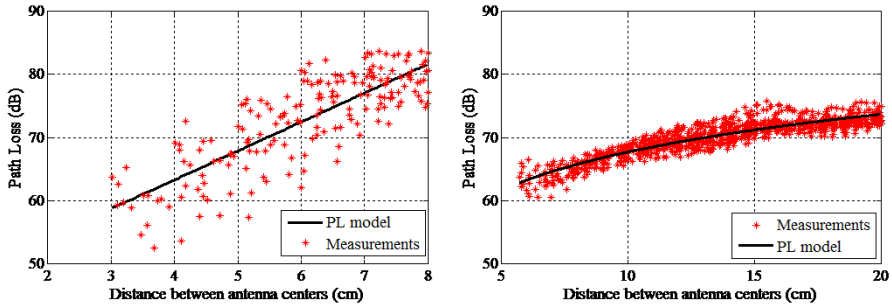

(a) In-body to in-body scenario (b) In-body to on-body scenario

Figure 5.8: Path loss as a function of the distance between the antenna centres in different layout scenarios. Reprinted from [69], © 2016, IEEE.

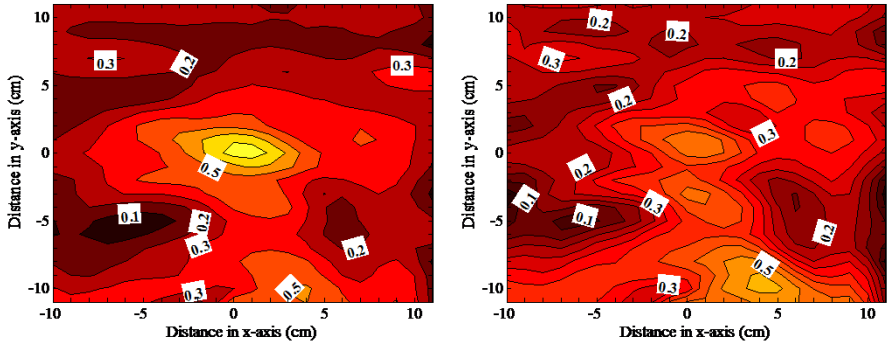

(a) $z = 1$cm (b) $z = 2$cm

Figure 5.9: Correlation coefficients at a z distance from the plane $z = 0$ in the experimental in-body to on-body scenario. Reprinted from [69], © 2016, IEEE.

5.4 Validation of a Colon Tumour Diagnosis System

The dielectric properties of the tissues change from one subject to another, that is why they are usually averaged after many measurements from different specimens that differ in age, gender and size. After that, authors normally fit the values of the relative permittivity to the Cole-Cole equation (Eq. 3.1) and report its fitting parameters for other authors to be able to get the values at any frequency. The most used reference is Gabriel's report [3], but it is not the only work that gathers dielectric data from different tissues in a wide frequency range. There are more works that report different tissues that have not been previously considered or assayed with different methods in order to compare their results with those of Gabriel or others, in order to increase the database. For instance, in [73] authors provide the results of the measurements of several tissues that had not been previously measured and they compare the results with those previously reported.

$$\varepsilon_r' - j\varepsilon_r'' = \varepsilon_\infty + \frac{\varepsilon_s - \varepsilon_\infty}{1 + (j\omega\tau)^{1-\alpha}} + \frac{\sigma_s}{j\omega\varepsilon_0} \qquad \text{(3.1 revisited)}$$

The fact is that there are more biological features that can change the dielectric properties of a tissue. One of these is the healthy or malignant nature of the present cells, and certainly there are authors focused on those studies due to the relevance it may have over cancer diagnosis systems. Colon is one of the tissues that has been reported to own differences between the healthy and malignant tissue [74]. The measurement of many surgery samples from human beings led to an accurate model of the dielectric properties in its different states, and one can observe that there is a significant variation in terms of values and relaxation frequency between the healthy and malignant tissue. This difference may be used in a cancer diagnosis system that measures the dielectric properties of the colon without the excision of the tissue [75]. This method would be less intrusive and fast than the typical pathological anatomy analysis. The collection of colon tissue samples is usually made through a colonoscope (Fig. 5.10a), which is introduced inside the intestine and displaced along it. It has both a camera and a clipping tool inserted in a cavity fitted out for it (Fig. 5.10b) in order to remove the polyps. As explained in Section 2.3, the open-ended coaxial technique makes use of a probe that measures the reflection coefficient of the MUT and then the relative permittivity is obtained with a mathematical conversion. The probe does not necessarily have to be rigid as the used ones in this thesis. This is just a way to simplify the system and avoid uncertainty in the measurements, since every single movement changes the reflections inside the probe. In this case, a flexible coaxial cable can be used

instead (Fig. 5.10c), with the advantage of being able to enter in the cavity of the colonoscope.

(a) Endoscope

(b) Endoscope tip

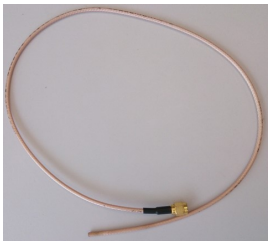

(c) Probe

Figure 5.10: Endoscope from different perspectives and the probe that is inserted into the available cavity. Images (a) and (b) by melvil, licensed under CC BY-SA 4.0.

The way to test this system was to prepare phantoms that imitate the dielectric properties of the healthy and malignant colon reported in [74]. This was possible by following the guidelines described in Section 3.3, from which there were achieved the results shown in Fig. 5.11 and whose compositions are reflected in Table 5.1. The approximation is quite proper, almost matching the curves in the whole frequency range. It can be noticed that the differences between the healthy and the malignant colon are more pronounced at low frequencies, so rising to higher ones is not desirable. Once the materials are prepared it is sufficient to test the system to see if it is able to distinguish between one material and another with precision.

Table 5.1: Phantom composition to fit the values of the healthy and malignant colon according to Fornes-Leal *et al.* [74].

Tissue	**Phantom composition**
Malignant colon	42% Acetonitrile, 1% NaCl
Healthy colon	48.5% Acetonitrile, 3% Ethanol, 1% NaCl

The sensitivity of the system was analysed by calibrating it and then producing spins similar to those it would experience in a human colon. After that, the phantoms were measured with the coaxial cable, keeping it inside the colonoscope. Results were not exactly the same as those obtained with the rigid coaxial probe, but the differences between the healthy and malignant colon were kept. This means that the system is not suitable for determining the relative permittivity of a material, but it may be useful to detect differences in its dielectric properties or assess if the measured values are within the region of a malignant or healthy tissue.

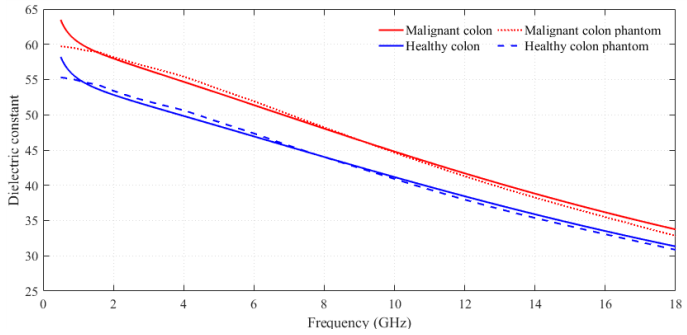

(a) Dielectric constant

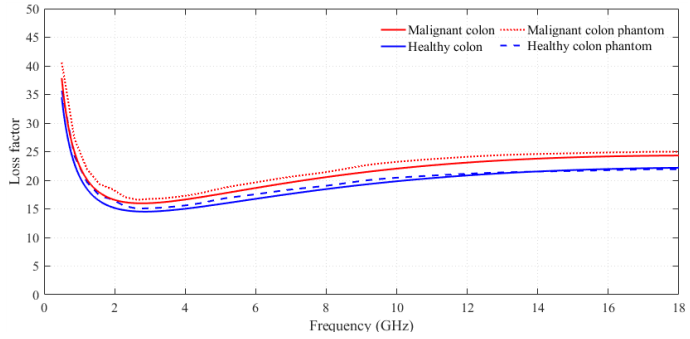

(b) Loss factor

Figure 5.11: Relative permittivity of the healthy and malignant colon tissues according to Fornes-Leal *et al.* [74] and that of their suggested phantoms from Table 5.1.

5.5 Study of the Penetration Ratio for Microwave Imaging

Microwave techniques have been suggested for imaging purposes in order to have an alternative to the commonly used X-radiation [76]. This way would allow a non-invasive technique to detect inclusions inside the healthy tissues, especially in the diagnosis of breast cancer. The challenge is the trade-off between the penetration ratio and the resolution that it is able to provide. On the one hand, the higher the frequency, the higher the resolution for detecting small particles. This is a desired feature because of the need of sensing the malignant regions at the earliest stages of cancer. On the other side, the lower the frequency, the better the penetration ratio due to the lower propagation

losses. The relative permittivity of the tissue also affects the penetration that the electromagnetic wave will achieve (see Section 1.1). Breasts are mostly made of fat and gland tissue, both with different dielectric properties [77]. That is, they are a heterogeneous tissue with different features that have to be taken into account in order to design the devices for microwave imaging. Fat has low values of relative permittivity, whereas the tendon and other parts own high dielectric properties. Thus, the penetration ratio will be different depending of the kind of penetrated tissue, and this is something that should be checked. Phantoms appear here as the best way to assess this penetration ratio after the design and fabrication of the devices.

This kind of study can be found in [78], where the penetration is assessed with fat and muscle phantoms, which are the extreme cases regarding the dielectric properties. This penetration is studied by means of two different antennas, designed specifically for the intended application. The external antenna is designed to work from 2.8 to 13.8 GHz in the air but near the tissues, with a high directivity in order to focus the power forward in order to improve the penetration. This antenna is described in [79] and shown in Fig. 5.12. The internal antenna is designed to receive signal from an external device and to be omnidirectional. It is described in [70], and conceived for working in the UWB frequency band directly wrapped in tissue.

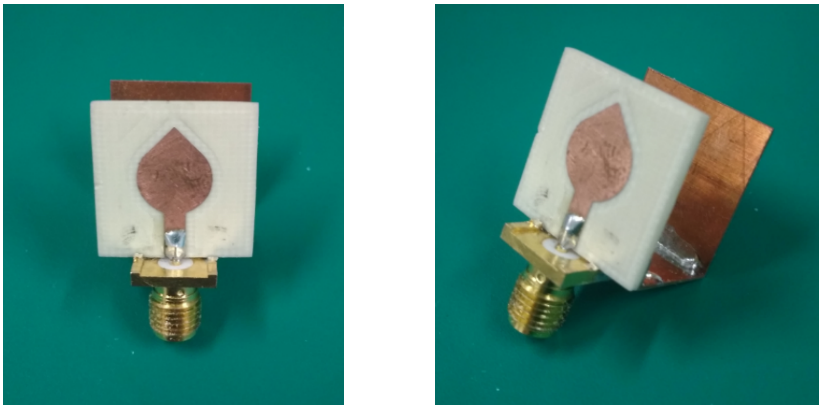

(a) Frontal view (b) Perspective view

Figure 5.12: Antenna designed for microwave imaging in the breast region. Reprinted from [78], © 2019, IEEE.

The test consisted in the measurement of the relationship between the transmitted and received power, i.e., the scattering parameters. The experiments are carried out with the Keysight ENA E5072A, the same VNA that was used

to obtain the dielectric properties. The setup is depicted in Fig. 5.13, where one can see that the external antenna is placed outside the phantom container, two centimetres away, and the internal antenna is immersed in the phantom. The fat phantom is that one depicted in Fig. 4.12 and the muscle one is that shown in Fig. 4.1. The transmitting antenna was kept fixed during the whole experiment, whereas the internal one was moved in one only dimension, closer or away from the wall parallel to the outside antenna.

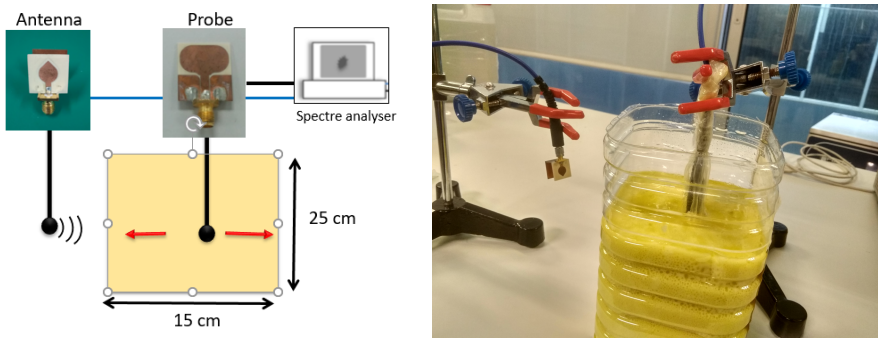

(a) Scheme

(b) Picture

Figure 5.13: Representation of the setup for the penetration measuring system. Reprinted from [78], © 2016, IEEE.

The frequency band that was chosen for the experiment was the UWB, since it is the band they have in common and it is supposed to own high resolution and enough penetration depth. It is necessary that both antennas are matched in the working frequency range to obtain suitable values. Then, the reflection coefficients are computed as well (S_{11} and S_{22}), being the transmitting antenna connected to the port 1 and the receiving one connected to the port 2. The antennas were considered to be radiating properly when the reflection coefficient was under -10 dB, i.e., most of the energy was transmitted instead of returned. The results of the experiment for the fat phantom can be observed in Fig. 5.14.

The S_{11} and S_{22} parameters show that the matching of the antennas is good within the whole frequency range in accordance to the established criteria. The S_{21} parameter is the relation between the received power and the transmitted one, so the higher are the values, the higher is the received signal. The four graphs from Fig. 5.14 depict the results as the immersed antenna is moved away from the wall closest to the external antenna.

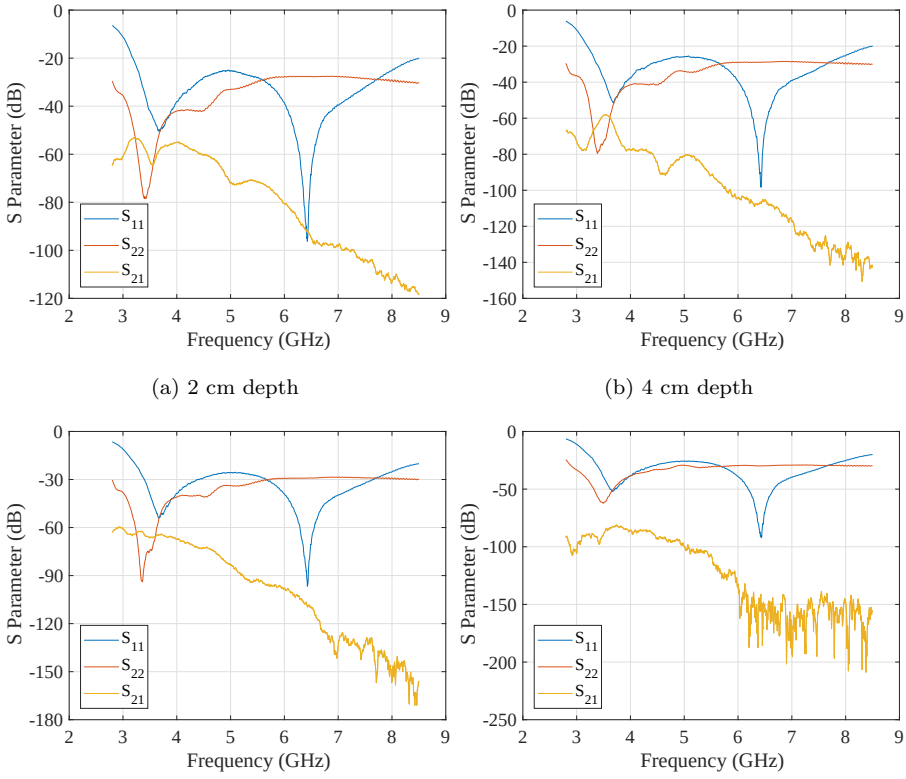

(a) 2 cm depth

(b) 4 cm depth

(c) 6 cm depth

(d) 10 cm depth

Figure 5.14: Scattering parameters (S) of the transmitting (port 1) and receiving (port 2) antennas on fat phantom, when the transmitting one is placed 2 cm away from the surface of the container and the receiving one changes its distance from the same surface in reverse.

It can be appreciated that the S_{21} becomes lower as the depth (distance from the wall) increases. There is a region between -150 and -200 dB where the values are kept almost invariable when the frequency grows. Theoretically, they should decrease with the frequency due to the greater propagation losses. However, there is a noise lever, in which the received signal cannot be discriminated from the environmental radiation background. Then, the signal is no longer useful and the results can be discarded. The distance at which the signal is considered suitable to receive useful signal with the fat phantom was 17 cm. This would represent the penetration that the signal achieves and so the depth for the images.

The same experiment was replicated with the wideband muscle phantom, whose results are shown in Fig. 5.15. In this case, the distance achieved before losing the useful signal was 9 cm of depth. As expected, the penetration with the muscle tissue is much lower that that achieved in the fat because of its higher losses. Fortunately, breasts are mainly formed by fat and the final penetration will be closer to 17 cm than to 9 cm. This range of values makes this technique suitable for microwave imaging with the purpose of cancer tumour detection. Further experiments with tumour discrimination techniques should be carried out and combined with data processing with the aim of calibrating and checking the system.

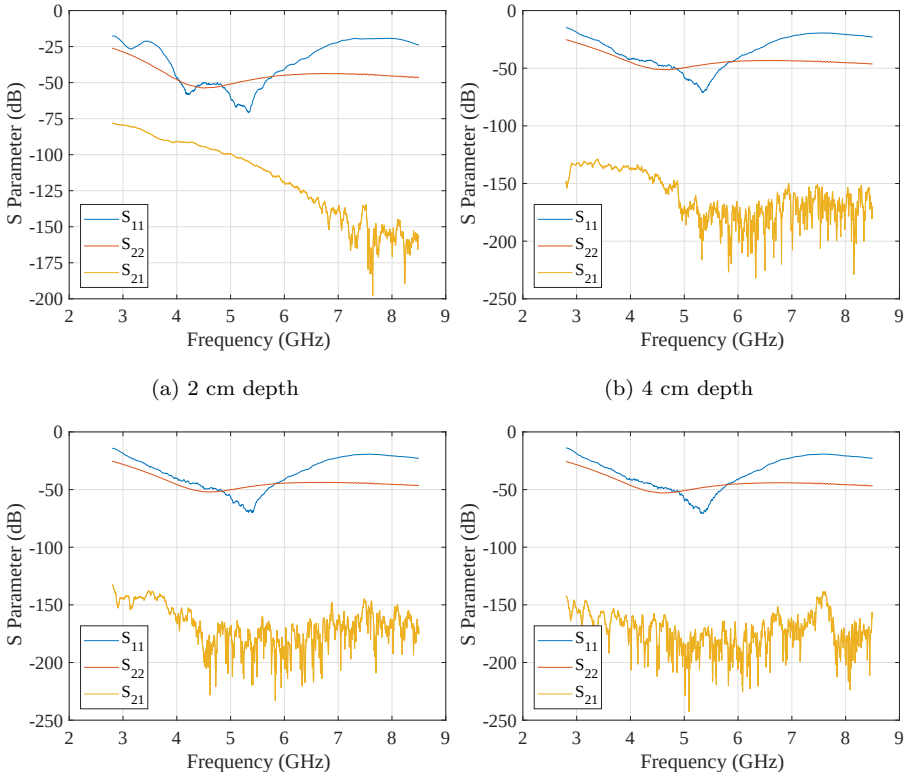

(a) 2 cm depth

(b) 4 cm depth

(c) 6 cm depth

(d) 10 cm depth

Figure 5.15: Scattering parameters (S) of the transmitting (port 1) and receiving (port 2) antennas on muscle phantom, when the transmitting one is placed 2 cm away from the surface of the container and the receiving one changes its distance from the same surface in reverse.

Chapter 6

Conclusions & Perspective

The arrival of the massive presence of wireless networks in the daily life is a fact. The need to connect more and more devices as well as the bandwidth requirements lead to the deployment of new access points. The increase in the offered bandwidth is usually covered by a shift of the frequency band to higher values. Devices require more power to generate the signals at these higher frequencies and they also have more losses, that is why a greater number of access points needs to be installed. Besides, as the frequency rises, the influence of the objects from the environment is larger, including that of the human body. The combination of both effects, the closeness of the devices to the body and its growing influence over the propagation of the signals, is the main motivation to study this influence. The claim becomes even more obvious when it comes to WBANs, since these are constantly in contact with the body when this is not the propagation medium itself.

Phantoms are presented as necessary in order to validate these scenarios for two main reasons: for modelling the propagation losses that suffer a transmitted signal in a particular scenario and for assessing the influence that these electromagnetic waves may have on the body tissues. There are both computer and experimental phantoms, but the last ones are the only choice to certificate devices in real conditions, e.g., SAR. These are currently used in the literature for all kinds of experiments in which the human body is involved. Regarding the experimental phantoms, which are those within the scope of this thesis, the number of reported tissue-equivalent materials is limited. There is no integral model that attempts to cover several parts of the body in a large bandwidth. Most researchers focus on a single tissue within a restricted band. This lack of models limits the accuracy that can be reached in the research of this topic. This thesis aims at filling the gap of available materials that mimic the electro-

magnetic properties of the body tissues for the maximum possible bandwidth. The purpose is to offer the models in different formats, liquid or semisolid, in order to increase its versatility for all types of experiments.

The main points of this thesis are summarised in Section 6.1, whereas the suggested future works are described in Section 6.2.

6.1 Concluding Remarks

The scope of this thesis was to find the most suitable materials to develop the synthetic models called phantoms. **Chapter 3** was the starting point for this objective. The materials reported by the researchers for imitating the dielectric properties of the body tissues do not normally meet the trend of the values from tissues. The main reason is the fact that most of them are basic compounds, easy to find and prepare. This certainly has many advantages when preparing an experiment, or in terms of accessibility, but these are not always accurate enough to recreate a realistic scenario. First experiments were intended to determine the limitations of these kinds of compounds. Sucrose and salt were combined in different proportions in order to establish their influence over the relative permittivity of the water mixtures. These combinations showed that the relaxation frequency of the water is too affected by the effect of sucrose, whereas the salt influence is mainly noticed at low frequencies. The values from these mixtures were fitted, first to a Cole-Cole model, for making them available to anyone without having to replicate the experiments, and secondly to a linear model. This last model was made for 2.4 GHz, since these mixtures were discarded for wideband phantoms, and this is an extensively used ISM non-licensed frequency band. It consisted of two equations, one for each part of the relative permittivity, where the concentrations of sucrose and salt yields to the dielectric values.

Afterwards, a selection of candidate polar compounds that actually follow the trend of the body tissues was pursued. The choice was based on the range of frequencies and its main polarisation effects described in Section 1.2. After several analyses with the polar compounds, acetonitrile was found out to be the most suitable compound to be mixed with water and achieve the trend of the tissues. One should consider that acetonitrile mixtures are flammable and toxic when there is prolonged exposure, so it is recommended to work with them under an extraction hood with the necessary safety conditions. As in the case of the sucrose, several combinations of acetonitrile and salt with water were prepared. The behaviour of the mixtures showed that acetonitrile reduces the values of the relative permittivity, provokes a reduction of the slope of the dielectric constant and an increase of the peak of the loss factor at higher

frequencies. The results from these mixtures were then fitted to the same 2.4 ISM band, which could then be used to compare the accuracy obtained with one model or another. This time, though, a new mathematical model with four equations was presented. It allowed to match the dielectric properties of a tissue within a wide frequency band, especially at UWB frequencies, by a non-linear optimisation solving method.

Thereafter, the possibility of converting these liquid samples into gels was analysed. Authors usually use agar or gelatin to prepare gel solutions, but these were not possible to replicate with acetonitrile mixtures. Besides, a gel with better mechanical characteristics that allowed manufacturing large shapes was pursued. For this reason, two synthetic polymers were studied (PAM and PHEA), which own the ability to be swollen in many kinds of liquids. The features that were taken into account to choose the most suitable polymer were the swelling index and the influence over the relative permittivity. It was shown that PAM is able to hold a larger amount of water, but PHEA is better with acetonitrile mixtures. This fact allows the ratio of liquid to gel to be much higher. Consequently, the resulting relative permittivity will be closer to that of the swelling liquid. However, the influence of the polymer over the dielectric properties was assessed in order to design the future gels phantoms. The main influence of the polymer was found out to be the reduction of the values from the relative permittivity of the liquid without changing the relaxation frequency, i.e., the slope of the dielectric constant. Moreover, a mechanical test was carried out to compare the compression strength that these gels are able to hold. These were shown to be much more resistive than the natural gels.

The previous analyses were aimed at getting the required guidelines to design the phantoms theirselves. This is what is done in **Chapter 4**, where the findings of the previous chapter are applied in the development of the phantoms. The equations of the models at 2.4 GHz for both, sucrose and acetonitrile mixtures, were applied for estimating the compositions of several tissue phantoms. After preparing the calculated liquid mixtures, their dielectric properties were measured and compared with the actual values of the tissues. Results showed that the acetonitrile mixtures own a remarkable accuracy at 2.4 GHz, much higher than sucrose mixtures. The latter attain an acceptable imitation for the heart tissue, despite it is not as high as in the other mixtures. A heart phantom for this frequency band was not found in the literature, so this is a way to get one for researchers that work with the cardiovascular zone, e.g., pacemakers. One should evaluate which is more convenient with regard to this tissue, either using a cheap and more accessible phantom at the expense of accuracy, or preparing the acetonitrile aqueous mixtures with their benefits.

Nevertheless, the acetonitrile mixtures were intended to pursue wideband phantoms, which is also attempted in this chapter. After using the equations

proposed in Chapter 4 for the UWB frequencies, these were used here in order to estimate the required compositions to imitate several phantoms in the frequency range from 0.5 to 26.5 GHz. The accuracy obtained in all of them is very high, much better than most of the reported phantoms in Table 1.1. Besides, there are some tissues that had not been previously imitated, at least in this frequency band. In some cases, slope that produces the inclusion of acetonitrile is too steep to reach that of the tissue. Because of that, a third polar compound, ethanol, which has a lower relaxation frequency, was added in the mixture. It permitted a finer adjustment of the slope of the dielectric constant. A great number of tissues can be obtained by combining all these variables, especially those with a high water amount, i.e., soft tissues. Regarding the tissues with low water content, these can be imitated with great precision with oil/water gels. On this basis, the two types of fat reported by Gabriel were prepared in a liquid format by including a surfactant in the composition. Results showed that it was possible to prepare a stable emulsion in the liquid form without loosing accuracy with regards to the aforementioned oil/water gels. In this way, one can choose between the two formats depending on the test requirements.

As mentioned in Chapter 1, the phantoms were not intended just for WBANs, but also for the upcoming high frequencies in 5G technologies, i.e., millimetre waves. This goal was sought by means of alcoholic solutions, since these are also polar compounds, and the dielectric properties of this band are mainly influenced by the orientation polarisation, although not as much as in the UWB frequency band. Three different alcohols were chosen to be included in the mixtures, methanol, ethanol and 1-propanol. The alcohol that better approximation got to that of the skin was 1-propanol, since it was the one that most reduced the values of the loss factor and produced a fall in the relaxation frequency. The reason for that is probably the fact that it is the largest molecule among the studied ones, and this impedes the correct orientation movement of the water molecules. A concentration of 15% 1-propanol was found out to be near the boundaries of a 10% deviation from the average skin values, which is normally considered by researchers that is the acceptable deviation with respect to the dielectric values of tissues.

There is a great deal of possible combinations with them, so a theoretical model was used in order to predict their dielectric properties, the so-called mixing rules. The results obtained after comparing the measured results with the estimated values from that theoretical model revealed that the assumptions made by this model are not appropriate. The mixing rules assume that there is no interaction between the different inclusions in the mixture, i.e., between the polar molecules, but this is not true. Thus, an experimental model based on the Cole-Cole fitting was used instead, in which the parameters were related

to the concentrations of the different alcohols. This fitting resulted in a lesser deviation from the actual values.

Afterwards, these mixtures were gelled with κ-carrageenan, which was able to be naturally cross-linked in presence of these mixtures, unlike the case of acetonitrile mixtures. This is probably due to the fact that acetonitrile is a better solvent than the alcohols. Despite the worse mechanical properties of κ-carrageenan in comparison to those of the synthetic polymers, it can form the gel with just 1% weight in the final composition. Several alcoholic mixtures with different amounts of κ-carrageenan concentrations were prepared and measured. The measurements of the relative permittivity of these gels showed that the influence of the natural polymer is almost negligible from the initial liquid mixture. This is an important advantage, since one can limit to imitating a tissue using only liquids, and add the polymer in the mixture when the suitable composition is found.

The last part from the chapter of tissue phantoms was the development of gel phantoms by using the synthetic polymers studied in Chapter 3. Since these kinds of materials are semisolid, the pressure applied during the measurements affects the observed results, that is why a careful procedure, in which the pressure was controlled, was followed. The main advantage of these gels, in addition of the better mechanical properties, is the fact that they can be swollen with the acetonitrile aqueous mixtures that were found out to be suitable for mimicking the tissues in a large bandwidth. Another advantage that these own is the tailoring capability in terms of the cross-linking degree. As these gels are synthesised from the initial steps, their swelling degree can be adjusted by changing this parameter. The final dielectric properties of the combinations of the liquids and the gels were analysed in a wide frequency range. Several tissues were mimicked thanks to these materials, which proved to be suitable as phantoms from 2 up to 26.5 GHz. The main way to reduce their dielectric properties is to increase the cross-linking degree, which reduces the amount of liquid they absorb, so that the liquid/polymer ratio decreases. The accuracy of the obtained tissue-equivalent gels was calculated by means of the RMSE values. Table 6.1 shows a comparison of those liquid and solid phantoms which have been found in the literature that include the accuracy within the same frequency range than those presented in this thesis.

The list of phantoms that have been found in the literature within the same frequency range that include the accuracy is short. One can see that the accuracy of the liquid phantoms reported in this thesis is significantly higher than those previously reported, whereas the semisolid phantoms own a similar deviation. However, the enhancements for the latter are the better mechanical properties and the tailoring capacity, which allows the number of tissues to be increased.

Table 6.1: Comparison between the accuracy of some of the phantoms obtained in this thesis and those previously presented in the literature.

Phantom	**This study [RMSE](Re/Im)**	**Previously reported [RMSE](Re/Im)**
Muscle	Liquid (1.17/0.30 S/m), semisolid (5.00/2.83 S/m)	Liquid (5.61/2.38 S/m) [10], semisolid (4.60/2.49 S/m) [21]
Wet skin	Liquid (1.3/0.73 S/m), semisolid (3.63/1.82 S/m)	Semisolid (2.62/2.44 S/m) [21]
Blood	Liquid (1.59/0.04 S/m)	Semisolid (5.04/1.06 S/m) [21]
Liver	Liquid (0.9/1.11), semisolid (0.55/2.12)	Solid ([5.58, 8.55, 7.77]/[5.49, 5.77, 6.47]) [27]

In fact, most of the imitated tissues had not been previously reported within this frequency band. In other cases, like the fat tissue, it had been previously reported but just in semisolid form. The fat phantom suggested here introduces the liquid format keeping the accuracy and reducing the number of ingredients.

Chapter 5 showed the use and need of phantoms in some biomedical applications. First, the matching of an antenna from a wearable medical band was assessed in order to validate that it still works properly when it is placed in a patient wrist. The presence of the human body affects heavily the quality of the communications in these kinds of devices that try to use the minimum amount of power. Later, a SAR evaluation test, like the ones that are conducted to commercial wireless devices, was carried out at three different frequencies. The novelty here, was the possibility to perform it at several frequencies without changing the phantom in use, since these normally are narrow band and need to be adjusted for every single frequency. Thereafter, a propagation experiment for UWB frequencies, from which several analyses were conducted, was achieved. Once again, the chance of imitating the full band with a single phantom allowed to draw conclusions in many aspects that had not been possible to study before. The versatility of the wideband phantoms presented in this thesis was used to imitate both a healthy and a malignant colon tissue. This experiment was performed in order to check the sensitivity of a prototype that is intended to detect cancerous cells from changes in the relative permittivity of the tissues. Finally, another application regarding the cancer detection was tested with the phantoms. In this case, the penetration ratio of a UWB signal inside the breast tissue was established. Thanks to the fat and muscle wideband phantoms, it was possible to compute the exact distance or depth that the system is able to reach for detecting abnormalities.

6.2 Future Work

This thesis aimed at developing tissue-equivalent phantoms to provide them as a tool for researchers that work with microwave devices that are placed near or inside the human body. The main reason is to avoid, or at least reduce, the human or animal experimentation due to ethical and moral reasons.

The focus was placed in the 2.4 GHz ISM and UWB biomedical bands, and later in the millimetre waves. The first ones for the WBANs, which use the human as the transmitting medium so that they depend entirely on the use of models for the design of devices. The millimetre waves due to the upcoming 5G technology, whose usage frequencies will be much more influenced by all objects in general and by the body in particular. This combined with the greater presence and closeness of the access points makes crucial to take into account the presence of the human body in these networks. However, there are other medical bands like the MICS ones, which work at lower frequencies and are more used nowadays than those aforementioned. Although the influence of body tissues is not so strong here (that is why they are currently used), it would be convenient to enlarge the number of available phantoms for these technologies as well.

Acetonitrile was found out to be the perfect candidate to achieve the dielectric properties of most of the high water content tissues. The trend that these values achieve at their maximum measured frequency (26.5 GHz), suggests that these will probably imitate the tissues at higher frequencies. Therefore, these samples should be measured at the part of the spectrum that corresponds to millimetre waves, since they would probably get a better approximation than alcoholic mixtures.

Further investigation about the mixing rules should be done, since they have been valuable in the literature to estimate the dielectric properties of tissues at large bandwidths. It is certainly not the same as a mixture, but maybe there is the possibility to introduce a correction factor or to use different formulas that consider these interactions that have the molecules. If the possibility of not having to prepare all the mixtures to study the effect on permittivity was introduced, a significant time would be saved.

The solid models have been entrusted to the 3D printing, since it is not possible to reach such rigidity with materials without a large content of liquid, like the gels. Then, the solution is to print a plastic casing with the shape of the tissue in question and fill it with the liquid phantom. Mimicking the shape of the tissues can be possible with MRI images, which can recreate 3D models of real people at the present time. The relative permittivity of polymers is near that of the air, so the contour would be practically negligible in terms of electromagnetic fields. PET is a promising candidate polymer that should be

studied in the future. It is not as used or reported as the ubiquitous PLA or ABS, but still it is a material that can be 3D-printed with FDM technology.

Regarding the gels, they were synthesised in small samples and without the shape of any particular tissue. The open-ended coaxial method is theoretically suitable for measuring semisolid materials. However, it has been shown that the pressure applied to the analysed sample has a significant influence on the measured values. A different method such as the transmission line should be carried out in order to compare, even if the measurable frequency bandwidth is narrower.

Manufacturing a gel with the shape of a particular tissue or region becomes necessary as the next step. The vessel where the gel should be prepared is a 3D printed model like in the case of the solid models. In this case, the container would be just in the manufacturing steps and then removed from the material. At the end, the final purpose is the attainment of a heterogeneous manikin model with the maximum amount of mimicked tissues to be as realistic as possible. How the dielectric properties are placed in the space determines the behaviour of the electromagnetic waves in the medium.

Finally, the possibility of working with the different applications where the phantoms are required, motivates the finding of new requirements. This search of new challenges leads to new ideas that are captured in new models or features for the existing ones. Then, more usage cases that currently have limitations in the testing stage should be pursued. At the end, it consists in replacing the real tissues in all the possible senses for facilitating the research.

Appendix A

Dielectric Properties of the Human Body

A.1 Dispersion Regions

The dielectric properties of the human body have been largely studied for different reasons. Some researchers try to analyse the tissue composition by studying the different phenomena that appear when particular frequencies are applied to the tissue under test. Other authors just want to provide the numerical values as a tool for different calculations or to try to imitate them, like in the case of the phantoms. Like any kind of material, when it suffers a polarisation process, there is a change on its values of relative permittivity. One of the pioneers in studying the dielectric properties and the classifications of the different mechanisms that suffer the tissues was Schwan [80]. He reported three main dispersion regions, which are frequency bands where there is a change in the trend of the dielectric properties due to certain mechanisms. This behaviour has been classified in the α dispersion, from 10 Hz to 10 kHz, the β dispersion, from 10 kHz to 100 MHz, and the γ dispersion, from 100 MHz to 100 GHz. These regions can be appreciated in Fig. A.1, where the dielectric properties of the muscle are depicted in logarithmic scale, to better appreciate these effects.

Internally, the polarisation mechanisms are due to the movement of the tissue constituents, including cells, proteins, surfaces, charges, etc. Later on, Scwan [81] also described why these mechanisms are due. The α dispersion is mainly caused by the conductance and capacitance of the cell membranes and surfaces, largely produced by the response of the counterion atmosphere near the charged cell surface.

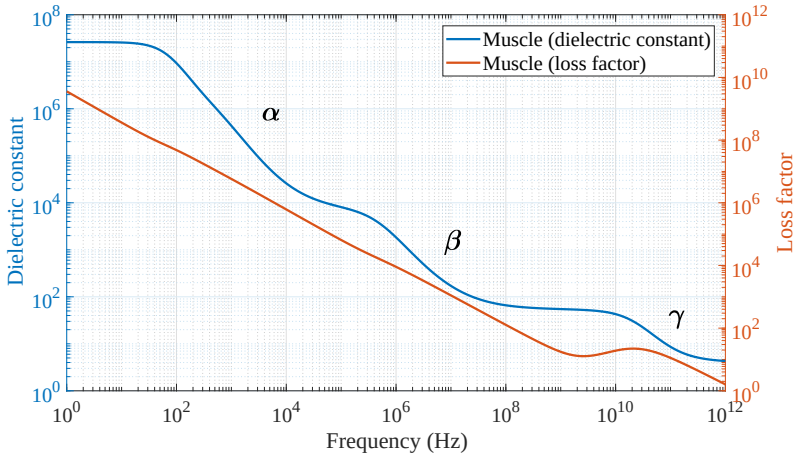

Figure A.1: Dielectric properties of the muscle tissue and its dispersion regions, according to Gabriel [3].

The β dispersion is due to the cellular structure of tissues with poorly conducting membranes. These membranes are charged through the conducting phases inside and outside. The γ dispersion is influenced by the water polarisation, and it is included within the tissue dispersion region because tissues and cells contain a large amount of water. This effect also includes a subsidiary dispersion effect, the δ dispersion, which is due to the protein bound water. All these regions actually represent relaxation effects, i.e., they appear when the movement of the charges is not fast enough to reach the frequency of the applied electric field. Charges can be as little as an electron or as big as long molecule chain. Depending on how much it costs to move the charge in question, the polarisation mechanism will take more or less time. Since tissues are large and complex structures, they reach enormous dielectric constants at extremely low frequencies. However, these rapidly disappear, leading to the polarisation mechanisms of the smaller particles. These regions are just appreciated in the dielectric constant, since the high losses due to electrical conductivity hide them until the γ dispersion region, where the ionic polarisation mechanism disappears (see Fig. 1.7).

A.2 Variability Factors

There are plenty of factors that can affect the actual dielectric properties of the body tissues. The main features are the free water and the ionic conduc-

tivity [82, 83], which are really important in soft tissues. These are directly affected for aspects like species, gender or age [84]. Precisely the water content varies a lot depending on the measuring conditions of the subject. Tissues become dehydrated quickly after being excised from the specimen, i.e., at *ex vivo* conditions [85]. Thus, the ideal conditions to perform the dielectric measurements are *in vivo* with the subject at body temperature. Temperature modify both the values and the relaxation frequency of the materials, and so with tissues [86]. That is why it must be specified in any measurement campaign, and researchers try to reproduce that of the normal body. The measurement technique can also modify the obtained results, like in [87], where authors report a average deviation of 10% by using different methods. However, most authors use the open-ended coaxial system due to its versatility and wideband measurement capability.

Some authors are interested in the changes that malignant cells may have on tissues [77, 88]. Breasts [89], colon [74], liver [90, 91] or prostate [92], among others, have been tissues that have been studied in this sense. The values for their dielectric properties have shown that there are significant variations between their healthy and malignant state. The main purpose of these studies are intended for cancer detection techniques [93, 94].

A.3 Cole-Cole Parametric Fitting

The dielectric properties of the tissues are typically fitted to the Cole-Cole model (Eq. 3.1), including as many poles as dispersion regions are present in the studied frequency band. Authors that want to offer the measured data for other to reproduce them usually provide the fitting parameters. These parameters are the dielectric constant at infinite frequency (ε_∞), the static dielectric constant (ε_0), the angular frequency (ω) in rad/s, the relaxation time (τ) in s^{-1}, the exponential parameter (α), and the static conductivity (σ_s) in S/m.

$$\varepsilon_r' - j\varepsilon_r'' = \varepsilon_\infty + \sum_{i=1}^{poles} \frac{\varepsilon_s - \varepsilon_\infty}{1 + (j\omega\tau)^{1-\alpha}} + \frac{\sigma_s}{j\omega\varepsilon_0} \qquad \text{(3.1 revisited)}$$

The most widespread reference data of body tissues is the Gabriel's database [3], who gathered the previously reported dielectric properties in the literature [95], enlarged it with new measurements [96], and provided the data in parametric models [97]. These data are based on the combination of measurements from different animals and in different conditions, although human tissues or *in vivo* were prioritised over animal tissues or *in vitro*. The data were obtained through three different experimental techniques in the frequency

range 10 Hz to 20 GHz and fitted to a 4-pole Cole-Cole model. These data are openly offered in a website [11]. There are also other open resources to find the dielectric properties of many body tissues, like in this other website [98], where a database of 20 tissues is available, based on the results published in [73]. The results of this latter study have been obtained from recent measurements where the conditions were more controlled. In this particular case, the measurements were carried out with *in vivo* porcine specimens, from 0.5 to 26.5 GHz, keeping characteristics such as weight, race, age or gender. This offers the data for a 2-pole model due to the measured frequency range, although on the website one can introduce the number of points and download the values for each frequency. The uncertainty for each tissue is also provided, which is an added value for researchers.

Thesis Contributions

Publications and Activities Stemming from this Thesis

International Journals

[J1] **S. Castelló-Palacios**, C. Garcia-Pardo, A. Fornes-Leal, N. Cardona, and A. Vallés-Lluch, "Tailor-Made Tissue Phantoms Based on Acetonitrile Solutions for Microwave Applications up to 18 GHz," *IEEE Transactions on Microwave Theory and Techniques*, vol. 64, no. 11, pp. 3987-3994, November 2016.

[J2] **S. Castelló-Palacios**, C. Garcia-Pardo, M. Alloza-Pascual, A. Fornes-Leal, N. Cardona, and A. Vallés-Lluch, "Gel Phantoms for Body Microwave Propagation in the (2 to 26.5) GHz Frequency Band," *IEEE Transactions on Antennas and Propagation*, vol. 67, no. 10, pp. 6564-6573, October 2019.

Patents

[P1] N. Cardona Marcet, **S. Castelló Palacios**, A. Fornés Leal, C. García Pardo, and A. Vallés Lluch, "Synthetic Model of Biological Tissues for Evaluating the Wireless Transmission of Electromagnetic Waves," Patent WO 2017/109252 Al, June 29, 2017.

International Research Visits

[V1] Universiteit Gent, imec - WAVES, Ghent (Belgium). February - April 2017 (3 months).

THESIS CONTRIBUTIONS

Research Projects

[RP1] European Coalition for Cancer Detection Based on Electromagnetic Techniques (EUIN2017-88272).

- Funding institution: Agencia Estatal de Investigación, Spain.
- Start date: 01/01/2017
- Duration: 24 months

[RP2] Electromagnetic Probe for Early Tumour Detection (UPV-FE-2017-B04).

- Funding institution: Universitat Politècnica de València, Spain.
- Start date: 01/05/2018
- Duration: 18 months

International Conferences

[C1] **S. Castelló-Palacios**, A. Vallés-Lluch, C. Garcia-Pardo, A. Fornes-Leal, and N. Cardona, "Formulas for easy-to-prepare tailored phantoms at 2.4 GHz ISM band," *2017 11th International Symposium on Medical Information and Communication Technology (ISMICT)*, Lisbon, 2017, pp. 27-31.

[C2] **S. Castelló-Palacios**, C. Garcia-Pardo, A. Fornes-Leal, N. Cardona, and A. Vallés-Lluch, "Wideband phantoms of different body tissues for heterogeneous models in body area networks," *2017 39th Annual International Conference of the IEEE Engineering in Medicine and Biology Society (EMBC)*, Seogwipo, 2017, pp. 3032-3035.

[C3] **S. Castelló-Palacios**, C. Garcia-Pardo, A. Fornes-Leal, N. Cardona, and A. Vallés-Lluch, "Full-spectrum phantoms for cm-wave and medical wireless communications," *12th European Conference on Antennas and Propagation (EuCAP 2018)*, London, 2018, pp. 1-3.

[C4] **S. Castelló-Palacios**, C. Garcia-Pardo, A. Fornes-Leal, N. Cardona, M. Alloza-Pascual, and A. Vallés-Lluch, "Initial Results of Semisolid Phantoms Based on Synthetic Hydrogels for the cmWave Band," *2018 IEEE 29th Annual International Symposium on Personal, Indoor and Mobile Radio Communications (PIMRC)*, Bologna, 2018, pp. 1128-1129.

[C5] **S. Castelló-Palacios**, C. Garcia-Pardo, N. Cardona, A. Vallés-Lluch, R. Aminzadeh, G. Vermeeren, and W. Joseph, "Elaboration of Simple Gel Phantoms for 5G/mm Wave Communications," *2018 IEEE 29th Annual International Symposium on Personal, Indoor and Mobile Radio Communications (PIMRC)*, Bologna, 2018, pp. 1215-1219.

COST Technical Documents

[TD1] **S. Castelló-Palacios**, C. Garcia-Pardo, A. Fornes-Leal, N. Cardona, and A. Vallés-Lluch, "Tailor-Made Tissue Phantoms Based on Acetonitrile Solutions for Microwave Applications up to 18 GHz," *2nd Technical Meeting, European COST CA15104 action*, Durham, United Kingdom, October 2016.

[TD2] **S. Castelló-Palacios**, C. Garcia-Pardo, N. Cardona, A. Vallés-Lluch, R. Aminzadeh, G. Vermeeren, and W. Joseph, "Elaboration of Simple Gel Phantoms for 5G/mm Wave Communications," *7th MC and Technical Meeting, European COST CA15104 action*, Cartagena, Spain, May 2018.

Publications and Activities Related to this Thesis

International Journals

[J3] C. Andreu, **S. Castelló-Palacios**, C. Garcia-Pardo, A. Fornes-Leal, A. Vallés-Lluch, and N. Cardona, "Spatial In-Body Channel Characterization Using an Accurate UWB Phantom," *IEEE Transactions on Microwave Theory and Techniques*, vol. 64, no. 11, pp. 3995-4002, November 2016.

[J4] C. Andreu, C. Garcia-Pardo, **S. Castelló-Palacios**, A. Vallés-Lluch, and N. Cardona, "Frequency Dependence of UWB In-Body Radio Channel Characteristics," *IEEE Microwave and Wireless Components Letters*, vol. 28, no. 4, pp. 359-361, April 2018.

[J5] C. Garcia-Pardo, C. Andreu, A. Fornes-Leal, **S. Castelló-Palacios**, S. Perez-Simbor, M. Barbi, A. Vallés-Lluch, and N. Cardona, "Ultrawideband Technology for Medical In-Body Sensor Networks: An Overview of the Human Body as a Propagation Medium, Phantoms, and Approaches for Propagation Analysis," *IEEE Antennas and Propagation Magazine*, vol. 60, no. 3, pp. 19-33, June 2018.

[J6] C. Andreu, C. Garcia-Pardo, **S. Castelló-Palacios**, and N. Cardona, "Experimental Assessment of Time Reversal for In-Body to In-Body UWB Communications," *Wireless Communications and Mobile Computing*, vol. 2018, Article ID 8927107, 12 pages, 2018.

[J7] A. Fornes-Leal, N. Cardona, M. Frasson, **S. Castelló-Palacios**, A. Nevárez, M. Frasson, and C. Garcia-Pardo, "Dielectric Characterization of *In Vivo* Abdominal and Thoracic Tissues in the 0.5-26.5 GHz Frequency Band for Wireless Body Area Networks," *IEEE Access*, vol. 7, pp. 31854-31864, 2019.

International Conferences

[C6] A. Fornes-Leal, C. Garcia-Pardo, N. Cardona, **S. Castelló-Palacios**, and A. Vallés-Lluch, "Accurate broadband measurement of electromagnetic tissue phantoms using open-ended coaxial systems," *2017 11th International Symposium on Medical Information and Communication Technology (ISMICT)*, Lisbon, 2017, pp. 32-36.

[C7] S. Perez-Simbor, M. Barbi, C. Garcia-Pardo, **S. Castelló-Palacios**, and N. Cardona, "Initial UWB in-body channel characterization using a novel multilayer phantom measurement setup," *2018 IEEE Wireless Communications and Networking Conference Workshops (WCNCW)*, Barcelona, 2018, pp. 384-389.

[C8] M.F. Awan, S. Perez-Simbor, K. Kansanen, P. Bose, **S. Castelló-Palacios**, and N. Cardona, "Experimental phantom-based evaluation of Physical Layer Security for Future Leadless Cardiac Pacemaker," *2018 IEEE 29th Annual International Symposium on Personal, Indoor and Mobile Radio Communications (PIMRC)*, Bologna, 2018, pp. 333-339.

[C9] A. Fornes-Leal, C. Garcia-Pardo, **S. Castelló-Palacios**, N. Cardona, M. Frasson, A. Nevárez, and V. Pons Beltrán, "Variability of the Dielectric Properties Due to Tissue Heterogeneity and Its Influence on the Development of EM Phantoms," *2018 IEEE 29th Annual International Symposium on Personal, Indoor and Mobile Radio Communications (PIMRC)*, Bologna, 2018, pp. 365-369.

[C10] H. Benchakroun, **S. Castelló-Palacios**, A. Nevarez, M. Cabedo-Fabrés, and M. Ferrando-Bataller, "Study of penetration ratio using UWB antenna with an in vivo subject," *13th European Conference on Antennas and Propagation (EuCAP 2019)*, Krakow, 2019, pp. 1-5.

[C11] M.F. Awan, K. Kansanen, S. Perez-Simbor, C. Garcia-Pardo, **S. Castelló-Palacios**, and N. Cardona, "RSS-Based Secret Key Generation in Wireless In-Body Networks," *2019 13th International Symposium on Medical Information and Communication Technology (ISMICT)*, Oslo, 2019, pp. 1-6.

COST Technical Documents

[TD3] C. Garcia-Pardo, R. Chávez-Santiago, A. Fornes-Leal, **S. Castelló-Palacios**, A. Vallés-Lluch, C. Andreu, I. Balasingham, and N. Cardona, "Experimental Ultra Wideband Path Loss Models for Implant Communications," *2nd Technical Meeting, European COST CA15104 action*, Durham, United Kingdom, October 2016.

[TD4] M. Barbi, S. Perez-Simbor, C. Garcia-Pardo, **S. Castelló-Palacios**, C. Andreu, A. Fornes-Leal, and N. Cardona, "Localization of Capsule Endoscopy at UWB Frequencies Using an Experimental Multilayer Phantom," *5th MC and Technical Meeting, European COST CA15104 action*, Graz, Austria, September 2017.

[TD5] C. Andreu, C. Garcia-Pardo, **S. Castelló-Palacios**, A. Vallés-Lluch, and N. Cardona, "Frequency Dependence of UWB In-Body Radio Channel Characteristics," *7th MC and Technical Meeting, European COST CA15104 action*, Cartagena, Spain, May 2018.

National Journals

[NJ1] C. Garcia Pardo, C. Andreu Estellés, A. Fornes Leal, **S. Castelló Palacios**, S. Pérez Simbor, M. Barbi, A. Vila Jiménez, M. Cabedo Fabrés, V. Pons Beltrán, M. Frasson, A. Vallés Lluch, and N. Cardona, "Wireless Communications for Medical In-Body Devices: Challenges for In-Body Propagation," *Waves*, year 9, pp. 17-28, 2017.

National Conferences

[NC1] C. Garcia Pardo, C. Andreu Estellés, S. Pérez Simbor, **S. Castelló Palacios**, A. Fornes Leal, M. Barbi, A. Vallés Lluch, and N. Cardona, "UWB Propagation for Medical In-body Devices," *XXXIII Simposium Nacional de la Unión Científica Internacional de Radio (URSI 2018)*, Granada, Spain, 2018.

Acronyms

ABS Acrylonitrile Butadiene Styrene

APS Ammonium Persulfate

EGDMA Ethylene Glycol Dimethylacrylate

FDM Fused Deposition Modelling

HA Hyaluronic Acid

HEA 2-Hydroxyethyl Acrylate

ICNIRP International Commission on Non-Ionizing Radiation Protection

ISM Industrial, Scientific and Medical

MICS Medical Implant Communication Service

MRI Magnetic Resonance Imaging

MSE Mean Square Error

MUT Material Under Test

NMBA N,N'-Methylenebis(Acrylamide)

PAM Polyacrilamide

PCL Polycaprolactone

PEG Polyethylene Glycol

PET Polyethylene Terephthalate

PHEA Poly(2-Hydroxyethyl Acrylate)

PHEMA Poly(2-Hydroxethyl Methacrylate)

PLA Polylactic Acid

PP Polypropylene

PVA Polyvinyl Alcohol

RMSE Root Mean Square Error

SAR Specific Absorption Rate

UV Ultraviolet

UWB Ultrawideband

VNA Vector Network Analyser

WBAN Wireless Body Area Network

WPAN Wireless Personal Area Network

References

[1] 3rd Generation Partnership Project (3GPP), "NR; User Equipment (UE) radio transmission and reception; Part 2: Range 2 Standalone," TS 38.101-2 (V15.6.0), Jun. 2019.

[2] OpenStax, *College Physics*. OpenStax, 2016, ch. 19. Electric Potential and Electric Field. [Online]. Available: https://pressbooks.bccampus.ca/collegephysics/chapter/capacitors-and-dielectrics/ [Accessed: 2-May-2019], pp. 746–753.

[3] C. Gabriel, "Compilation of the dielectric properties of body tissues at RF and microwave frequencies," Occupational and Environmental Health Directorate, Radiofrequency Radiation Division, Brooks Air Force Base, Texas (USA), Technical Report AL/OE-TR-1996-0037, Jun. 1996.

[4] S. Oh, Y.-C. Ryu, G. Carluccio, C. T. Sica, and C. M. Collins, "Measurement of SAR-induced temperature increase in a phantom and in vivo with comparison to numerical simulation," *Magnetic Resonance in Medicine*, vol. 71, no. 5, pp. 1923–1931, 2014.

[5] Y. Wang, A. M. Abbosh, B. Henin, and P. T. Nguyen, "Synthetic bandwidth radar for ultra-wideband microwave imaging systems," *IEEE Transactions on Antennas and Propagation*, vol. 62, no. 2, pp. 698–705, Feb. 2014.

[6] P. Homolka, M. Figl, A. Wartak, M. Glanzer, M. Dünkelmeyer, A. Hojreh, and J. Hummel, "Design of a head phantom produced on a 3D rapid prototyping printer and comparison with a RANDO and 3M lucite head phantom in eye dosimetry applications," *Physics in Medicine and Biology*, vol. 62, no. 8, pp. 3158–3174, Mar. 2017.

[7] D. Kurup, W. Joseph, G. Vermeeren, and L. Martens, "Path loss model for in-body communication in homogeneous human muscle tissue," *Electronics Letters*, vol. 45, no. 9, pp. 453–454, Apr. 2009.

[8] A. R. Guraliuc, M. Zhadobov, O. De Sagazan, and R. Sauleau, "Solid phantom for body-centric propagation measurements at 60 GHz," *IEEE Transactions on Microwave Theory and Techniques*, vol. 62, no. 6, pp. 1373–1380, Jun. 2014.

[9] C. Gabriel, "Tissue equivalent material for hand phantoms," *Physics in Medicine and Biology*, vol. 52, no. 14, pp. 4205–4210, Jul. 2007.

[10] H. Yamamoto, J. Zhou, and T. Kobayashi, "Ultra wideband electromagnetic phantoms for antennas and propagation studies," *IEICE Trans. Fundam. Electron. Commun. Comput. Sci.*, vol. E91-A, no. 11, pp. 3173–3182, 2008.

[11] D. Andreuccetti, R. Fossi, and C. Petrucci, "An Internet resource for the calculation of the dielectric properties of body tissues in the frequency range 10 Hz-100 GHz," IFAC-CNR, Florence (Italy), 1997. Based on data published by C. Gabriel *et al.* in 1996. [Online]. Available: http://niremf.ifac.cnr.it/tissprop/ [Accessed: 12-Mar-2019].

[12] N. Chahat, M. Zhadobov, and R. Sauleau, "Broadband tissue-equivalent phantom for BAN applications at millimeter waves," *IEEE Transactions on Microwave Theory and Techniques*, vol. 60, no. 7, pp. 2259–2266, Jul. 2012.

[13] M. Saviz and R. Faraji-Dana, "A theoretical model for the frequency-dependent dielectric properties of corneal tissue at microwave frequencies," *Progress In Electromagnetics Research*, vol. 137, pp. 389–406, 2013, doi: 10.2528/PIER12112510.

[14] C.-K. Chou, G.-W. Chen, A. W. Guy, and K. H. Luk, "Formulas for preparing phantom muscle tissue at various radiofrequencies," *Bioelectromagnetics*, vol. 5, no. 4, pp. 435–441, 1984.

[15] A. A. Bakar, A. Abbosh, P. Sharpe, M. Bialkowski, and Y. Wang, "Heterogeneous breast phantom for ultra wideband microwave imaging," *Microwave and Optical Technology Letters*, vol. 53, no. 7, pp. 1595–1598, 2011.

[16] S. Romeo, L. Di Donato, O. M. Bucci, I. Catapano, L. Crocco, M. R. Scarfi, and R. Massa, "Dielectric characterization study of liquid-based materials for mimicking breast tissues," *Microwave and Optical Technology Letters*, vol. 53, no. 6, pp. 1276–1280, 2011.

[17] X. Li, S. K. Davis, S. C. Hagness, D. W. van der Weide, and B. D. Van Veen, "Microwave imaging via space-time beamforming: experimental investigation of tumor detection in multilayer breast phantoms," *IEEE Transactions on Microwave Theory and Techniques*, vol. 52, no. 8, pp. 1856–1865, Aug. 2004.

[18] M. Lazebnik, E. L. Madsen, G. R. Frank, and S. C. Hagness, "Tissue-mimicking phantom materials for narrowband and ultrawideband microwave applications," *Physics in Medicine and Biology*, vol. 50, no. 18, pp. 4245–4258, Aug. 2005.

[19] K. Ito, "Human body phantoms for evaluation of wearable and implantable antennas," in *The Second European Conference on Antennas and Propagation, EuCAP 2007*, Edinburgh, UK, Nov. 2007, pp. 1–6.

[20] A. Abu Bakar, A. Abbosh, and M. Bialkowski, "Fabrication and characterization of a heterogeneous breast phantom for testing an ultrawideband microwave imaging system," in *Asia-Pacific Microwave Conference 2011*, Melbourne, VIC, USA, Dec. 2011, pp. 1414–1417.

[21] T. Yilmaz, R. Foster, and Y. Hao, "Broadband tissue mimicking phantoms and a patch resonator for evaluating noninvasive monitoring of blood glucose levels," *IEEE Transactions on Antennas and Propagation*, vol. 62, no. 6, pp. 3064–3075, Jun. 2014.

[22] Y. Baskharoun, A. Trehan, N. K. Nikolova, and M. D. Noseworthy, "Physical phantoms for microwave imaging of the breast," in *2012 IEEE Topical Conference on Biomedical Wireless Technologies, Networks, and Sensing Systems (BioWireleSS)*, Santa Clara, CA, USA, Jan. 2012, pp. 73–76.

[23] S. Alshehri, A. Jantan, R. S. A. Raja Abdullah, R. Mahmud, S. Khatun, and Z. Awang, "A UWB imaging system to detect early breast cancer in heterogeneous breast phantom," in *International Conference on Electrical, Control and Computer Engineering 2011 (InECCE)*, Pahang, Malaysia, Jun. 2011, pp. 238–242.

[24] I. J. Youngs, A. S. Treen, G. Fixter, and S. Holden, "Design of solid broadband human tissue simulant materials," *IEE Proceedings - Science, Measurement and Technology*, vol. 149, no. 6, pp. 323–328, Nov. 2002.

[25] J. Bourqui, M. A. Campbell, and E. C. Fear, "Antenna evaluation for ultra-wideband microwave imaging," *International Journal of Antennas and Propagation*, vol. 2010, no. 850149, pp. 1–8, 2010.

[26] J. Garrett and E. Fear, "Stable and flexible materials to mimic the dielectric properties of human soft tissues," *IEEE Antennas and Wireless Propagation Letters*, vol. 13, pp. 599–602, 2014.

[27] P. Prakash, M. C. Converse, D. M. Mahvi, and J. G. Webster, "Measurement of the specific heat capacity of liver phantom," *Physiological Measurement*, vol. 27, no. 10, pp. N41–N46, Aug. 2006.

[28] W. C. Khor, F. Y. Hui, M. E. Bialkowski, and S. Crozier, "Investigations into microwave properties of various substances to develop a breast phantom for a UWB breast tumour radar detecting system," in *MIKON 2008 - 17th International Conference on Microwaves, Radar and Wireless Communications*, Wroclaw, Poland, May 2008, pp. 1–4.

[29] S. A. Kumar and T. Shanmuganantham, "Design of implantable CPW fed monopole H-slot antenna for 2.45 GHz ISM band applications," *AEU - International Journal of Electronics and Communications*, vol. 68, no. 7, pp. 661–666, Jul. 2014.

[30] T. Takahashi, M. Miyakawa, M. Tamura, and T. Ogawa, "High fidelity breast phantom and its microwave imaging by CP-MCT," in *Asia-Pacific Microwave Conference 2011*, Melbourne, VIC, USA, Dec. 2011, pp. 1490–1493.

[31] K. Fukunaga, S. Watanabe, and Y. Yamanaka, "Dielectric properties of tissue-equivalent liquids for safety evaluation tests of mobile phones," in *2003 Annual Report Conference on Electrical Insulation and Dielectric Phenomena*, Albuquerque, NM, USA, Oct. 2003, pp. 44–47.

[32] A. Hellerbach, V. Schuster, A. Jansen, and J. Sommer, "MRI phantoms - are there alternatives to agar?" *PLoS One*, vol. 8, no. 8, Aug. 2013.

[33] J. Lacik, V. Hebelka, J. Velim, Z. Raida, and J. Puskely, "Wideband skin-equivalent phantom for V- and W-band," *IEEE Antennas and Wireless Propagation Letters*, vol. 15, pp. 211–213, 2016.

[34] R. Aminzadeh, M. Saviz, and A. A. Shishegar, "Theoretical and experimental broadband tissue-equivalent phantoms at microwave and millimetre-wave frequencies," *Electronics Letters*, vol. 50, no. 8, pp. 618–620, Apr. 2014.

[35] S. K. H. Gulrez, S. Al-Assaf, and G. O. Phillips, *Progress in Molecular and Environmental Bioengineering*. IntechOpen, 2011, ch. 5.

Hydrogels: Methods of Preparation, Characterisation and Applications. [Online]. Available: https://www.intechopen.com/books/progress-in-molecular-and-environmental-bioengineering-from-analysis-and-modeling-to-technology-applications/hydrogels-methods-of-preparation-characterisation-and-applications [Accessed: 2-May-2019], pp. 117–150.

[36] F. Franks, *Chemistry and Technology of Water-Soluble Polymers*. New York, NY, USA: Springer US, 1983, ch. 9. Water Solubility and Sensitivity-Hydration Effects, pp. 157–178.

[37] W. Shei, "Structure, dynamics, and properties of artificial protein hydrogels assembled through coiled-coil domains," Ph.D. dissertation, California Institute of Technology, Pasadena, CA, USA, 2005.

[38] B. D. Ratner and A. S. Hoffman, *Hydrogels for Medical and Related Applications*. Washington, DC, USA: American Chemical Society, 1976, ch. 1. Synthetic Hydrogels for Biomedical Applications, pp. 1–36.

[39] A. S. Hoffman, "Hydrogels for biomedical applications," *Advanced Drug Delivery Reviews*, vol. 64, pp. 18–23, 2012.

[40] B. V. Slaughter, S. S. Khurshid, O. Z. Fisher, A. Khademhosseini, and N. A. Peppas, "Hydrogels in regenerative medicine," *Advanced Materials*, vol. 21, no. 32-33, pp. 3307–3329, 2009.

[41] Y. Qiu and K. Park, "Environment-sensitive hydrogels for drug delivery," *Advanced Drug Delivery Reviews*, vol. 53, no. 3, pp. 321–339, 2001.

[42] T. V. Chirila, "An overview of the development of artificial corneas with porous skirts and the use of PHEMA for such an application," *Biomaterials*, vol. 22, no. 24, pp. 3311–3317, 2001.

[43] J. A. Stammen, S. Williams, D. N. Ku, and R. E. Guldberg, "Mechanical properties of a novel PVA hydrogel in shear and unconfined compression," *Biomaterials*, vol. 22, no. 8, pp. 799–806, 2001.

[44] E. Tziampazis, J. Kohn, and P. V. Moghe, "PEG-variant biomaterials as selectively adhesive protein templates: model surfaces for controlled cell adhesion and migration," *Biomaterials*, vol. 21, no. 5, pp. 511–520, 2000.

[45] J. A. Burdick and G. D. Prestwich, "Hyaluronic acid hydrogels for biomedical applications," *Advanced Materials*, vol. 23, no. 12, pp. H41–H56, 2011.

[46] A. D. Augst, H. J. Kong, and D. J. Mooney, "Alginate hydrogels as biomaterials," *Macromolecular Bioscience*, vol. 6, no. 8, pp. 623–633, 2006.

[47] T. A. E. Ahmed, E. V. Dare, and M. Hincke, "Fibrin: A versatile scaffold for tissue engineering applications," *Tissue Engineering Part B: Reviews*, vol. 14, no. 2, pp. 199–215, 2008.

[48] C. H. Lee, A. Singla, and Y. Lee, "Biomedical applications of collagen," *International Journal of Pharmaceutics*, vol. 221, no. 1, pp. 1–22, 2001.

[49] E. Karadağ and D. Saraydın, "Swelling of superabsorbent acrylamide/sodium acrylate hydrogels prepared using multifunctional crosslinkers," *Turkish Journal of Chemistry*, vol. 26, no. 6, pp. 863–875, Jan. 2002.

[50] H. Towbin, T. Staehelin, and J. Gordon, "Electrophoretic transfer of proteins from polyacrylamide gels to nitrocellulose sheets: procedure and some applications," *Proceedings of the National Academy of Sciences of the United States of America*, vol. 76, no. 9, pp. 4350–4354, Sep. 1979.

[51] R. Weinberg, U. Loening, M. Willems, and S. Penman, "Acrylamide gel electrophoresis of HeLa cell nucleolar RNA," *Proceedings of the National Academy of Sciences of the United States of America*, vol. 58, no. 3, pp. 1088–1095, Sep. 1967.

[52] U. Loening, "The fractionation of high-molecular-weight ribonucleic acid by polyacrylamide-gel electrophoresis," *Biochemical Journal*, vol. 102, no. 1, pp. 251–257, Jan. 1967.

[53] T.-H. Yang, "Recent applications of polyacrylamide as biomaterials," *Recent Patents on Materials Science*, vol. 1, no. 1, pp. 29–40, 2008.

[54] T. P. Marsland and S. Evans, "Dielectric measurements with an open-ended coaxial probe," *IEE Proceedings H - Microwaves, Antennas and Propagation*, vol. 134, no. 4, pp. 341–349, Aug. 1987.

[55] A. Nyshadham, C. L. Sibbald, and S. S. Stuchly, "Permittivity measurements using open-ended sensors and reference liquid calibration-an uncertainty analysis," *IEEE Transactions on Microwave Theory and Techniques*, vol. 40, no. 2, pp. 305–314, Feb. 1992.

[56] M. A. Stuchly, M. M. Brady, S. S. Stuchly, and G. Gajda, "Equivalent circuit of an open-ended coaxial line in a lossy dielectric," *IEEE Transactions on Instrumentation and Measurement*, vol. IM-31, no. 2, pp. 116–119, Jun. 1982.

[57] A. Fornes-Leal, C. Garcia-Pardo, N. Cardona, S. Castelló-Palacios, and A. Vallés-Lluch, "Accurate broadband measurement of electromagnetic tissue phantoms using open-ended coaxial systems," in *2017 11th International Symposium on Medical Information and Communication Technology (ISMICT)*, Lisbon, Portugal, Feb. 2017, pp. 32–36.

[58] E. Porter and M. O'Halloran, "Investigation of histology region in dielectric measurements of heterogeneous tissues," *IEEE Transactions on Antennas and Propagation*, vol. 65, no. 10, pp. 5541–5552, Oct. 2017.

[59] S. Nelson, "Technical note: Coaxial-probe contact-force monitoring for dielectric properties measurements," *Applied Engineering in Agriculture*, vol. 28, no. 1, pp. 149–152, 2012.

[60] R. Buchner, G. T. Hefter, and P. M. May, "Dielectric relaxation of aqueous NaCl solutions," *The Journal of Physical Chemistry A*, vol. 103, no. 1, pp. 1–9, 1999.

[61] J. Barthel and R. Buchner, "High frequency permittivity and its use in the investigation of solution properties," *Pure and Applied Chemistry*, vol. 63, no. 10, pp. 1473–1482, 1991.

[62] L. Guerin, *CK-12 Chemistry Concepts - Intermediate*. CK-12 Foundation, 2013, ch. 9.19. Hydrogen Bonding. [Online]. Available: https://www.ck12.org/book/CK-12-Chemistry-Concepts-Intermediate/section/9.19/ [Accessed: 2-May-2019].

[63] C. Beck, S. Nägele, J. Nagel, H. Guth, U. Gengenbach, and G. Bretthauer, "Low-cost head phantom for the evaluation and optimization of RF-links in ophthalmic implants," *Biomedical Engineering / Biomedizinische Technik*, vol. 58 (Suppl. 1), Aug. 2013.

[64] International Commission on Non-Ionizing Radiation Protection, "Latest publications on radio frequency-EMF guidelines, ICNIRP guidelines for limiting exposure to time-varying electric, magnetic and electromagnetic fields," *Health Physics*, vol. 74, pp. 494–522, 1998.

[65] G. Ancans, V. Bobrovs, A. Ancans, and D. Kalibatiene, "Spectrum considerations for 5G mobile communication systems," *Procedia Computer Science*, vol. 104, pp. 509–516, 2017.

[66] R. Aminzadeh, M. Saviz, and A. A. Shishegar, "Comments on 'Wideband skin-equivalent phantom for V- and W-band'," *IEEE Antennas and Wireless Propagation Letters*, vol. 16, pp. 3257–3257, 2017.

[67] "IEEE standard for local and metropolitan area networks - Part 15.6: Wireless body area networks," *IEEE Std 802.15.6-2012*, pp. 1–271, Feb. 2012.

[68] M. Patel and J. Wang, "Applications, challenges, and prospective in emerging body area networking technologies," *IEEE Wireless Communications*, vol. 17, no. 1, pp. 80–88, Feb. 2010.

[69] C. Andreu, S. Castelló-Palacios, C. Garcia-Pardo, A. Fornes-Leal, A. Vallés-Lluch, and N. Cardona, "Spatial in-body channel characterization using an accurate UWB phantom," *IEEE Transactions on Microwave Theory and Techniques*, vol. 64, no. 11, pp. 3995–4002, Nov. 2016.

[70] C. Andreu, C. Garcia-Pardo, A. Fornes-Leal, M. Cabedo-Fabrés, and N. Cardona, "UWB in-body channel performance by using a direct antenna designing procedure," in *2017 11th European Conference on Antennas and Propagation (EUCAP)*, Paris, France, Mar. 2017, pp. 278–282.

[71] C. Andreu, C. Garcia-Pardo, S. Castelló-Palacios, A. Vallés-Lluch, and N. Cardona, "Frequency dependence of UWB in-body radio channel characteristics," *IEEE Microwave and Wireless Components Letters*, vol. 28, no. 4, pp. 359–361, Apr. 2018.

[72] C. Andreu, C. Garcia-Pardo, S. Castelló-Palacios, and N. Cardona, "Experimental assessment of time reversal for in-body to in-body UWB communications," *Wireless Communications and Mobile Computing*, vol. 2018, no. 8927107, pp. 1–12, Apr. 2018.

[73] A. Fornes-Leal, N. Cardona, M. Frasson, S. Castelló-Palacios, A. Nevárez, V. Pons Beltrán, and C. Garcia-Pardo, "Dielectric characterization of *in vivo* abdominal and thoracic tissues in the 0.5-26.5 GHz frequency band for wireless body area networks," *IEEE Access*, vol. 7, pp. 31 854–31 864, 2019.

[74] A. Fornes-Leal, C. Garcia-Pardo, M. Frasson, V. Pons-Beltrán, and N. Cardona, "Dielectric characterization of healthy and malignant colon tissues in the 0.5-18 GHz frequency band," *Physics in Medicine and Biology*, vol. 61, no. 20, pp. 7334–7346, 2016.

[75] A. Fornés Leal, "Dielectric characterization of biological tissues for medical applications," Ph.D. dissertation, Universitat Politècnica de València, Valencia, Spain, 2019.

[76] E. C. Fear and M. A. Stuchly, "Microwave detection of breast cancer," *IEEE Transactions on Microwave Theory and Techniques*, vol. 48, no. 11, pp. 1854–1863, Nov. 2000.

[77] M. Lazebnik, D. Popovic, L. McCartney, C. B. Watkins, M. J. Lindstrom, J. Harter, S. Sewall, T. Ogilvie, A. Magliocco, T. M. Breslin, W. Temple, D. Mew, J. H. Booske, M. Okoniewski, and S. C. Hagness, "A large-scale study of the ultrawideband microwave dielectric properties of normal, benign and malignant breast tissues obtained from cancer surgeries," *Physics in Medicine and Biology*, vol. 52, no. 20, pp. 6093–6115, 2007.

[78] H. Benchakroun, S. Castelló-Palacios, A. Nevarez, M. Cabedo-Fabrés, and M. Ferrando-Bataller, "Study of penetration ratio using UWB antenna with an in vivo subject," in *2019 13th European Conference on Antennas and Propagation (EuCAP)*, Krakow, Poland, Apr. 2019, pp. 1–5.

[79] H. Benchakroun, M. Cabedo-Fabrés, M. Ferrando-Bataller, Z. Mahlaoui, and A. Latif, "New approach for the design of UWB monopoles with directive radiation for BAN applications," in *2018 12th European Conference on Antennas and Propagation (EuCAP)*, London, UK, Apr. 2018, pp. 1–5.

[80] H. P. Schwan, "Electrical properties of tissue and cell suspensions," *Advances in Biological and Medical Physics*, vol. 5, pp. 147–209, 1957.

[81] ——, "Electrical properties of tissues and cell suspensions: mechanisms and models," in *Proceedings of 16th Annual International Conference of the IEEE Engineering in Medicine and Biology Society*, vol. 1, Baltimore, MD, USA, Nov. 1994, pp. A70–A71 vol.1.

[82] S. R. Smith and K. R. Foster, "Dielectric properties of low-water-content tissues," *Physics in Medicine and Biology*, vol. 30, no. 9, pp. 965–973, Sep. 1985.

[83] H. F. Cook, "The dielectric behaviour of some types of human tissues at microwave frequencies," *British Journal of Applied Physics*, vol. 2, no. 10, pp. 295–300, Oct. 1951.

[84] C. Gabriel, "Dielectric properties of biological tissue: Variation with age," *Bioelectromagnetics*, vol. 26, no. S7, pp. S12–S18, 2005.

[85] A. Shahzad, S. Khan, M. Jones, R. M. Dwyer, and M. O'Halloran, "Investigation of the effect of dehydration on tissue dielectric properties in *ex vivo* measurements," *Biomedical Physics & Engineering Express*, vol. 3, no. 4, p. 045001, Jun. 2017.

[86] F. Jaspard and M. Nadi, "Dielectric properties of blood: an investigation of temperature dependence," *Physiological Measurement*, vol. 23, no. 3, pp. 547–554, 2002.

[87] P. Wang and C. L. Brace, "Tissue dielectric measurement using an interstitial dipole antenna," *IEEE Transactions on Biomedical Engineering*, vol. 59, no. 1, pp. 115–121, Jan. 2012.

[88] W. T. Joines, Y. Zhang, C. Li, and R. L. Jirtle, "The measured electrical properties of normal and malignant human tissues from 50 to 900 MHz," *Medical Physics*, vol. 21, no. 4, pp. 547–550, 1994.

[89] A. J. Surowiec, S. S. Stuchly, J. R. Barr, and A. Swarup, "Dielectric properties of breast carcinoma and the surrounding tissues," *IEEE Transactions on Biomedical Engineering*, vol. 35, no. 4, pp. 257–263, Apr. 1988.

[90] S. R. Smith, K. R. Foster, and G. L. Wolf, "Dielectric properties of VX-2 carcinoma versus normal liver tissue," *IEEE Transactions on Biomedical Engineering*, vol. BME-33, no. 5, pp. 522–524, May 1986.

[91] A. P. O'Rourke, M. Lazebnik, J. M. Bertram, M. C. Converse, S. C. Hagness, J. G. Webster, and D. M. Mahvi, "Dielectric properties of human normal, malignant and cirrhotic liver tissue: *in vivo* and *ex vivo* measurements from 0.5 to 20 GHz using a precision open-ended coaxial probe," *Physics in Medicine and Biology*, vol. 52, no. 15, pp. 4707–4719, 2007.

[92] R. J. Halter, A. Schned, J. Heaney, A. Hartov, S. Schutz, and K. D. Paulsen, "Electrical impedance spectroscopy of benign and malignant prostatic tissues," *Journal of Urology*, vol. 179, no. 4, pp. 1580–1586, 2008.

[93] E. C. Fear, S. C. Hagness, P. M. Meaney, M. Okoniewski, and M. A. Stuchly, "Enhancing breast tumor detection with near-field imaging," *IEEE Microwave Magazine*, vol. 3, no. 1, pp. 48–56, March 2002.

[94] E. C. Fear, P. M. Meaney, and M. A. Stuchly, "Microwaves for breast cancer detection?" *IEEE Potentials*, vol. 22, no. 1, pp. 12–18, Feb. 2003.

[95] C. Gabriel, S. Gabriel, and E. Corthout, "The dielectric properties of biological tissues: I. literature survey," *Physics in Medicine and Biology*, vol. 41, no. 11, pp. 2231–2249, Nov. 1996.

[96] S. Gabriel, R. W. Lau, and C. Gabriel, "The dielectric properties of biological tissues: II. measurements in the frequency range 10 Hz to 20 GHz," *Physics in Medicine and Biology*, vol. 41, no. 11, pp. 2251–2269, Nov. 1996.

[97] ——, "The dielectric properties of biological tissues: III. parametric models for the dielectric spectrum of tissues," *Physics in Medicine and Biology*, vol. 41, no. 11, pp. 2271–2293, Nov. 1996.

[98] A. M. Abad-García, A. Fornes-Leal, and N. Cardona, "Electromagnetic characterization of biological tissues of the abdominal and thoracic regions at *in vivo* conditions," iTEAM-UPV, Valencia (Spain), 2018. Based on data published by A. Fornes-Leal *et al.* in 2019. [Online]. Available: https://www.mcg.upv.es/studer-results/ [Accessed: 28-Jun-2019].